Condition monitoring of a gearbox through the Internet

GS Grobler

20688245

Dissertation submitted in fulfilment of the requirements for the degree *Magister* in Mechanical Engineering at the Potchefstroom Campus of the North-West University

Supervisor: Dr CB Nel

May 2015

ABSTRACT

Condition monitoring of rotating machines used at factories and mines could significantly reduce production losses to allow continuous production. Unexpected machine failures could be eliminated, and specific problems then identified and solved as a predictive maintenance approach.

In this study a cost-effective continuous condition-monitoring system for a gearbox was developed. The monitoring system measured vibration and temperature at short time intervals, and these parameters were effectively used as early warnings when problems started and developed over time. In addition, electrical current was also measured for changing power and torque which were then also determined for the gearbox regarding different applied loading conditions.

A mathematical model was developed to describe all the different defect frequencies for each of the ball-bearings in the gearbox. This model also described the gear-mesh frequencies for the gears in the gearbox. This mathematical model was implemented in a computer program, and the information obtained used in the analysis of measured data regarding possible damage at the bearings and gears.

The condition-monitoring system comprised electronic hardware coupled to appropriate sensors and also to a computer. A second computer program was written so that the measured parameters could be captured and indicated. In addition, a second mathematical model was developed to convert measured time domain acceleration data into the frequency domain by using a series of Fourier coefficient amplitudes at certain frequencies and corresponding phase angles. Acceleration signals were also converted to corresponding velocity and displacement signals. The time domain signals were used to determine single overall RMS vibration magnitudes. This model was then also implemented in this computer program.

The computer programs were both implemented in a Matlab environment. By using certain input parameters for the bearings and for the gears respectively as characterised, the first program computed bearing-defect frequencies and gear-mesh frequencies. This was regarded as necessary because amplitudes at these frequencies normally represent wear.

The second computer program made it possible to capture measured acceleration data obtained from instrumentation, and time domain signals were then constructed for each of the four acceleration meter inputs. The program constructed trends and graphs for the measured time and frequency domain vibration signals. This computer program also captured measured temperature and electrical current data obtained from instrumentation. The measured electrical current magnitudes were used to compute changing power and torque, and corresponding trends were also constructed. Trends for temperature were also constructed. Alarm settings were programmed for certain measured parameters.

This system was developed, built and thoroughly tested to ensure accuracy and reliability of the measured data. A test setup was built in the laboratory for the experimental phase of this work. A small gearbox coupled to an electrical motor with a brake at the output shaft for loading purposes was used. Instrumentation coupled to a laptop and connected to the Internet was part of this test setup.

Extensive time and frequency domain vibration signal analysis was done for a broad range of frequencies up to 12500 Hz. The vibration signal analysis was very effective in clearly distinguishing between ball-bearing wear and wear at gear teeth.

The measured parameters, namely vibration, temperature, electrical current, power and torque were made available on the Internet during real time. The main advantage here was that the gearbox condition could be observed by other people, even in a different town or country, compared to where the gearbox was actually installed and used, while the gearbox was running. For example, vibration signal analysis could thus be done by experts in this field far away from where the gearbox was running, so that specific problems could be identified at an early stage.

Keywords: Gears, ball bearings, wear, Internet, condition monitoring, vibration, electrical current, temperature.

SAMEVATTING

Toestandmonitering van roterende masjiene wat gebruik word in fabrieke en myne kan produksieverliese aansienlik verminder om deurlopende produksie moontlik te maak. Onverwagte masjienfaling kan uitgeskakel word, en spesifieke probleme kan dan geïdentifiseer en opgelos word as 'n voorspelde instandhoudingsbenadering.

In hierdie studie is 'n koste-effektiewe, deurlopende toestandmoniteringstelsel vir 'n ratkas ontwikkel. Die moniteringstelsel het vibrasie en temperatuur op kort tyd intervalle gemeet, en hierdie parameters is effektief gebruik as vroeë waarskuwings wanneer probleme begin het en met verloop van tyd ontwikkel het. Daarbenewens is elektriese stroom ook gemeet vir verandering in drywing en wringkrag wat dan bepaal is vir die ratkas oor verskillende toegepaste lastoestande.

'n Wiskundige model is ontwikkel om al die verskillende defek-frekwensies vir elk van die koeëllaers in die ratkas te beskryf. Hierdie model het ook die rat inkam-frekwensies vir die ratte in die ratkas beskryf. Hierdie wiskundige model is geïmplementeer in 'n rekenaarprogram en die inligting wat verkry word is in die analise van die gemete data, aangaande moontlike skade aan die laers en ratte, gebruik.

Die toestandmoniteringstelsel bestaan uit elektroniese hardeware wat gekoppel is aan toepaslike sensors en ook aan 'n rekenaar. 'n Tweede rekenaarprogram is so geskryf dat die gemete parameters vasgelê en aangedui kon word. Daarbenewens is 'n tweede wiskundige model ontwikkel om gemete tyddomein versnellingsdata om te skakel na die frekwensiedomein deur die gebruik van 'n reeks van Fourier-koëffisiënt-amplitudes op sekere frekwensies en hulle ooreenstemmende fasehoeke. Versnellingseine is ook omgeskakel in ooreenstemmende snelheids- en verplasingseine. Die tyddomeinseine is gebruik om 'n totale RMS vibrasiewaarde te bepaal. Hierdie model is ook in die rekenaarprogram geïmplementeer.

Die rekenaarprogram is albei geïmplementeer in 'n Matlab-omgewing. Deur die gebruik van sekere inset-parameters wat vir die laers en vir die ratte onderskeidelik gekarakteriseer is, het die eerste program laer defekfrekwensies en rat inkamfrekwensies bereken. Dit is nodig geag omdat amplitudes by hierdie frekwensies normaalweg slytasie verteenwoordig. Die

tweede program op die rekenaar het dit moontlik gemaak om gemete versnellingsdata, wat verkry is van instrumentasie, vas te lê, en tyddomeinseine is toe gekonstrueer vir elk van die vier versnellings se meterinsette. Die program het tendense en grafieke gekonstrueer vir die gemete tyd en frekwensie domeinvibrasieseine. Hierdie rekenaarprogram het ook gemete temperatuur en elektriese stroomdata wat verkry is van instrumentasie, vasgevang. Die gemete elektriese stroomwaardes is gebruik om veranderende drywing en wringkrag te bereken, en die ooreenstemmende tendense is ook gekonstrueer. Tendense vir temperatuur is ook gekonstrueer. Alarminstellings is geprogramer vir sekere gemete parameters.

Hierdie stelsel is ontwikkel, gebou en deeglik getoets om akkuraatheid en betroubaarheid van die gemete data te verseker. 'n Toetsopstelling is in die laboratorium gebou vir die eksperimentele fase van hierdie werk. 'n Klein ratkas, gekoppel aan 'n elektriese motor met 'n rem op die leweringsas vir lasdoeleindes, is gebruik. Instrumentasie gekoppel aan 'n skootrekenaar en gekonnekteer aan die Internet was deel van hierdie toetsopstelling.

Uitgebreide tyd en frekwensie domeinvibrasie seinanalise is gedoen vir 'n wye reeks van frekwensies tot so hoog as 12500 Hz. Die vibrasie seinanalise was baie effektief om duidelik te kan onderskei tussen koeëllaersslytasie en slytasie by rattande.

Die gemete parameters, naamlik vibrasie, temperatuur, elektriese stroom, drywing en wringkrag is intyds op die Internet beskikbaar gestel . Die belangrikste voordeel hiervan was dat die ratkas se toestand waargeneem kon word deur ander mense, selfs in 'n ander dorp of land teenoor waar die ratkas eintlik geïnstalleer en gebruik was, terwyl die ratkas geloop het. Byvoorbeeld, vibrasie seinanalise kan dus gedoen word deur kundiges op hierdie gebied ver weg van waar die ratkas loop, sodat spesifieke probleme op 'n vroeë stadium geïdentifiseer kan word.

Sleutelwoorde: Ratte, koeëllaers, slytasie, Internet, toestand monitering, vibrasie, elektriese stroom, temperatuur.

ACKNOWLEDGEMENTS

As in many walks of life no big task can be done by a person on his own, and I want to dedicate this page to thank the many who helped me accomplish this wonderful milestone. Thank you, to each one who had an impact on my life to help me finish this degree. In particular I would like to thank the following special contributors:

- My Heavenly Father for His loving kindness and grace. I do not deserve what I get and I give Him all the honour and praise. He finished what He started and my life is evidence of His grace and faithfulness. Thank you, Father.
- Dr CB Nel for his professional and yet personal guidance, help and motivation throughout the project. It was greatly appreciated and needed.
- My supporting and loving family, especially my parents, for always giving me motivation and love and keeping me in their prayers during the span of my studies. Without love we are nothing.
- The wonderful lady in my life. Vidette, thank you for being behind me and by my side during the latter part of this big project and for all the help, support and love.
- The technical support personnel of the Mechanical Engineering School for helping with manufacturing and with problem-solving during challenges.
- Prof AL Combrink for language editing of this document.

INDEX

LIST OF FIGURES

LIST OF TABLES

LIST OF SYMBOLS

Upper case symbols:

Bd	: Ball diameter of roller element bearings balls	[m]
Bd	: Ball diameter of roller element bearings balls	[m]
D_1, D_2, D_3, D_4	: Gear pitch diameter for Gear 1 to 4	[m]
F	: Power factor of gearbox	
I	: Electrical current	[amp]
N	: Input shaft speed	[rpm]
Nb	: Number of balls in roller element bearing	
P	: Power	[W]
Pd	: Pitch diameter in roller element bearing	[m]
S	: Running speed frequency of shafts	[Hz]
T	: Torque	[Nm]
T	: Period	[s]
V	: Electrical potential difference	[V]
X	: Displacement amplitude	[m]
$\dot{X}$	: Velocity amplitude	[m/s]
$\ddot{X}$	: Acceleration amplitude	[m/s^2]

Lower case symbols:

$a_{0,1,2,\ldots,n}$	: Constant coefficient in Fourier series	[m/s^2]
$b_{1,2,\ldots,n}$	: Constant coefficients in Fourier series	[m/s^2]
c_n	: n_{th} Constant coefficient in Fourier series	[m/s^2]
c_0	: First constant coefficient in Fourier series	[m/s^2]
f_1, f_2, f_3, f_4	: Shaft speed at Gear 1 to 4	[Hz]
f_{bpi}	: Ball pass frequency of the inner race	[Hz]
f_{bpo}	: Ball pass frequency of the outer race	[Hz]
f_{bs}	: Ball spin frequency	[Hz]
f_{ft}	: Fundamental train frequency	[Hz]
f_{gm1}	: Gear mesh frequency of gear pair 1	[Hz]
f_{gm2}	: Gear mesh frequency of gear pair 2	[Hz]
g_r	: Total gear reduction ratio of gearbox	
m	: m_{th} Fourier coefficient of series	
t	: Time	[s]
t_1, t_2, t_3, t_4	: Number of teeth for Gear 1 to 4	
$x(t)$	: Periodic Displacement	[m]
$\dot{x}(t)$	: Periodic velocity	[m/s]
$\ddot{x}(t)$	: Periodic acceleration	[m/s^2]
$\dot{x}_{rms}$	: Root Mean Square velocity	[m/s]

$\ddot{x}_{rms}$	: Root Mean Square acceleration	[m/s^2]

Symbols:

θ	: Contact angle at roller element bearing	[°]
η	: Mechanical efficiency	
ϕ_n	: n_{th} Phase angle	[rad]
ϕ_{an}	: n_{th} Phase angle for acceleration in Fourier series	[rad]
ϕ_{vn}	: n_{th} Phase angle for velocity in Fourier series	[rad]
ϕ_{dn}	: n_{th} Phase angle for displacement in Fourier series	[rad]
ω_n	: n_{th} Frequency in Fourier series	[rad/s]

Abbreviations:

BPFI	: Ball Pass Frequency Inner
BPFO	: Ball Pass Frequency Outer
BSF	: Ball Spin Frequency
DI	: Diagnostic Instruments
FFT	: Fast Fourier Transform
FTF	: Fundamental Train Frequency
IH	: Input shaft measured in the horizontal direction
IPS	: Instantaneous Power Spectrum distribution
IV	: Input shaft measured in the vertical direction
NI	: National Instruments
OH	: Output shaft measured in the horizontal direction

OV : Output shaft measured in the vertical direction

RMS : Root Mean Square

1. Literature study

1.1 Introduction

The purpose of this literature study was to make a study of the literature on the topic of condition monitoring of industrial gearboxes and the possible use of the Internet for this task. The recent developments and the current status of technology in this field were investigated. The literature survey included different condition monitoring techniques used by previous researchers. Their specific measured parameters chosen as Indicators for rotating machine condition including details regarding instrumentation and in some cases also computer software that were used were important and relevant regarding this study. Special attention was given to the analysis of measured data. Recent different work done as reported in the literature on early warnings of condition-monitoring systems regarding different possible defects that could be present at rotating machines, including roller element bearings and gear teeth problems, was investigated with due care.

1.2 Condition monitoring of rotating machinery

Condition monitoring is a predictive maintenance approach, where certain measured data can be used to determine possible problems with industrial rotating machines such as gearboxes driven by electrical motors, as early warnings. These problems could then be addressed and certain maintenance actions carried out in time, before unnecessary production losses in factories and mines start occurring. In addition, catastrophic failures could virtually be eliminated when this approach is applied correctly.

1.2.1 Condition-monitoring techniques

Rao (2011) mentioned and explained several machine condition-monitoring techniques that could be used. These techniques could be visual and aural inspections, operational variables related to machine performance, oil analysis to determine wear, vibration and temperature measurements. Vibration as the preferred parameter for condition monitoring at rotating machines is widely accepted (Bloch & Geitner, 1997; Taylor, 2003)

1.2.2 Vibration causes

Rao (2011) listed the following defects at a gearbox that could result in excessive vibration:

- Bent shaft
- Eccentric shaft
- Misaligned components
- Unbalanced components
- Faulty bearings
- Faulty gears
- Mechanical loose parts

Each of these above-mentioned defects will result in a vibration pattern, and when vibration signals are measured the shape of the frequency domain signal and phase relationships between signals could reveal important information regarding the diagnostic analysis (Rao, 2011).

According to Rockwell Automation (2005) condition monitoring may be the most misused and misunderstood of the tools used in plant optimization. According to this author, condition monitoring should not only be seen as a plant maintenance tool, but should also be seen as a tool to optimize plant operations and management. It should be used in plant asset management, logistics and labour requirements. For example, mines in South Africa are usually located far from major suppliers, thus asset management and planning is critical to ensure overall plant performance. Four condition monitoring tools at machines were suggested to be used effectively in the management of a plant:

- Vibration analysis
- Oil analysis
- Infrared thermography (temperature)
- Motor-electrical current analysis

1.3 Vibration signal analysis

Vibration response in a single degree of freedom system is determined by the mass, stiffness and damping properties of the system as well as an external shaking force at a certain forced frequency (Davies, 1998). The external shaking force could be related to mass imbalance, eccentricity, misalignment, mechanical looseness, etc., which represents the defect in the machine system. Response amplitude, phase at a certain frequency are the two characteristics to define any vibration (Bentley & Hatch, 2002). Response amplitude could be expressed in terms of acceleration, velocity or displacement (Davies, 1998; Rao, 2011; Dunton, 1991). It can be shown, however, that velocity is normally the preferred measured parameter to be used to examine the presence of structural defects such as, mass imbalance, eccentricity, misalignment, mechanical looseness, etc., because it is independent of frequency for a large frequency range (Bentley & Hatch, 2002). For bearing defects and gear teeth problems, however, acceleration has proven to be a more sensitive measured parameter. The literature shows that vibration signal analysis could be classified in certain main techniques when a gearbox mechanical condition is considered, as described in the next few Paragraphs.

1.3.1 Time waveform analysis

Time-domain analysis is based on the time history of a vibration signal obtained from measurements taken by using a feasible sensor and an amplifier as instrumentation. Acceleration meters are regarded as the best sensors to be used at gearboxes where roller element bearings are used (Bentley & Hatch, 2002; Davies, 1998; Kalaitszlou *et al.*, 2009; Stander & Heyns, 2000; Taylor, 2003). Any non-steady or transient impulse could be observed from these time waveforms. This type of analysis is often used at vibration monitoring of gearboxes (Rao 2011; Ozturk *et al.*, 2010). Cracks at inner rings of bearings and broken teeth on gears could be seen from these time-wave signals (Rao, 2011).

In recent years the limitations of FFT analysis is being discovered and time waveform analysis is used to support FFT analysis (Dunton, 1991; Ganeriwala, 2010). Time waveform analysis is a powerful tool and is not used to its full potential by condition-monitoring engineers. It is a confusing and difficult technique and these are the reasons why it is not used to its full potential. A time waveform can consist of easily identified periodic events or more complex signals. The frequency of a periodic event can be calculated by taking the

inverse of the periodic time in seconds between events. Pattern recognition is elementary on time waveform analysis.

1.3.2 Frequency domain analysis

The data of a measured time domain vibration signal could be converted into the frequency domain with an approach based on a mathematical model developed by Fourier (Ewins, 2000; Rao, 2011; Stander & Heyns, 2000). This procedure could be done by a numerical algorithm based on this mathematical model which is known as Fast Frequency Transform or alternatively also Fast Fourier Transform (Ewins, 2000, Ozturk *et al.*, 2010; Randall & Robert, 2011). Frequency domain analysis is based on the presence of amplitudes at certain frequencies in measured frequency domain signals. Depending on the shape of this graph and also amplitudes at certain fundamental frequencies and also harmonics, specific problems such as the presence of mass imbalance, eccentricity, misalignment, mechanical looseness, etc. could be clearly identified. In addition, this analytical approach could clearly identify the presence of possible roller element bearing defect frequencies, and also gear mesh frequencies regarding faults at bearings and gear teeth (Akerblom, 2001; Antoni & Randall, 2002; Archer & Basaraba, 1995; Bentley, 2002; Bloch & Geitner, 1997; Dalpiaz *et al.*, 2008; Davies, 1998; Ganeriwala, 2010; Limmer, 1997; Pryor, 2011; Randall & Sawalhi, 2011). This frequency domain spectrum approach could be used, as early warnings and specific amplitudes at certain frequencies could increase or change as problems developed. The magnitudes of roller element bearing defect frequencies, and also gear mesh frequencies could be theoretically calculated and are based on geometry and shaft speed.

For gear impacts it is clearly visible as a spike in the time waveform (see Paragraph 1.3.1) if there are defects present. In the frequency spectrum signal only a small amplitude is normally observed at running speed first order, but the time waveform clearly shows the impact amplitudes on a single revolution.

1.3.3 Cepstrum analysis

Quefrency domain analysis could be used at gearboxes and is based on a parameter known as *cepstrum*, similar to *frequency* that serves as the abscissa for the parameter of spectrum (Rao, 2011). Cepstrum can be used to detect local gear tooth defects early in their development (Ozturk *et al.*, 2010; Randall & Robert, 2011).

Dalpiaz *et al.*, (2008) concluded that the cepstrum analysis was unable to detect a gear crack.

1.3.4 Wavelet transform analysis

Wavelet transform analysis is based on complex mathematical functions which are well suited for expansion of non-stationary signals (Dalpiaz *et al.*, 2008; Ozturk *et al.*, 2010). From experimental work, it was found that for the initiation and progression of a fatigue crack at a gear tooth that the wavelet transform technique is the best for early detection diagnosis (Ozturk *et al.*, 2010; Stander & Heyns, 2000). Wavelet transform is very sensitive to changes in gear vibration and will detect gear faults and reflect the progression of the fault. It can be used for early fault detection in gears (Jena *et al.*, 2013; Ozturk *et al.*, 2010).

1.3.5 Time synchronous averaging

Time synchronous averaging in vibration analysis, according to Dalpiaz *et al.* (2008) is used to attenuate the parts of a signal that are not coherent and not synchronous to a level that leaves it negligible. It is a fundamental process to analyse shafts, gears and balance algorithms. The attenuation is done to a level of $\sqrt{1/\mathrm{N}}$ as a rule of thumb, where N is the number of averages (Stander & Heyns, 2000).

1.3.6 High-frequency detection

High-frequency detection is used to focus in the high frequency range from 5-60 kHz (Dunton, 1991). It is not used very widely since the enveloping technique has developed which also focussed on the high-frequency range. High-frequency detection is not as complex as enveloping and can also be used for very early stage damage detection at roller element type of bearings. It is not very trendable, because so many small changes could influence the readings.

1.3.7 Envelope spectrum

Envelope spectrum analysis is very effective at roller-element bearing analysis, but could also effectively be used in gear fault diagnostics. The technique takes the high frequency harmonics generated by a bearing and displays it in the low frequency band used in current data collectors. A velocity processed signal may not show the defect on a bearing, but an enveloped signal will show the defect. This technique provides a method for early detection of defects at roller element type of bearings. According to SKF (1999) bearing-fault signals

are of short duration and not easy to detect when masked by machine noise. Enveloping firstly filters out the low-frequency noise from rotating components. The high-amplitude and low-frequency rotational signals are filtered out. Thus the amplitudes at the first three or four running speed signals are filtered out and only the high frequency repetitive signals are kept which take care of most of the noise. The band pass filter selected should not only filter the low-frequency harmonics out, but also the very high-frequency components which are amplified by the acceleration meter resonance. The lower filter limit should be at least ten times the rotation speed, but it should be selected to pass the most bearing-defect frequencies and not the very high-frequency noise. The next aspect of enveloping is to reduce the complex signals to a display of all repetitive impulse responses. The signal will show the repetitive bearing defect signal enhanced and the non-repetitive signal suppressed. Enveloping can also be successfully used in early detection of faults in gearboxes. It must be noted that amplitudes of an enveloped signal cannot be compared to normal signal amplitudes because the amplitude is a summation of the harmonic series of the bearing defect. Very slow bearing speeds, of as low as 3.5 rpm, have been successfully monitored with vibration enveloping (Stander & Heyns, 2000).

Alexej *et al,* (2011) explained that difficulties were experienced when bearing enveloping algorithms were applied to gearing. Dynamic loads on bearings at gears showed additional lines in the envelope spectrum. Gear-defect shocks did not interfere with bearing-defect detection. When the envelope vibration spectra taken at bearings were analysed, good results for low-rotating gears were reported.

Dalpiaz *et al.* (2008) used demodulation and found that for a gear-tooth crack the demodulations had to be done for every gear to have a full machine diagnosis. It was found with amplitude demodulation that the crack could be localized on a tooth and is sensitive to crack size. Vibration was measured in the radial direction, but the small crack could not be detected on these data. A phase-modulation derivative was done to get better crack detection. The presence and position of the crack could clearly be observed with this technique and even better than with amplitude demodulation. It was found from this study that the transducer position and direction were important with this method.

Alexej *et al.* (2011) listed three tasks in enveloping diagnostics. Firstly, selection of the frequency band was done. When one excludes harmonic components, their Root Mean Square values are higher than the half value of the sum of all the random components in the frequency band. If they are not excluded it will be difficult to detect bearing and gear shock loads on bearings. Secondly, the defect severity is estimated. Vibration enveloping should be measured for every bearing at a gearbox. Different bearings will have different clearances. Gear mesh defects are transferred through the bearings. Thirdly, the diagnostic characteristics of bearings and gears are separated. This is random vibration modulation from shaft rotation and their multiples. It is unknown on which bearing the defect is. When a defect is present at a bearing the modulation almost always appears in the random vibration of this bearing. For gears the rule is that the modulation will be seen on the bearings of the shaft the faulty bearing is on and the bearings of the shaft of the meshing gear. It can also be seen on other shaft bearings. Gear-mesh defect modulation will not be observed in bearing envelope spectra. When this is present it must be considered that the frequency band may be incorrect (Alexej *et al.*, 2011).

1.3.8 Spike Energy

The Spike Energy technique was developed in the 1970s to detect the signals from rolling element bearings with defects (Dunton, 1991). The term is used to describe the very short impulse when a rolling element goes through a crack or defect. All metal to metal impact flaws could be measured. This method is also a high-frequency detection method and effective to detect early defects.

1.4 Vibration severity

Figure 1.1 shows a vibration severity diagram according to ISO standard 10816-1 (Reliability direct, 2014). This diagram could only be used for structural defects such as mass imbalance, eccentricity, misalignment, mechanical looseness, etc. and is not applicable to bearing and gear-wear problems. It can be seen that velocity magnitudes indicate different machine conditions for different classes of machines based on power in kW and also mounting configurations which could be either very stiff or very flexible. A cut-off frequency at 1000 Hz is normally used for the overall velocity magnitudes indicated at this diagram.

VIBRATION SEVERITY PER ISO 10816-1						
Machine			Class I	Class II	Class III	Class IV
	in/s	mm/s	Small Machines	Medium Machines	Large Rigid Foundation	Large Soft Foundation
Vibration Velocity Vrms	0.01	0.28				
	0.02	0.45				
	0.03	0.71		GOOD		
	0.04	1.12				
	0.07	1.80				
	0.11	2.80		SATISFACTORY		
	0.18	4.50				
	0.28	7.10		UNSATISFACTORY		
	0.44	11.20				
	0.70	18.00				
	1.10	28.00		UNACCEPTABLE		
	1.77	45.90				

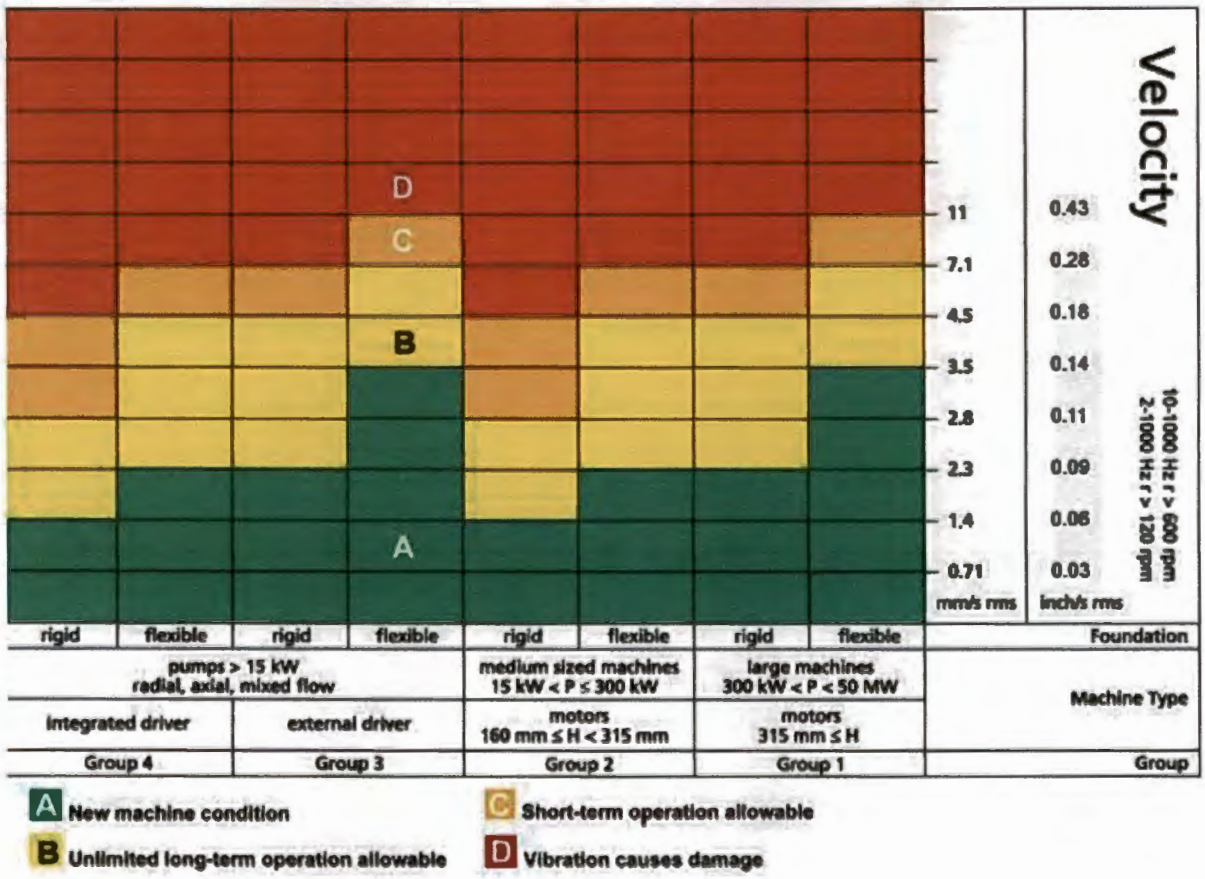

Figure 1.1: ISO 10816-1 vibration severity chart

1.5 Internet condition-monitoring system

1.5.1 Background

The Internet is a way to deliver data between two points in our modern world. Condition-monitoring data based on measurements taken could also be made available on the Internet. Many contractors, however, use portable instrumentation to measure for example vibration signals and temperature, and often travel far distances to visit different plants as a periodic condition-monitoring approach. The measured data are then downloaded to a computer and a report then typically constructed on a monthly basis. This approach is also time-consuming and it is clear that an alternative Internet approach eliminates these disadvantages. The main advantage of the Internet approach is that the rotating machine (or gearbox) condition could be observed by other people, even in a different town or country compared to where the machine was actually installed and used. For example, vibration signal analysis could thus be done by experts in this field far away from where the machine is running so that possible problems could be effectively identified at an early stage.

There are many setups using the Internet for monitoring critical machines, but many improvements can still be made because the technology is not commonly used and is relatively young. The current technologies are described in the next Paragraphs.

Vibration is regarded as the best parameter to evaluate a machine's condition. Two types of vibration analysis are used, namely off-line and on-line or also known as periodic and continuous. Off-line analysis consists of a person walking around on site and taking measurements with a portable device and downloading the data to a computer to be analysed in an office.

For on-line monitoring a permanent connection to the plant is installed. This gives opportunity for continuous monitoring and surveillance. The period between surveillances can be decreased without additional cost to get better fault detection. Dangerous areas in the industry can be monitored without risking the safety of a technician and further remote sites can be monitored at any interval.

Continuous monitoring is advancing rapidly and full protection of an asset is possible. Critical equipment can be monitored continuously to detect damage in the early stages. In the past overall values were monitored and equipment was shut down when certain values were passed. New technology makes it possible to look at spectral bands. A certain frequency band indicates a certain fault and this is used to set spectral band alarms that will indicate what type of fault is present.

Continuous on-line condition monitoring do not have to be implemented on all equipment in a plant. The equipment should be ranked according to their criticality when failing. Rockwell Automation considered the effect of failure on production, the failure mode, the replacement cost, the health and safety consequences and the environmental consequences.

The answers to these questions can further be examined to see where the most time and money can be saved. The failure modes, for example, take into account how long a certain piece of equipment will still be running after damage has occurred. Electrical motors can run for many hours when a bearing has started to fail but turbine bearings could fail after a few hours after the onset of bearing damage.

When the equipment is ranked the correct condition monitoring technique can be implemented on every machine.

1.5.2 Companies with Internet condition monitoring

A company called Ludeca focuses on machine reliability. Ludeca is located in Miami Florida and is the suppliers of laser shaft and geometric aligning systems, laser sheave aligning tools, and vibration and condition-monitoring systems to the industry. Vibroweb R is an online condition-based machine monitor developed by Ludeca. Permanently installed transducers are connected to it and a plug and play card configures the sensors automatically. Up to 32 channels can be accessed. The system can be used on rolls, presses, conveyors, motors, pumps, gearboxes and fans. Parameters monitored include: vibration, bearing condition, temperature, process parameters, FFT spectrum, envelope and time signals. The conditions can then be monitored and checked via a network connection and alarm notifications can be seen on the Internet. The exact method used to connect to the Internet was not explained.

Prosig is a USA and UK-based company focusing on data capturing and the analysis of noise and vibration. The system's hardware and software are designed and developed by their own engineers over decades. The software environment used in their system is not named.

Their online condition-monitoring system is called Protor. This system is implemented on turbine generators, main boiler feed pumps and other plant equipment. The system has a remote measurement data-acquisition system linked by Ethernet. More than one remote measurement data-acquisition system can be connected via Ethernet connection. The systems are mounted close to the transducer and makes cabling costs lower. Personal computers and work-stations are able to look at the data either via modem or WAN which is Internet-accessible. Protor user-software is used to look at the data. A graphical user interface is used with display changes that can be made with a mouse. Power plant control room engineers helped with the design of the display layout. Real-time display of Mimics, Trends, Waterfalls and Orbits can be displayed. Data history can be accessed. For diagnostics full frequency spectra and time histories are used and a configuration editor is also available.

ABB is a global leader in power and automation technologies. MACHsense-R is a service that ABB delivers for condition monitoring of motors and generators. The data from sensors are fed to a fixed data-analysis unit developed by ABB near the equipment monitored. Data are wirelessly transferred to an ABB server which makes it possible for the user to access the data online. The output of the system is one of five, namely rotor bar defects, installation problems, bearing problems, operating parameters and cooler fouling.

The ABB system is able to measure four vibration channels using acceleration meters and five temperature channels using resistance temperature detectors. Their data analysis system uses a Linux-based processor that does in-time analysis. The raw data are processed on board and only the useful results are seen. The alarms for faults send a SMS or e-mail to the dedicated person and also the ABB local service centre. Detailed information about the equipment and fault is seen in the SMS. The Internet connection method is not explained.

Min-Chun Pan *et al.* (2008) applied condition monitoring on a machine through the Internet. The system worked remotely and used the Borland C++ Builder software and Internet transmission communication. Their study did a full monitoring cycle and used artificial

neural networks for pattern recognition. Data-acquisition, signal-processing, feature extraction, pattern recognition and online video surveillance were done. The acquisition hardware used an 8-AD/12-DA data-acquisition card (DAQ) with a TMS320C32 DSP card and the sensors for capturing the vibration data. For privacy reasons a server/client network was used with the server end set at the sites to be monitored and one client end from where monitoring was done. At the server end the sensor captured the signal, a data acquisition system was present and the raw data were sent from the Host computer/port, IP, socket to the client end. Here a fault diagnostics and decision-making system was present which did the signal processing, feature extraction and pattern recognition. The Socket of the TCP/IP was used for the Internet communication and was programmed with the BCB programming language. The DAQ card had 8 Channels available for measurement. The system was tested on a transmission element test rig.

Some other online condition monitoring services available from Internet searches are:

- Condition Monitoring Services Inc (California).
- Schaeffler (UK) Ltd.
- Proviso Systems Ltd (UK based)
- General Electric Bentley Nevada hardware and software (USA).
- OneproD XPR online monitoring system from 01dB-METRAVIB in France was installed in Namibia for De Beers by a Cape Town firm: Ideas Solutions.
- Eriks (UK) based online condition-monitoring system.
- Alstom MSc Machinery Health Monitoring Services (Australia).

1.6 Gears

According to Åkerblom (2001) the most used gear profile for spur, helical, cylindrical and conical gears are the involute. The involute profile gives many useful characteristics, namely that rotational motion can be transferred uniformly even with small errors in centre distance. When contact forces are summed, they will always be constant and all act in the same direction; gears with different numbers of teeth can mate and manufacturing is relatively easy. Perfectly manufactured gears with this profile will transmit speed and torque constantly if no friction is present, and without vibration and noise. But in practice there are friction, geometrical errors and deflections present that create noise and wear.

1.6.1 Gear failures

Transmission error is the difference between the actual position of the gear to the position it would occupy if the gear drive were perfectly conjugate (Åkerblom, 2001). Transmission error is an important excitation mechanism for gear noise and vibration. Causes for transmission error are deflections, geometrical errors and geometrical modifications.

Examples of deflections are contact deformations in the gear mesh, gear-bending deflections, gear-blank deflections, shaft deflections and gearbox-casing deflections. In addition, examples of geometrical errors are involute alignment deviation, involute form deviation, lead deviation, lead-form deviation, lead deviation, gear-tooth bias, pitch errors, run-out and the bearing position in the casing. Finally a list of geometrical modifications are lead crowning, helix angle modification, profile crowning and tip relief and root relief.

Gear noise is caused by the tooth-mesh frequency and its harmonics. The once per revolution is not the main problem, but when the once per revolution transmission error causes sidebands to the gear-mesh frequency, plus when tooth-mesh frequency and the shaft rotational frequency are present. Ghost and phantom frequencies are also present because of manufacturing and dressing of the tools. It is concluded that when pitch error is present, transmission error will be generated at the frequencies of tooth contact and its harmonics. Transmission error is measured with optical encoders at several thousands of pulses per revolution. Two gears' meshing optical readings will be compared to measure the error.

Bloch and Heinz (1997) studied gear-fault detection. Gear-fault vibrations could be observed on a signal at the frequency of the product of the shaft speed and the number of teeth. The product gives the cycles per minute of the gear-vibration signal. Gearbox vibration should be measured in acceleration because the close fit in a gearbox's assembly does not give room for velocity to be developed. When the gearbox condition deteriorates, velocity amplitudes may change in small margins but acceleration amplitude could double or triple. Gear teeth are not often shown on drawings and the engineer should count them when inspecting the gearbox. It should be noted that gear defects occur at synchronous frequencies. As machine condition degrades, sideband frequencies were generated around the gear-mesh harmonics. The spacing of these sidebands is equal to the shaft speed. When

gear-mesh frequency increased, a problem developed and when harmonics of the gear mesh frequency are seen the problem is more severe and finally sidebands form which indicate near failure conditions.

According to Smith (1983) gears can have many different forms of damage of which some are unimportant or easily fixed. Visual inspection is sometimes the only way to see some failure and the level of skill of the viewer is important. Commonly seen, gear failures, namely pitting, scuffing, root cracking and wear were listed by Smith (1983).

According to Smith (1983) pitting occurs because of fatigue from contact stresses that are higher than the surface can handle. The maximum shear stress is under the surface and a crack forms before it breaks out to form a crater. This is initial pitting. Progressive pitting occurs when new craters are continuously formed even after high spots are removed after initial pitting. The whole flank of the gear can be destroyed. Spalling is a form of pitting that can be described when larger pieces of material are breaking out.

Scuffing occurs when the thin oil film between the gear contact surfaces break down and metal to metal contact occurs which results in local welding and tearing. When a machine runs at low speed the oil film is prone to break and is known as cold scuffing. Warm scuffing is present when the oil temperature is high enough for the film to break.

Gear teeth do not commonly break, but cracks on the root, known as root cracking, are the starting point (eye) for failure. Cracks propagate from the eye in a circular way and large pieces of teeth break off and sometimes whole teeth. Because the result is catastrophic, root cracks should be searched for at inspection and gears must be replaced immediately.

Wear is defined as the undesired removal or displacement of material by mechanical action of a contacting solid liquid or gas. Wear is known as the steady removal of metal from the gear flank covering the whole face. Wear and scuffing may look the same on visual inspection. Helical gears wear more consistently over the whole surface than spur gears. Wear is considered undesired in general, but it is an important aspect of a new machine when wearing or breaking in. A gear pair that is worn in will run smoother than a new gear pair. Surface origin pitting is a wear type listed as a contact stress fatigue or pitting fatigue and occurs at gear contact where a rolling and sliding action occurs (Materials Engineering

Institute). The sliding action tends to drag each surface in the direction of sliding and lubrication becomes critical. With the continued contact small diagonal fatigue cracks form on the surface and progress downward into the metal. Over time a small piece of metal surrounded by cracks, usually a fraction of a millimetre deep, falls out, leaving an arrowhead-shaped pit. The piece of metal that was removed creates other wear problems in the gearbox.

When a gear has a defect it changes the contact between meshing gears (Alexej *et al.*, 2011). This increases the vibration amplitudes at the gear-mesh frequency and the harmonic amplitudes. Three defects that can be experienced on gears are displacement of one gear against the next gear, shaft misalignment and lubrication problems

For a worn, cracked or missing tooth a shock will be produced once per revolution for this gear. The gear housing will show increases in vibration at multiples of the faulty gear frequency. The gear-mesh harmonics creates sidebands. These sidebands are spaced at intervals equal to the rotational frequency of the gear. Hunting tooth frequency will be seen when both meshing gears have a defect and the two faulty teeth contact each other. A high shock vibration will be excited and will excite the gear structure's fundamental frequency and multiples of the tooth repeat frequency.

1.6.2 Gear-fault diagnostic methods

Ozturk *et al.* (2010) investigated how effective some techniques are in the early detection of gear failure. The methods were used on real gear vibrations and at gear-tooth cracks. The conclusion was that conventional time and frequency domain analysis techniques were unable to detect cracks early but only when the fault is significantly developed.

Dalpiaz *et al.* (2008) compared vibration analysis techniques for the detection of gear faults. A test setup was used and they looked at gear-crack detecting at different depths with a change in transducer placement. The setup was a power circulating gear-testing machine. Two identical single stage gear units were connected back to back with a locked-in torque. Vibration signals were measured on the gearbox casing in two different positions with Bruel & Kjaer 4369 piezo-electric acceleration metres. One was mounted parallel to the shaft axis and the other radially on the shaft axis. A Bruel & Kjaer 2635 charge amplifier was used to get the velocity signals. The tests were done on 385 Nm nominal torques on the pinion gear

and at a speed of 1000 rpm. This gives a meshing frequency of 466.67 Hz. Magnetic tape was used for recording. The frequency range worked in was between 0 and 5000 Hz because it includes the meshing harmonics. Signal processing was done with LMS Cada-X and Matlab software. Some signals were pre-processed using synchronizing techniques to compensate variations in machine angular speed.

1.7 Bearings

Bearings are an important component in rotating machinery. A bearing carries a component in rotation at very low friction. Railroad speeds were limited in the past because of the lack of bearings. Oil-soaked rags were stuffed into the wheel axle journal boxes, called stuffing boxes. Friction caused high temperatures resulting in fires and train stoppages. Today high speeds and loads can be carried on trains because of tapered roller bearings. According to Bloch and Heinz (1997) there exist many bearing types, each designed to better carry the loads for a certain application. Because the bearing is the component in a machine that carries the load it is the component that fails first. Condition monitoring on bearings is a field of study that enjoys a lot of attention. Vibration analysis is a tool to measure and predict the condition of a bearing. Bearing defects is seen at asynchronous frequencies according to Archer and Basabara (1995).

Bearing fault frequencies are non-integer multiples of machine operating speeds. For bearing condition monitoring the vibration frequency techniques are divided into three categories, namely low (0-20kHz), medium (20-100 kHz) and high (>100kHz).

During routine machinery monitoring the signals looked at are in the low range. Amplitude and energy levels for signals in this range are very high compared to those of bearing amplitude and energy content. In the medium range sensor position becomes critical. Sometimes the signal can be amplified or attenuated. In the high frequency range machinery material problems do not show. These signals can be analysed for their energy content which will guide us in the fault detection on a bearing (Bloch & Heinz, 1997).

1.7.1 Bearing failures

A bearing failure may occur for many reasons such as fatigue, poor lubrication, contamination, faulty mounting and careless handling. Fatigue is mainly influenced by the

number of revolutions performed by the bearing, and the magnitude of the loads carried by the bearing, especially the dynamic fluctuating loads. Fatigue is the result of material stresses appearing immediately below the load carrying surface. When cracks form on the surface and grow into the material, surface distress is at hand. As the rolling elements pass over these cracks, fragments of material break away. This is known as spalling or flaking which progressively increases in extent, and the increase in damage eventually causes the bearing to become unusable. One of the reasons that vibration is measured on the bearing housings is that all the forced frequencies are transmitted through the bearings from the rotating element. These detectable forces as function of measured vibration responses are also at work degrading the life of the bearing. Degradation manifests itself in any of four ways, namely as damage to the outer race, damage to the inner race, damage to the rolling elements or damage to the bearing cage. Each of these four flaws will generate a specific frequency depending on the geometry and the shaft speed inside the bearing, which can be theoretically computed (Bloch & Geitner, 1997; Moheb *et al.*, 2011). These frequencies are known as bearing-defect frequencies, and will appear in frequency domain vibration signals at small amplitudes when spalling damage has started (Bloch & Geitner, 1997; (Paez & Piersol, 2010).

SKF (1999) identified four stages of bearing damage, from minor to more severe, numbered from one to four. In stage one micro-pitting is present but the bearing is still in a good condition. During stage two the bearing has some wear but replacement is unnecessary. Pinpoint spalling is present in the raceways. The bearing is becoming terminal in stage three and monitoring intervals should be closer together because bearing degrading is not linear anymore. Sidebands of shaft speed are beginning to show on vibration signals. When stage four is reached immediate action should be taken because bearing life from here is very short. Defect-frequency amplitudes in the bearing defect region are developing and in an enveloped signal high-amplitude defect frequencies as well as first and second order speed sidebands are showing looseness. Cage-defect frequencies will appear.

One of the most common failures when bearings are first put into service is seizure. This happens when the rolling elements fail to rotate and then the surface temperature rises rapidly, making the metal unfit for the task. Micro-welding starts and bearing failure sets in

rapidly. Three reasons for seizing are insufficient clearance, lack of lubrication and excessive mechanical load (Paez & Piersol, 2010).

During installation a bearing can be damaged with the incorrect installation methods and can result in a race fracture. Insufficient clearance between bearing parts or shock loads can result in fractures of bearing components. The inner race will also fracture over an oversized shaft.

Retainer failure may also occur at a bearing. The retainer is the cage that secures the rolling elements in their position. Reasons for failure can be damage because of foreign matter entering the bearing, damage during installation or high bearing speed.

Rust is caused by improper care during storage, maintenance and when the machine is out of operation. Exposure to moisture during handling, storage and operation can start rust. Small pits form and the most damage occurs when the rust is on the race. Do not handle a bearing with bare hands during installation and prevent moisture or acidic gases from coming into contact with a bearing.

Wear is part of the natural life of a bearing but when excessive wear sets in damage and failure are the result. Contamination of lubrication is a reason for premature wear. Another cause is the softening of races' surfaces because of overheating.

Load carrying surfaces are roughened when foreign material enters the lubricant of the bearing and is called roughening. Small dents are formed on the surface when a particle is pressed between a load surface and a rolling element. In severe cases of roughening flaking can set in.

When the rolling elements form dents in the load carrying surface after a shock or when a machine is static in a high vibration environment and is termed Brinelling. Applying a shock force during installation on the wrong race can also result in Brinelling.

When bearings are subject to small movement between rollers and raceways during storage or shipment under excess load false Brinelling occurs. Microscopic cracks form and become dark brown and can even form Brinelling.

When rolling elements start to slip and not roll smearing sets in. Over-lubrication is also a cause of smearing.

When a bearing race starts to slip on its mounting surface it is termed creeping. The outer race of a bearing is much more prone to creeping because it has a much looser fit than the inner race. When a fit is accurate not much damage will be done but fretting will speed up the looseness (Paez & Piersol, 2010).

1.7.2 Bearing fault diagnostic methods

Ganeriwala (2010), Dunton (1991) and Pryor (2011) reviewed several techniques that are used in current industrial products to analyse bearing faults. These techniques are listed and briefly explained in Paragraph 1.3. It was evident from the literature that if more than one vibration analysis technique is used, it should result in a better fault diagnostic procedure.

1.8 Separation of gear and bearing vibrations

Antoni *et al* (2002) studied the differential diagnosis of gear and bearing faults. Gear faults and bearing faults on vibration signals give a challenge to detect and to separate the two. Gear faults are periodic, but bearing faults experience some randomness and are cyclo-stationary. Localized and distributed faults were studied. Gear and bearing faults were simulated and advanced spectral analysis were used to diagnose the faults. Experimental and actual vibration signals were used to check the effectiveness of the proposed procedure.

Randall and Robert (2011) looked at a new method for separating discrete components from a signal. A procedure to separate a signal was used. Firstly, parts of the signal were transformed to the frequency domain using the FFT algorithm. Secondly the phase angle was stored while the log amplitude was processed using the inverse FFT algorithm. This gave the real cepstrum. The next step was to remove harmonic families (rahmonics = uniformly spaced components in the cepstrum). The edited cepstrum was transformed using forward FFT. This gave the edited log amplitude cepstrum. In the following step the phase angle and the edited log amplitude cepstrum were combined to give the complex spectrum. Then the inverse FFT was applied to get the time signal of the residual random part.

A gear test rig was used for testing. A variable speed electrical motor drove the rig. Changeable load is applied with a circulating power loop involving a hydraulic pump supplying a hydraulic motor. The motor speed is 10 Hz with 50 Nm load. Two 32 spur gears meshed together and a bearing with an inner race defect was monitored by an acceleration meter on its casing.

The new method is superior to time-synchronous averaging and discrete/random separation methods because it could remove sidebands, remove harmonics, remove periodic narrow band noise peaks and operate over limited band regions.

Rafiee (2010) used wavelet functions to automatically diagnose gear bearing faults. Feature extraction was considered in detail and 324 mother wavelet candidates studied. The statistical features used are standard deviation, variance, kurtosis, and fourth central moment of continuous wavelet coefficient of synchronized vibration signals.

Jena *et al.* (2013) used adaptive wavelet transform of vibration signals to diagnose gear and bearing faults. They tried to build a robust wavelet function to address any specific class of problem. Each rotating system has a unique defect signature and this made their challenge more difficult. They concluded that statistical parameters are insensitive in determining the severity of defects. Their method was suitable and reliable to see the severity of gear and bearing defects.

The decomposition of vibration signals into deterministic and non-deterministic components was investigated by Barscz *et al.* (2009). This researcher considered the possibility of using it for fault detection and identification. He used the Wold theorem to decompose the signal where the deterministic part was the gear and shaft related component and the bearing and noise as the non-deterministic component. A signal was simulated with a bearing fault on which the algorithm was tested. A self-adaptive filter was programmed in Matlab computer programming and used for the decomposition algorithm. Finally the algorithm was tested on a wind turbine signal with an outer ring bearing defect. Speed fluctuation in the component tested must be avoided because it will make the algorithm useless

Karagulle and Kiral (2006) considered vibration analysis of rolling element bearings under the action of an unbalanced force. This study simulated the bearing defects and vibrations all in computer models and software. No actual vibration measurement was done on a bearing. Visual basic was used for the computer code and the finite element package IDEAS for the vibration analysis. RMS, crest factor, kurtosis and band energy ratio was used to do vibration analysis on the bearing. Three points were simulated where vibrations were measured from. Localized bearing defects in the bearing were simulated and an unbalanced force rotated with the shaft. Parameters inspected were rotational speed, sensor location, angular position and the number of outer ring defects and defect type which were on the inner ring and on the rolling elements. Kurtosis and crest factor are uninfluenced by the number of defects. RMS ratio was a good indicator for inner ring defects at all speeds. Acceleration crest factor detect defects at the middle speed region but not at high and low speeds. Kurtosis detects defects at low bearing speeds. RMS was the best defect indicator of the three methods for inner ring defects. Acceleration RMS ratio gave good defect detection at high speeds but poor detection at lower speeds. Crest factor was effective for defect detection.

1.9 Gearbox condition monitoring

Loutas *et al.* (2009) considered condition monitoring on a single stage gearbox by artificially inducing gear damage and using vibration measurement and acoustic emission through the Internet. They laid emphasis on the signal processing of the vibration and acoustic emission signals received and used wavelet transform. It is concluded that acoustic emission measurement was a superior method over vibration measurement to detect early natural gear system wear. Their testing was done over 50 hours and the gear tooth was cut to simulate a tooth crack.

The setup consisted of a single stage gearbox with the gears running on ball-bearing shafts. The gearbox is driven by a three-phase electrical motor running at 1400 rpm. A single-phase generator with continuous power consumption was connected to the gearbox for load fluctuation. Two Bruel and Klaer acceleration meters were connected to the gearbox with a sampling frequency of 50 Hz and signal duration of 1 second were recorded. Three acoustic emission sensors were also installed at the gearbox. Their frequency response range was 100 to 800 kHz and they recorded signals continuously for 100 ms at a sampling rate of 2

MHz. A thermocouple measured the oil-bath temperature. The recordings of the sensors were done by National Instruments NI-6070 1MS/SEC FIREWIRE data acquisition device and Labview programming software assisted this.

It was their goal to get the most promising technique to use for damage detection on a gear system. More advanced signal processing techniques were used namely discrete wavelet transform which extracted wavelet based parameters from the signals. They compared the techniques capable of monitoring the damage. Frequency and time domain parameters for both the acoustic emission and vibration measurements were compared.

Kalaitszlou *et al.* (2009) concluded that they could see critical changes in the operation of the gearbox by looking at some of these parameters. The oil temperature was an important parameter in condition monitoring. Finally, acoustic emission was a better method to see early damage in gear systems than vibration measurements.

Arvani *et al.* (2007) looked at artificial neural network to do condition monitoring on a motorcycle gearbox. According to *Wikipedia,* an artificial neural network is a mathematical model where connections are used between inputs and outputs to solve a complex problem. An artificial neural network changes while running, which means that the structure changes during a learning phase. The artificial neural network is inspired by the neural networks in the brain.

The setup consisted of a four-speed motorcycle gearbox connected to an electrical motor running at 1400 rpm and a load mechanism applied a load to the gearbox. A multichannel pulse analyser system, a tri-axial acceleration meter, a tachometer and four shock absorbers was also part of the setup. The acceleration meter was mounted on the outer surface of the bearing case at the input shaft of the gearbox.

The test was done with ten different configurations and seven different fault conditions for every configuration were measured namely, slight worn, medium worn, broken gear teeth, three distinctive faulty bearing conditions and one faultless condition.

This study was done experimentally. Firstly, data of faulty conditions were acquired, then the data were processed with wavelet packet transform and finally the neural network was developed.

Arvani *et al.* (2007) concluded that the neural network identified the gear failures and detected the bearing defects 100% accurately.

Heyns and Stander (2000) investigated the detection of problems on a gearbox that had been used in coal mines under varying speeds and loads. On-line monitoring was a part of their research. The gearbox in question drove the cutting head of a continuous mining machine. The head cuts coal from the coal face and was under shock loads as it sheared coal from the face. As this equipment was working in such a high vibration environment it is difficult to monitor the state of the equipment from signals measured because of the noise. Gear monitoring techniques that were reviewed to remove noise and analyse the signals were:

- Time domain averaging (synchronous averaging)
- Amplitude and phase demodulation were used to enhance the defects in the signal.
- Short Time Fourier Transform is used to look for localised defects by looking at small sections of a signal or windows.
- Wavelet Analysis is used to enhance either the accuracy of the time resolution or the frequency resolution.
- Pattern recognition was implemented to show faults and how severe the faults were.
- Neural Networks or Artificial Neural Networks can be trained to help with failure and degradation recognition.

The work done by Heyns and Stander (2000) made it clear that at non-stationary load conditions it is more difficult to detect faults and monitor a gearbox.

The scenario explained above that included the coal cutter gearbox lead to the study by Heyns *et al.* (2001) on a gearbox working under fluctuating load conditions. A test rig was built with a gearbox on which fluctuating loads could be applied of up to 3 Hz. Three load functions were used namely, sinusoidal, step and chirp.

The experimental set-up consisted of a single-stage gearbox driven by a 5 HP Dodge Silicon Controlled Rectifier motor and a load was applied by a 5.5 kVA three phase alternator.

Four load conditions and three levels of damage were used to build a signal processing procedure that would be more sensitive to gear condition than to load fluctuation. An initial signal was measured with no damage. Face wear was induced by removing material from the gear face and a crack was simulated 180 degrees from the face wear position.

Heyns and Stander (2005) concluded that a gear under fluctuating load could be monitored if three things were provided for, namely, the fluctuation in machine speed, the input force that caused a response amplitude and the effects from amplitude and phase on the measured response.

They looked particularly at the effect of the transmission path phase and developed a method to resolve the influence that transmission path phase has on synchronous averaging. With adopting the new approach the rate of convergence improved significantly.

On-line vibration-monitoring systems are commercialised because of recent developments in the condition monitoring and asset management market according to Heyns and Stander (2005). These systems make use of conventional vibration monitoring methods which diagnose faults wrongly on gears working under fluctuating load. Heyns and Stander (2005) used instantaneous angular speed to monitor the condition of gears under fluctuating load. In their test it was seen that averaging done in the rotation domain will suppress the modulation from non-cyclic stationary load conditions, but not from cyclic conditions. It is possible to indicate a deteriorating gear fault condition.

1.10 Problem statement

The problem lies in the fact that industry often experiences unexpected failures at gearboxes used in production which sometimes results in large and unnecessary maintenance costs and occasionally extremely large production losses occur. This study must contribute to reduce these huge industrial problems by the development of a feasible, cost-effective, continuous condition-monitoring system.

A cost-effective condition-monitoring system for a gearbox needs to be developed. This continuous condition-monitoring system must measure vibration and temperature at short time intervals and these parameters must be used for early warnings when problems have started and increased over time when a gearbox is in service. In addition electrical current

must also be measured and changing power and torque then also determined for a gearbox subject to different operational loading conditions. Feasible hardware coupled to appropriate sensors and also coupled to a computer needs to be developed, built and thoroughly tested to ensure accuracy and reliability. A computer program must be written so that all the measured parameters are indicated. In addition, mathematical models need to be developed for vibration signal analysis and then be implemented in a computer program. The vibration signal analysis should be effective to clearly distinguish between ball bearing wear and wear on gear teeth for increasing stages of wear. Alarm settings must also be programmed for certain measured parameters. The measured parameters namely vibration, temperature, electrical current, power and torque must be made available on the Internet while the gearbox is running. A system that monitors the condition of a gearbox and which gives access to the real time measured monitored data of the gearbox via the Internet, must be developed.

In Chapter 2 mathematical models developed for this study are described. These models were implemented in computer programs and used to compute certain useful and relevant technical information as described in chapter 3.

2. Mathematical models

2.1 Introduction

Two different mathematical models were developed for this study. Part A was developed to allow gearbox defect computations, regarding bearings and gears inside the gearbox. Part B was developed for vibration signal construction, as well as for power and torque computations.

2.2 Part A: Gearbox-defect frequencies

Faults at bearings and gears are normally related to certain defect frequencies. These frequencies are described in Paragraphs 2.2.1 and 2.2.2. This was used for the development of a Matlab program for condition monitoring of the gearbox as described in Chapter 3. These frequencies were then used for the analysis as described in Chapter 5.

2.2.1 Bearing-defect frequencies

Ball rolling element type bearings are used in the gearbox. A bearing failure may occur for many reasons such as fatigue, poor lubrication, contamination, faulty mounting and careless handling. Fatigue is mainly influenced by the number of revolutions performed by the bearing, and the magnitude of the loads carried by the bearing, especially the dynamic fluctuating loads. Fatigue is the result of material stresses appearing immediately below the load carrying surface. When cracks form on the surface and grow into the material, surface distress is at hand. As the rolling elements pass over these cracks, fragments of material break away. This is known as spalling or flaking which progressively increases in extent, and the increase in damage eventually causes the bearing to become unusable. One of the reasons that vibration is measured on the bearing housings is that all the forced frequencies are transmitted through the bearings from the rotating element. These detectable forces as function of measured vibration responses are also at work degrading the life of the bearing. Degradation manifests itself in any of four ways, namely as damage to the outer race, damage to the inner race, damage to the rolling elements or damage to the bearing cage. Each of these four flaws will generate a specific frequency depending on the geometry and the shaft speed inside the bearing, which can be theoretically computed (Bloch & Geitner, 1997). These frequencies are known as bearing defect frequencies, and will appear in

frequency domain vibration signals at small amplitudes when spalling damage has started. With reference to Figure 2.1, the following characteristics of a specific bearing are needed to mathematically describe these bearing defect frequencies (Bloch & Geitner, 1997; Harris, 2010; Taylor, 2003):

- B_d = Rolling element diameter
- P_d = Pitch diameter
- N_b = Number of rolling elements
- θ = Contact angle
- S = running speed frequency of shaft at shaft at bearing

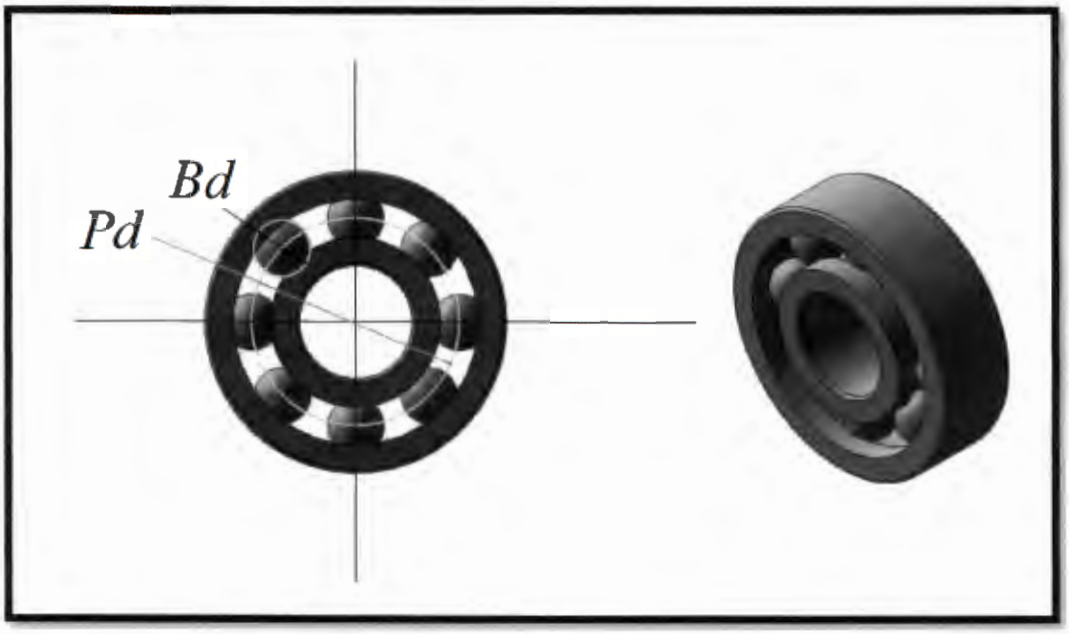

Figure 2.1: Ball roller element bearing illustration

As function of damage to the inner race, the Ball Pass Frequency Inner (BPFI) f_{bpi} is described as

$$f_{bpi} = \frac{Nb}{2} S[1 + (\frac{Bd}{Pd} \cos\theta)] \tag{2.1}$$

As function of damage to the outer race, the Ball Pass Frequency Outer (BPFO) f_{bpo} is described as

$$f_{bpo} = \frac{Nb}{2} S[1 - (\frac{Bd}{Pd} \cos\theta)] \tag{2.2}$$

As function of damage to the rolling ball, the Ball Spin Frequency (BSF) f_{bs} is described as

$$f_{bs} = \frac{Pd}{2Bd} S[1 - (\frac{Bd}{Pd}\cos\theta)^2] \tag{2.3}$$

As function of damage to the bearing cage, the Fundamental Train Frequency (FTF) f_{ft} is described as

$$f_{ft} = \frac{s}{2}[1 - (\frac{Bd}{Pd}\cos\theta)] \tag{2.4}$$

For all the ball bearings in the gearbox used in this study, the contact angle θ = 90° and then $\cos\theta$ = 1 in Equations (2.1) to (2.4). For increased damage at the bearing, harmonics (pure multiples) of these fundamental defect frequencies could appear in measured frequency domain signals.

2.2.2 Gear mesh frequencies

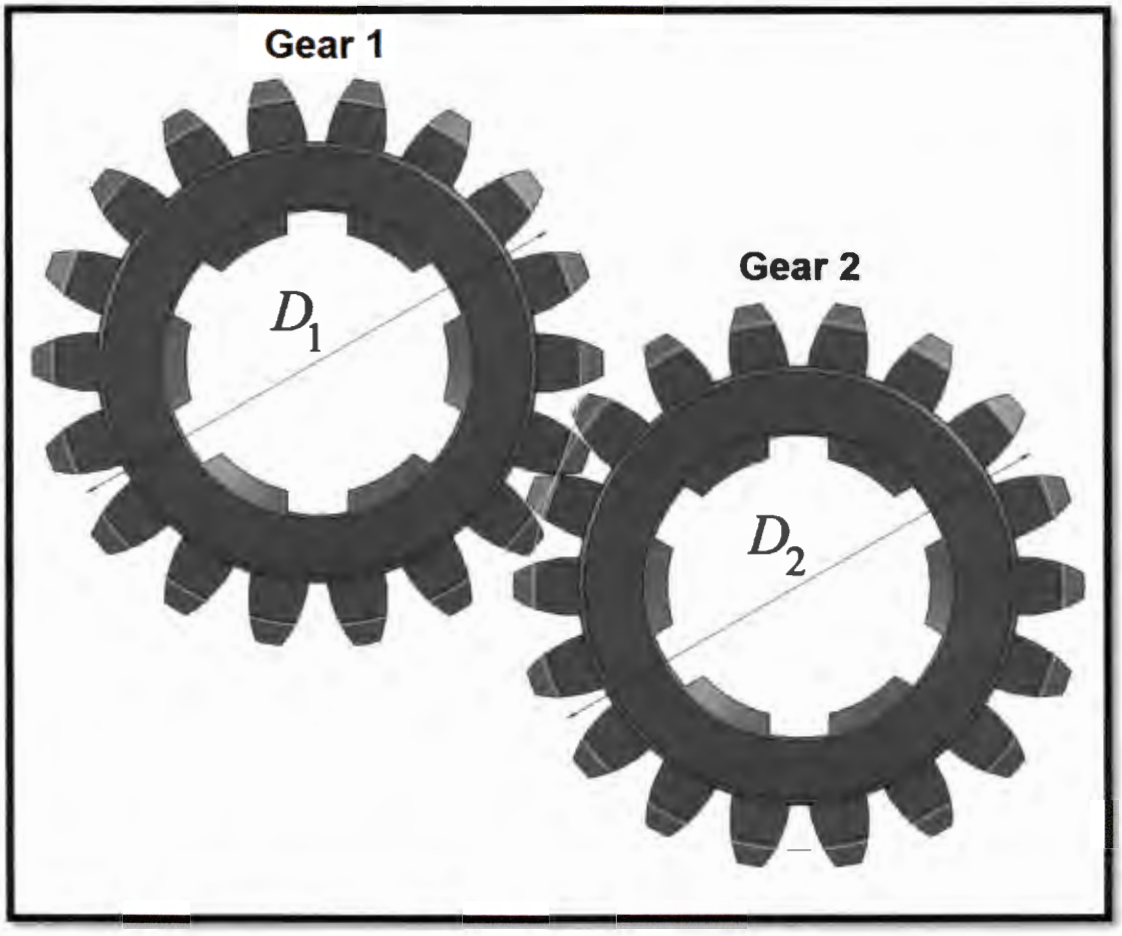

Figure 2.2: Schematic representation of gear pair 1 with Gear 1 and Gear 2

A gear pair comprising two gears normally generates a frequency related to the mesh of the gear teeth (Bloch & Geitner, 1997; Harris, 2010; Taylor, 2003), known as the gear mesh frequency and for the first gear pair in the gearbox used in the study f_{gm1} and is mathematically described as

$$f_{gm1} = f_1 t_1 = f_2 t_2 \tag{2.5}$$

where f_1 is the forced frequency of the shaft attached to Gear 1 with t_1 the number of teeth at Gear 1, and f_2 the forced frequency of the other shaft attached to Gear 2 with t_2 the number of teeth at Gear 2.

Similarly the gear mesh frequency and for the second gear pair in the gearbox used in the study f_{gm2} (see Chapter 4 Figure 4.3 for a schematic drawing of internal components) and is mathematically described as

$$f_{gm2} = f_3 t_3 = f_4 t_4 \tag{2.6}$$

where f_3 is the forced frequency of the shaft attached to Gear 3 with t_3 the number of teeth at Gear 3, and f_4 the forced frequency of the other shaft attached to Gear 4 with t_4 the number of teeth at Gear 4. For increased damage at the gear teeth or larger contact pressures at the teeth caused by misalignment, harmonics (pure multiples) of these fundamental gear mesh frequencies could appear in measured frequency domain signals.

For this gearbox

$$f_2 = f_3 \tag{2.7}$$

because Gear 2 and Gear 3 are both attached to the intermediate shaft (see Chapter 4 Figure 4.3 for a schematic drawing of internal components).

2.2.3 Gearbox reduction and shaft speeds

With reference to Figure 2.2, the frequency (speed) ratio for Gear 1 and Gear 2 of the first gear pair is given by

$$\frac{f_1}{f_2} = \frac{D_2}{D_1} = \frac{t_2}{t_1} \tag{2.8}$$

where f_1 is also the forced frequency (speed) of the input shaft attached to Gear 1 with D_1 the pitch diameter of Gear 1, where f_2 is also the forced frequency of the intermediate shaft attached to Gear 2 with D_2 the pitch diameter of Gear 2 (see Chapter 4, Figure 4.3 for a schematic drawing of internal components).

Similarly the frequency (speed) ratio for Gear 3 and Gear 4 of the first gear pair is given by

$$\frac{f_3}{f_4} = \frac{D_4}{D_3} = \frac{t_4}{t_3} \tag{2.9}$$

where D_3 is the pitch diameter of Gear 3, and f_4 is also the forced frequency of the output shaft attached to Gear 4 with D_4 the pitch diameter of Gear 4 (see Chapter 4 Figure 4.3 for a schematic drawing of internal components).

The total gear ratio g_r of this reduction gearbox is

$$g_r = \frac{f_1}{f_4} \tag{2.10}$$

2.3 Part B: Vibration signal constructions, power and torque

Part B was developed to allow vibration signal constructions during the vibration measurement phase of the work. The data acquisition for vibration in the experimental work provided acceleration data as a function of time. Time and frequency domain signals are needed to be constructed. In Paragraph 2.3.1 the underlying mathematics for these signals including the Fourier analysis and also the conversion of data from the time domain to the frequency domain are described. This was used for the development of a Matlab program for condition monitoring of the gearbox as described in Chapter 3. In addition power and torque computations for the gearbox are also described in Paragraph 2.3.2 because it is used in the same Matlab program based on data acquisition of electrical current measurements. The data acquisition system is described in Chapter 4, and the measured data obtained described in Chapter 5.

2.3.1 Vibration signal construction

If $\ddot{x}(t)$ is a periodic function for acceleration $\ddot{x}$ at time t with period T (Ewins, 2000; Rao, 2011), its Fourier series representation is given by

$$\ddot{x}(t) = \frac{a_0}{2} + \sum_{n=1}^{\infty} (a_n \cos \omega_n t + b_n \sin \omega_n t) \tag{2.11}$$

where ω_n is the frequency expressed in terms of the period T as

$$\omega_n = \frac{2\pi n}{T} \tag{2.12}$$

and where a_0, a_1, a_2, ..., a_n, b_1, b_2, ..., b_n are constant coefficients.

It can be shown (Ewins, 2000; Rao, 2011) that these constant coefficients can be expressed as follows:

$$a_0 = \frac{2}{T} \int_0^T \ddot{x}(t) dt \tag{2.13}$$

$$a_n = \frac{2}{T} \int_0^T \ddot{x}(t) \cos \omega_n t dt \tag{2.14}$$

$$b_n = \frac{2}{T} \int_0^T \ddot{x}(t) \cos \omega_n t dt \tag{2.15}$$

The harmonic function can alternatively (Ewins, 2000) also be expressed as

$$\ddot{x}(t) = c_0 + \sum_{n=1}^{\infty} c_n \cos(\omega_n t + \phi_n) \tag{2.16}$$

where c_0 and c_n are alternative constant coefficients with c_n expressed as the Pythagoras's component

$$c_n = \sqrt{a_n^2 + b_n^2} \tag{2.17}$$

The phase angle ϕ_n of the triangle is

$$\phi_n = \tan^{-1}\left(-\frac{b_n}{a_n}\right) \tag{2.18}$$

Alternatively, (Ewins, 2000) the periodic function could also be expressed in terms of acceleration amplitude $\ddot{X}_n$ in Fourier analysis as

$$\ddot{x}(t) = \sum_{-\infty}^{\infty} \ddot{X}_n e^{i\omega_n t} \tag{2.19}$$

where $i = \sqrt{-1}$ in the complex notation, where

$$\ddot{X}_n = \frac{1}{T}\int_0^T \ddot{x}(t) e^{-i\omega_n t}\, dt \tag{2.20}$$

When $\ddot{x}(t)$ is Fourier analysed, then the acceleration Fourier coefficients comprise a series of *m* sinusoidal acceleration amplitudes $\ddot{X}_n$ with corresponding frequencies ω_n and phase angles $\phi_{an,n=1,2,..m}$ where the time domain acceleration data is converted to frequency domain data (Heyns *et al.* 1994; Nel, 2000; Nel, 2007; Nel, 2009).

The series of *m* sinusoidal acceleration amplitudes could be described as a series of sinusoidal velocity amplitudes

$$\dot{X}_n = \frac{\ddot{X}_n}{\omega_n} \tag{2.21}$$

But each of the phase angles ϕ_{vn} for these velocity amplitudes of the series each lag by $\frac{\pi}{2}$ radians compared to corresponding phase angles ϕ_{an} for acceleration (Rao, 2011).

For a series of *m* sinusoidal acceleration amplitudes could also be described as a series of sinusoidal displacement amplitudes, where

$$X_n = \frac{\ddot{X}_n}{\omega_n^2} \tag{2.22}$$

The phase angles ϕ_{dn} for these displacement amplitudes of the series each lag by π radians compared to corresponding phase angles ϕ_{an} for acceleration (Rao, 2011).

By using each of the Fourier coefficients for acceleration, the corresponding acceleration as function of time (Ewins, 2000; Heyns *et al.* 1994; Nel, 2000; Nel, 2007; Nel, 2009), can be expressed as

$$\ddot{x}(t) = \sum_{n=1}^{m} \ddot{X}_n \cos(\omega_n t + \phi_{an}) \tag{2.23}$$

Similarly by using each of the Fourier coefficients for velocity, the corresponding velocity as a function of time can be expressed as

$$\dot{x}(t) = \sum_{n=1}^{m} \dot{X}_n \cos(\omega_n t + \phi_{vn}) \tag{2.24}$$

Similarly by using each of the Fourier coefficients for displacement, the corresponding displacement as function of time, can be expressed as

$$x(t) = \sum_{n=1}^{m} X_n \cos(\omega_n t + \phi_{dn}) \tag{2.25}$$

2.3.2 Power and torque calculations

For the electrical current I through one of the power supply lines, with V the potential difference between two supply lines, F the electrical power factor, and η the efficiency, then the electrical power (Nilsson, 2011) as consumed by the three-phase electrical motor at the gearbox is

$$P = IV\sqrt{3}F\eta \tag{2.26}$$

The torque at the input shaft is

$$\mathrm{T} = \frac{60P}{2\pi N} \tag{2.27}$$

where N is the speed of the input shaft.

These mathematical models were implemented in computer programs as described in Chapter 3. Useful and relevant technical information for condition monitoring could then be computed as explained in Chapter 3.

3. Computer implementation

3.1 Introduction

Two different computer programs were developed for this study. Program A was developed to allow gearbox defect computations regarding bearings and gears inside the gearbox. Program A is based on Part A of the mathematical models presented in Chapter 2. Program B was developed for vibration signal construction, as well as for power and torque computations. Program B is based on Part B of the mathematical models presented in Chapter 2.

3.2 Program A: Gearbox-defect frequencies

Faults at bearings and gears are normally related to certain defect frequencies. These frequencies are described in Paragraphs 2.2.1 and 2.2.2 of Chapter 2. The magnitudes of the different bearing defect frequencies for all six bearings at the gearbox, and also the magnitudes of the gear mesh frequencies for the two different gear pairs inside the gearbox were computed based on the equations described in Chapter 2. These computations were done in a Matlab environment (Matlab version 2014a) by Program A. The magnitudes of the bearing defect frequencies and also the gear mesh frequencies for the gearbox are indicated in Chapter 4. The Matlab code for Program A is included in Appendix D.

3.3 Program B: Vibration signal constructions, power and torque

Program B was developed in a Matlab environment (Matlab version 2014a) to allow vibration signal constructions during the vibration measurement phase of the work. The instrumentation hardware described in detail in Chapter 4 provided measured data regarding vibration, temperature and electrical current. All these measured parameters were captured in Program B. This was done by using the data acquisition sub-routine of Matlab located in the Data Acquisition Toolbox (DAQ), which interacted with the National Instruments (NI) software (Measurement and Automation Explorer) that was supplied with the National Instruments hardware. More information regarding the Measurement and Automation Explorer supplied by NI is described in Paragraph 3.4. More information regarding the Data-Acquisition Toolbox (DAQ) is described in Paragraph 3.5. Trends for vibration, temperature and electrical current were constructed. The measured electrical

current magnitudes were used to do computations regarding power and torque with mathematical equations presented in Chapter 2, Paragraph 2.3.2. Computations for power and torque trends were also done in Program B. These trends were shown in graphs by using the graphical capabilities of Matlab.

The data acquisition for vibration in the experimental work provided acceleration data as function of time. Vibration acceleration time domain data were captured and time domain signals constructed in Program B for the four acceleration meters attached to the gearbox (see also Chapter 4, Figures 4.9, 4.18 and 4.19). Corresponding frequency domain signals were then also constructed in Program B based on the mathematical model presented in Chapter 2, Paragraph 2.3.1. The underlying mathematics for these signals, including the Fourier analysis for the conversion of measured acceleration data from the time domain to the frequency domain, were also implemented in Program B. The Matlab built-in function *fft.m* located in the Signal Control Toolbox was used for Fourier transform. In addition, acceleration signals were converted to corresponding velocity and displacement signals. Time and frequency domain signals were thus constructed in Program B for acceleration, velocity and displacement. These signals were shown in graphs by using the graphical capabilities of Matlab. Three-dimensional representations of measured frequency domain vibration data were also constructed by using Matlab's extensive graphical capabilities (see Chapter 5).

Program B made provision for time settings to allow that these trends and signals could be updated sequentially with updated measured data as obtained from the continuous condition-monitoring system. In this study the time setting of 30 minutes was used in the experimental phase of the work (see Chapter 5 and Table 5.1 for more details regarding the 48-hour test).

Program B is based on a 'for' loop running for a certain number of iterations. The number of iterations indicates the number of different data-sets at this program based on information obtained from each of the sensors at the gearbox. A matrix was created in the program for the output data based on measured magnitudes at a specific time, to allow 17 different trends for 17 different measured parameters. This matrix with 18 columns and a number of rows that corresponds to the number of iterations, contained information as indicated in

Table 3.1. Note that the specific time is located in Column 9, while the other 17 columns were allocated for the different output parameters that corresponded to this time. Also note that abbreviations were used for the different overall vibration parameters are indicated in Columns 10 to 17. These abbreviations are related to type of response, position and direction and explained in Chapter 5, Paragraph 5.1. For the 48-hour test as described in Chapter 5, the total number of iterations was 96, based on measured data indicated in Table 3.1 collected every half an hour.

Table 3.1 Data matrix layout

Column	Data type (Row)
1	Temperature Input shaft
2	Temperature Intermediate shaft
3	Temperature Output shaft
4	Temperature of oil
5	RMS current @ Line 1
6	Power
7	Torque
8	% of full load
9	Time of measurement
10	Vibration RMS Xdotdot IV
11	Vibration RMS Xdot IV
12	Vibration RMS Xdotdot IH
13	Vibration RMS Xdot IH
14	Vibration RMS Xdotdot OV
15	Vibration RMS Xdot OV
16	Vibration RMS Xdotdot OH
17	Vibration RMS Xdot OH
18	RMS current @ Line 2

For each of these iterations, the data indicated in Table 3.1 are saved in a folder so that it could be used at a later stage if necessary.

The data indicated in Table 3.1 are obtained from three different sessions created in Program B. A session is created for each module so that data could be captured through the different sensors (also see Chapter 4 for more detail regarding the different modules and sensors). The session was closed directly after the data had been captured.

The first session was created for data through each of the four thermocouples connected to the NI 9211 module for temperature measurements. A single scan took 0.2 seconds to capture a single temperature value on each channel. The second session was created for data through two channels at the NI 9234 module for current measurements. A single scan also took 0.2 seconds to capture a current value. The third session was created for data through four input channels at the NI 9234 module for vibration measurements. Data was measured for 5 seconds at a sample rate of 25 000 scans per second. This resulted in a wide frequency range and a small frequency interval. Each vibration measurement was stored in a special matrix with five columns, one for each channel and one for time, and the number of rows corresponded to the sample rate multiplied by the duration of one signal. This matrix contained acceleration as function of time data. All these data are stored in the computer system's memory. The data are then used for computations and construction of signals and presented as graphs as displayed at two output screens (see Chapter 5, Figures 5.12 to 5.13 for examples of these output screens). The graphs at the two output screens were updated for every iteration.

These data are saved for that current date and time and used for the name of the file, at every iteration. These data could then be imported for construction of graphs at a later stage if so required.

Alarm settings were also programmed when certain measured parameters reached certain magnitudes. These parameters include vibration, power and temperature.

The Matlab code for Program B is included in Appendix E.

3.4 Measurement and Automation Explorer (supplied by NI)

Program B in a Matlab environment as described in Paragraph 3.3 interacted with the National Instruments (NI) software (Measurement and Automation Explorer) that were supplied with the National Instruments hardware. Alternatively it could be downloaded or updated from the NI-website. With this software all drivers for NI hardware could be installed. It is important that the latest version be used to avoid hardware synchronization problems. These drivers made it possible for National Instruments data acquisition devices to connect to the laptop. A new NI cDAQ 9188 chassis as a data-acquisition device was

automatically connected to the software platform. This made the interaction and control between Matlab and this data acquisition device possible.

The connection of instrumentation hardware devices to NI Measurement and Automation Explorer software are described in Paragraph 4.8.

3.5 Matlab Data Acquisition Toolbox (DAQ)

The Data Acquisition Toolbox in Matlab provided functions for connection to Matlab through data acquisition devices (NI modules, see also Chapter 4). The connection between Matlab and the NI hardware is activated with Matlab commands programmed in Program B, which then interacted with the data-acquisition toolbox of Matlab.

Matlab has two possible data-acquisition interfaces:

- Legacy-based interface
- Session-based interface

The legacy-based interface could only operate with a Windows 32-bit computer operating system. The NI cDAQ 9188 chassis is, however, session-based. The session-based interface could operate on both Windows 32-bit and Windows 64-bit operating systems. The laptop used in the study was, however, equipped with a Windows 64-bit operating system and was selected because it was faster.

An object is created and used to call the Matlab function at the DAQ toolbox to do a certain task. The following Matlab code in Program B was used to create a session for the hardware:

```
s = daq.createSession('ni')
```

When a session is created, a connection between Matlab and the data-acquisition hardware is activated, and data acquisition tasks could be done with the hardware during the session.

The following Matlab code in Program B was used to describe the chassis with module for 4 channels (0 to 3) to which acceleration meters were connected:

```
s.addAnalogInputChannel( 'cDAQ9188-16D666AMod1',0:3,'Accelerometer');
```

The following Matlab code in Program B was used to end the session for the hardware:

s = 0

This command code disconnects the link between the device and Matlab.

Certain parameters, for example the number of channels, type of input, sample rate and duration of the data-acquisition session could also be set in the Matlab program code. More information is included in Program B (see Appendix E).

The connection of instrumentation hardware devices to Matlab is described in Paragraph 4.9.

3.6 TeamViewer

One of the objectives in this research project was that condition monitoring of the gearbox should be done via the Internet. In the laboratory one laptop was used and linked to instrumentation for measurements and also to the Internet as described in Chapter 4 (also see Figure 4.9). For a remote connection to this laptop located in the laboratory, another laptop away from the laboratory was used. Special software known as TeamViewer was obtained and downloaded from the TeamViewer website. This software is free of charge when not commercially used. The TeamViewer software was installed on the remote computer and also on the host computer. TeamViewer created an ID number and a password for each of the two computers (the laptop in the laboratory and the other laptop away from the laboratory). These ID numbers will remain the same for each of the two computers respectively, but the Passwords will be changed at each of these computers respectively by TeamViewer, every time when TeamViewer is opened. The ID number and the Password allocated by TeamViewer to the laptop in the laboratory as the Partner ID are then used at the laptop away from the laboratory in the TeamViewer software. A TeamViewer window with information is observed at the host computer screen as shown in Figure 3.1. When TeamViewer is opened at the host computer, the ID number and the Password as automatically allocated to the host computer is indicated in the TeamViewer window as shown in Figure 3.1. At this point in time TeamViewer should also be opened at the remote computer. The partner ID number allocated to the remote computer by TeamViewer must be known and also typed in at the host computer (see Figure 3.1). When the "Connect to partner" button is selected with the click of the mouse, a second window will appear on the host computer screen. At this screen the Password for the remote

computer must also be known and typed in, and the "Connect" option then also selected with the mouse. The screen of the remote computer will then automatically appear at the screen of the host computer. Access to the remote computer will then become possible through the host computer. The remote computer could then be controlled from any host computer connected to the Internet, even located in another country. This made condition monitoring of a rotating machine possible via the Internet.

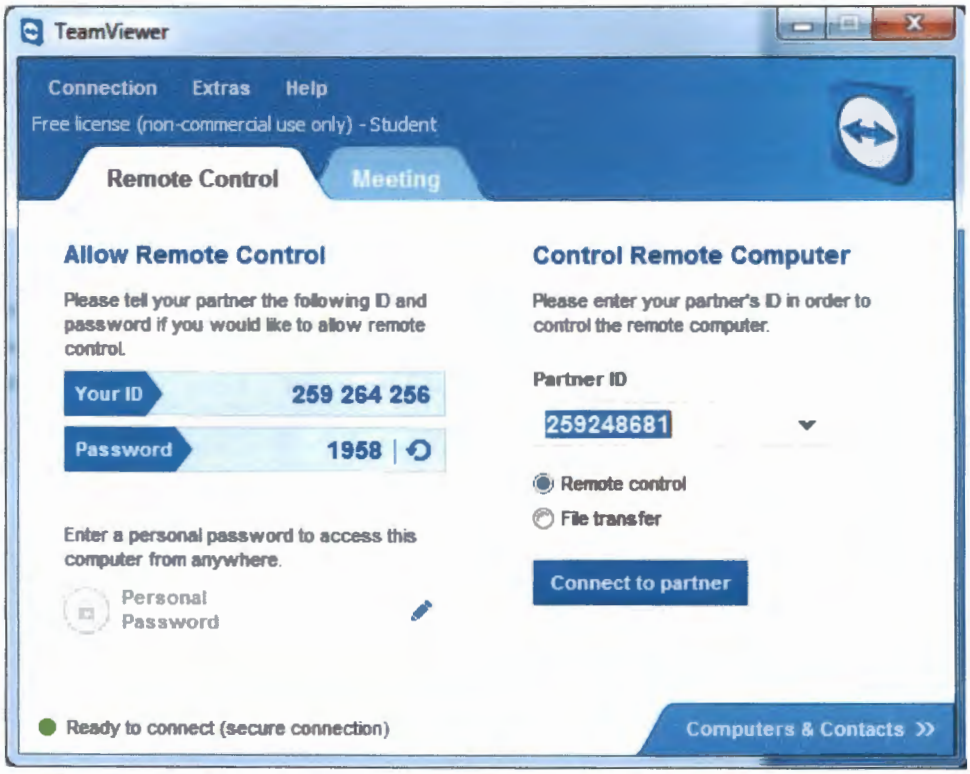

Figure 3.1: TeamViewer screen at the host computer to control the remote computer

All the input parameters used at these computer programs were characterised as described in Chapter 4. The test setup for the experimental phase in the laboratory and all equipment used during the study are also described in Chapter 4. The output data of the computer programs are indicated in Chapters 4 and 5.

4. Experimental characterization

4.1 Introduction

The characteristics of all the hardware at the test set-up are described in Chapter 4. A gearbox and motor were used and are shown in Figure 4.1.

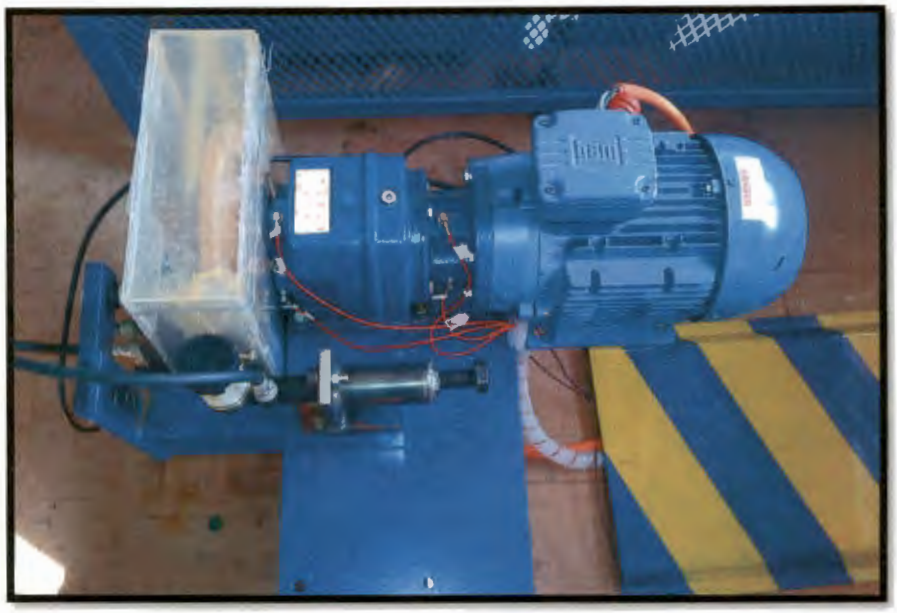

Figure 4.1: Gearbox assembly test setup

4.2 Gearbox linked to electrical motor

The gearbox supplier Dawid Brown donated the gearbox used for this study. The Radicon gearbox with model number MO2225.OBGCE1 and the specifications for this model number indicated are shown in Figure 4.2. The gearbox characteristics were available on the Radicon web page. The gearbox dimensions are shown in Appendix A.

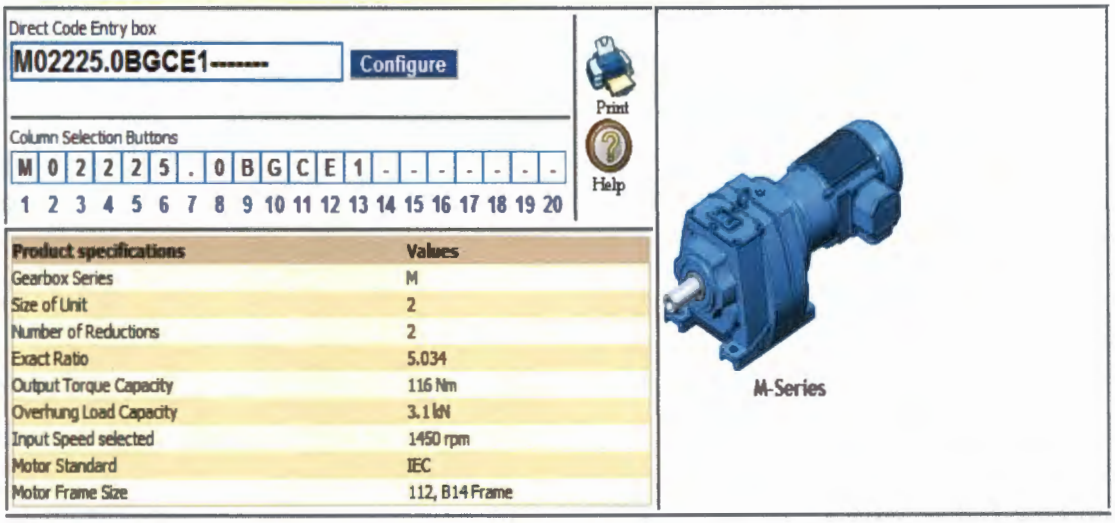

Figure 4.2: The specifications of the gearbox linked to an electrical motor

A schematic drawing of the internal components of the gearbox is shown in Figure 4.3.

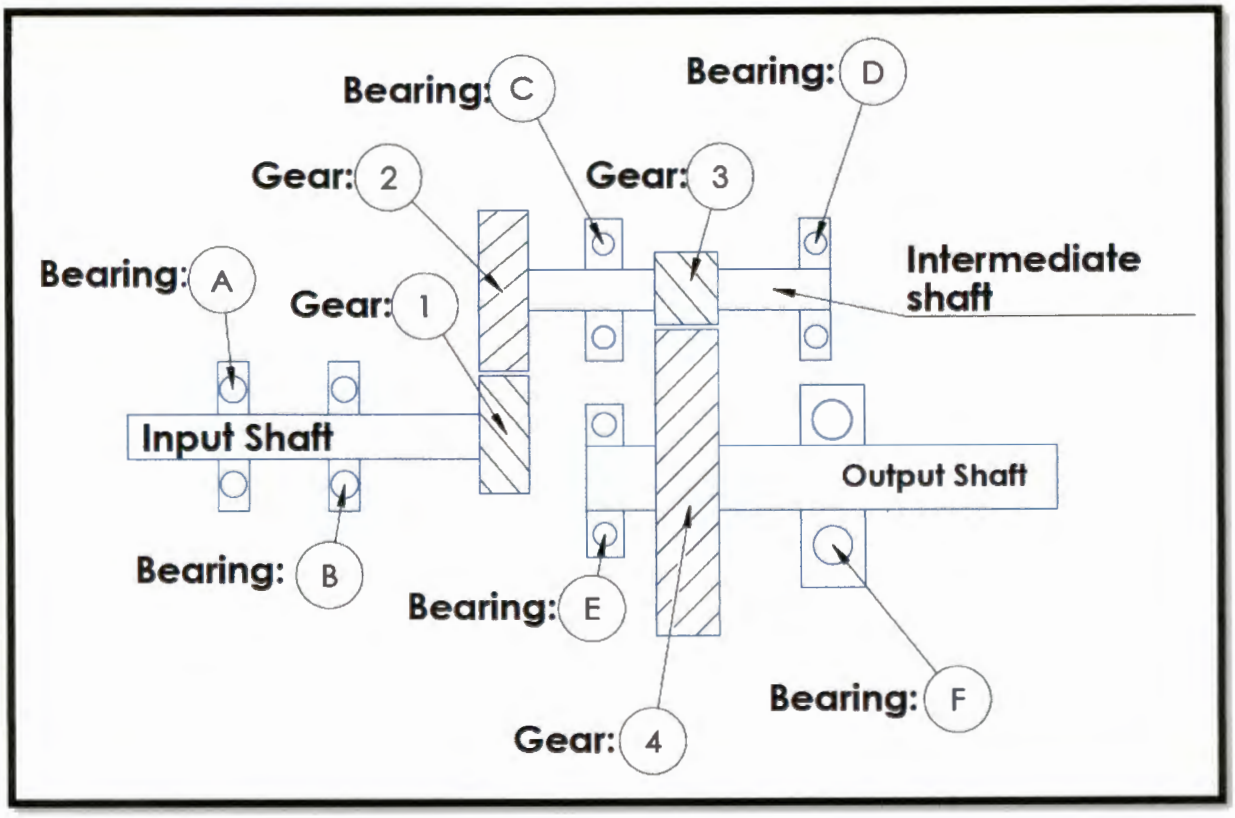

Figure 4.3: Schematic drawing of internal components of gearbox

Table 4.1: Bearing characteristics

Bearing:	Bearing number	Number of rollers [*Nb*]	Roller diameter [*Bd*] (mm)	Pitch diameter [*Pd*] (mm)
A	6008/2RS1-C3	12	7.94	54
B	6205-2RS1-C3	9	7.94	39.04
C	6202/C3	8	6	25.26
D	6202/C3	8	6	25.26
E	6005/C3	10	6.75	36
F	6206-2Z/C3	9	9.52	46

The bearing geometric characteristics were provided by SKF and indicated in Table 4.1 for Bearing A, B, C, D, E, and F (see also Figure 4.3).

The number of gear teeth for Gear 1, 2, 3, and 4 (see also Figure 4.3) was unfortunately not available at the Radicon website, but they were counted and indicated in Table 4.2.

Table 4.2: Number of gear teeth

Gear	Teeth
1	39
2	44
3	13
4	58

The reduction ratios were computed by using the number of teeth for the four different gears as indicated in Table 4.2. The three different shaft speeds were then computed as indicated in Table 4.4. The total reduction ratio corresponds to the value indicated in Figure 4.2 as obtained from the manufacturer and also indicated in Table 4.3.

Table 4.3: Gear reductions ratios

First reduction	1.12:1
Second reduction	4.46:1
Total reduction	5.034:1

The three different shaft speeds were then computed as indicated in Table 4.4.

Table 4.4: Gearbox shaft speeds

	[rpm]	[Hz]
Input shaft speed	1496.0	24.93
Intermediate shaft speed	1326.0	22.10
Output shaft speed	297.2	4.95

The gear-mesh frequencies for gear pair 1 as computed by Equation (2.5) in Chapter 2, and gear pair 2 as computed are indicated in Tables 4.5 and 4.6.

Table 4.5: Gear mesh frequencies of gear pair 1 with 5 harmonics.

f_{gm1}	[Hz]
X1	972.4
X 2	1944.8
X 3	2917.2
X 4	3889.6
X 5	4862.0
X 6	5834.4

Table 4.6: Gear mesh frequencies of gear pair 2 with 5 harmonics

f_{gm2}	[Hz]
X1	287.3
X 2	574.6
X 3	861.9
X 4	1149.2
X 5	1436.5
X 6	1723.8

In Table 4.7 the fundamental train frequency is labelled as f_{ft} and is the frequency of rotation of the cage computed by using Equation (2.4) as indicated in Chapter 2. The ball-pass frequency on the outer race is labelled as f_{bpo} and was computed by using Equation (2.2) while the frequency for the inner race, labelled as f_{bpi}, was computed by using Equation (2.1). The ball spin frequency which is labelled as f_{bs} was computed by using Equation (2.3). Harmonics as computed are pure multitudes of these fundamental frequencies. The computed magnitudes of the different bearing defect frequencies are indicated in Table 4.7.

Table 4.7: Bearing defect frequencies with 5 harmonics

Bearing:	Number:		f_{ft}	f_{bpo}	f_{bpi}	f_{bs}
A	6008/2RS1-C3	X 1	10.6	127.6	171.6	83.0
		X 2	21.3	255.3	343.3	165.9
		X 3	31.9	382.9	514.9	248.9
		X 4	42.5	510.5	686.5	331.9
		X 5	53.2	638.1	858.2	414.9
		X 6	63.8	765.8	1029.8	497.8
B	6205-2RS1-C3	X1	9.9	89.4	135.1	58.8
		X 2	19.9	178.8	270.1	117.6
		X 3	29.8	268.2	405.1	176.3
		X 4	39.7	357.6	540.2	235.1
		X 5	49.7	447.0	675.2	293.9
		X 6	59.6	536.4	810.3	352.6
C	6202/C3	X1	8.4	67.4	109.4	12.8
		X 2	16.9	134.8	218.8	25.5
		X 3	25.3	202.3	328.3	38.2
		X 4	33.7	269.7	437.7	51.0
		X 5	42.1	337.1	547.1	63.7
		X 6	50.6	404.5	656.5	76.5
D	6202/C3	X1	8.4	67.4	109.4	12.8
		X 2	16.9	134.8	218.8	25.5
		X 3	25.3	202.3	328.3	38.2
		X 4	33.7	269.7	437.7	51.0
		X 5	42.1	337.1	547.1	63.7
		X 6	50.6	404.5	656.5	76.5
E	6005/C3	X1	2.0	20.1	29.4	12.8
		X 2	4.0	40.3	58.8	25.6
		X 3	6.0	60.4	88.3	38.3
		X 4	8.1	80.5	117.7	51.1
		X 5	10.1	100.6	147.1	63.9
		X 6	12.1	120.8	176.5	76.7
F	6206-2Z/C3	X1	2.0	17.7	26.9	11.5
		X 2	3.9	35.4	53.8	22.9
		X 3	5.9	53.0	80.7	34.4
		X 4	7.9	70.7	107.6	45.8
		X 5	9.8	88.4	134.6	57.3
		X 6	11.8	106.1	161.5	68.7

4.3 Electrical motor

A three-phase, Weg, 3 kW, IEC standard electrical motor was also donated by Dawid Brown. The motor shown in Figure 4.4 was connected in delta to the electrical power supply.

Figure 4.4: The Weg three phase electrical motor

The motor characteristics indicated at the specification plate at the motor are shown in Table 4.8. The actual motor speed was measured as 1500 RPM and not 1410 RPM as indicated on the plate. The accurate input speed was very important as an input parameter used for the computation of bearing defect frequency and also gear mesh frequency values used for the vibration analysis.

Table 4.8: Motor characteristics indicated at specification plate

Motor characteristics: 3 kW			
Voltage [V]	**RPM**	**Current [Amp]**	**PF**
380	1410	6.63	0.84

The starter box was connected and set to trip at 6 amp to provide a safe overload. The full load current of 6.63 amp as well as the power factor of 0.84 was used to compute the electrical power. It was then found that the mechanical efficiency of 81.8% provided the maximum power of 3 kW as indicated in Table 4.8 (see Chapter 2 regarding the mathematical equation used). This procedure was performed by the computer program developed when electrical current magnitudes were measured, and power, torque and also % of full load magnitudes computed for condition monitoring.

4.4 Dynamometer

It was necessary to load the gearbox during testing to evaluate measured parameters of the condition-monitoring system. A brake system was designed and built to apply load at the gearbox output shaft as dynamometer. The design consisted of a Mazda Sting front disc brake assembly that was modified to fit to the gearbox output shaft as shown in Figure 4.5. A new calliper bracket designed was manufactured by the NWU mechanical engineering workshop. The hydraulic system shown in Figure 4.6 comprised an Isuzu motor vehicle clutch master cylinder and designed to be loaded with a threaded rod. This then applied a load on the piston inside of the calliper at the brake. When the rod was turned in by hand, the fluid inside the cylinder compressed and the calliper piston increased the pressure applied to the disc brake. This brake system provided sufficient power at the gearbox in the laboratory.

Figure 4.5: Brake calliper and its bracket at gearbox

After tests to obtain constant load had been done, it was found that the brake master cylinder was unable to provide a constant load after only a few seconds during a test done. The reason for this was that the rubber o-ring at the master cylinder failed in a short time under the high pressure as applied. This problem was overcome with the use of an electrical

hydraulic power pack that was linked with rubber pipes to the calliper for replacement of the initial master cylinder. This provided a constant load for a long time which was effective for evaluation of measured parameters of the condition-monitoring system. The master cylinder is shown in Figure 4.6 and the hydraulic power pack is shown in Figure 4.7.

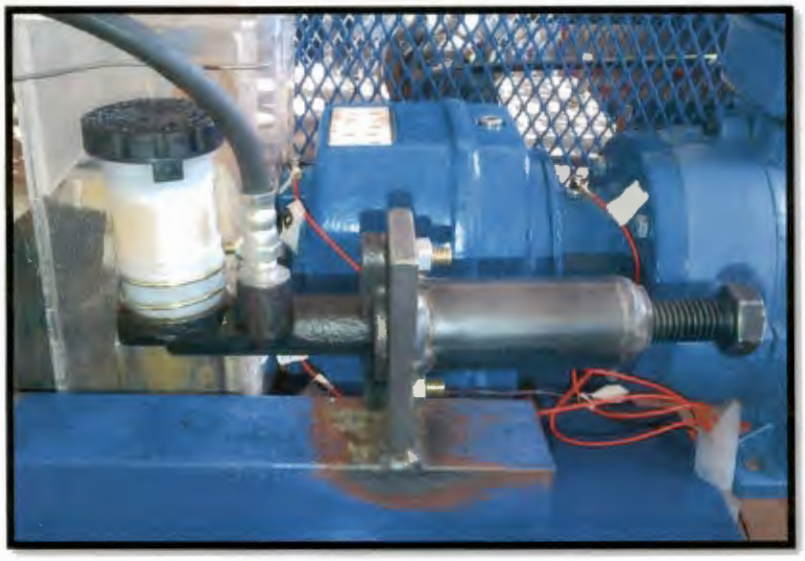

Figure 4.6: The hydraulic master cylinder

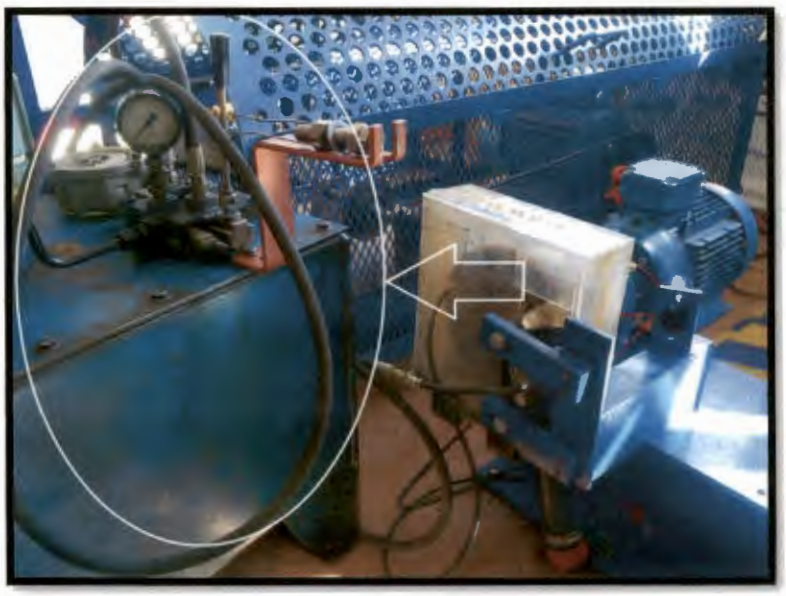

Figure 4.7: The hydraulic power pack

Effective cooling of the brake system was done by cold water supplied from a tap at a feasible flow rate and sprayed directly on the brake disc. The heated water flowed directly

into a nearby drain. Nozzles and a water cover box were installed as shown in Figure 4.8. Normal brake pads were used.

Figure 4.8: Cooling system and outlet water pipe

4.5 The data acquisition and Internet setup

The condition-monitoring system was designed as a remote Internet-accessible system. A schematic diagram for the condition-monitoring system hardware layout is shown in Figure 4.9. All the different instrumentation components and the laptop as indicated in Figure 4.9 are described in the following Paragraphs of this Chapter.

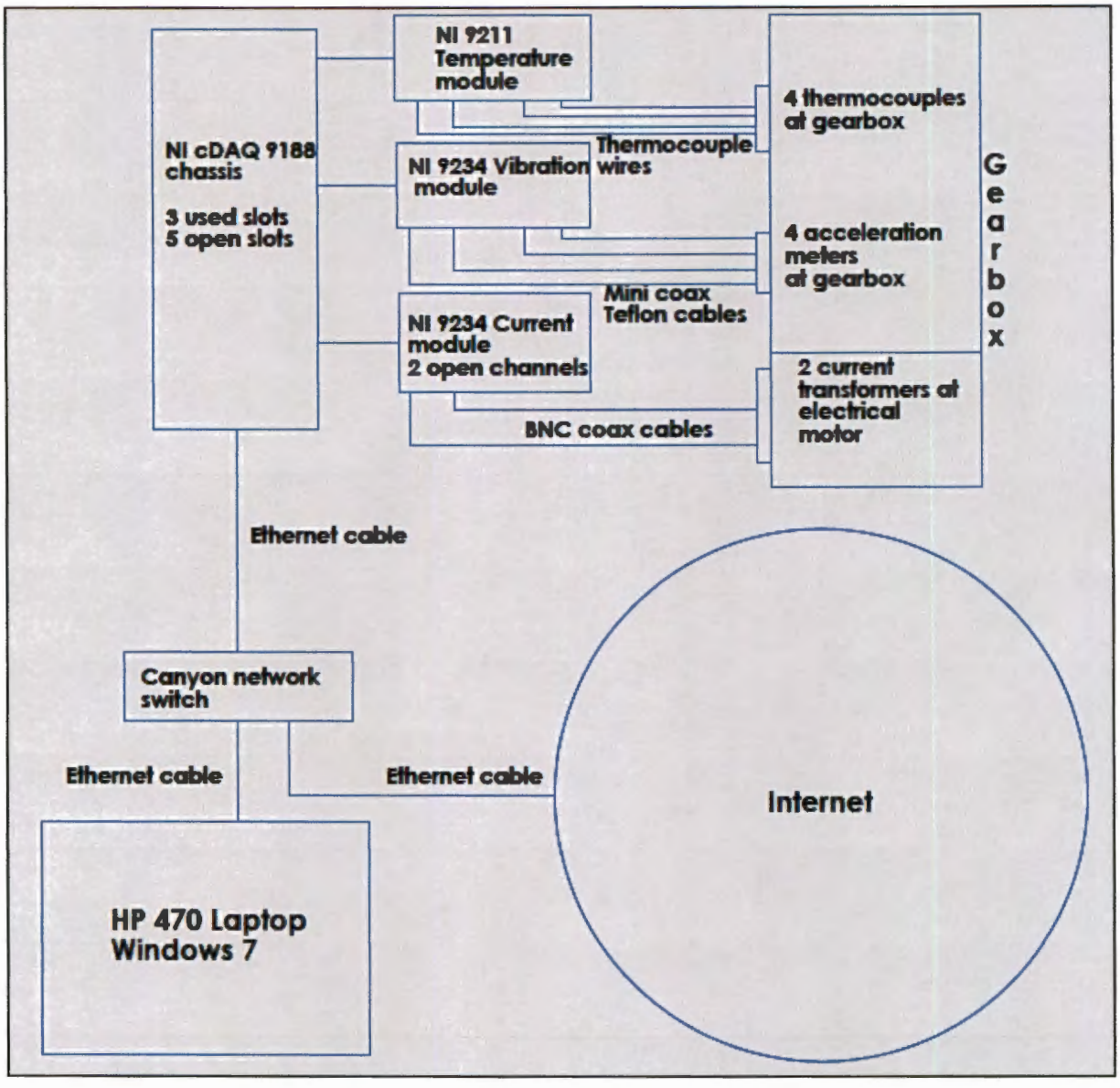

Figure 4.9: Schematic diagram of the condition-monitoring system hardware layout

4.6 The laptop, NI hardware and Canyon network switch

A safe was used to locate and store all the electrical instrumentation equipment and the laptop at the gearbox in the laboratory as shown in Figure 4.10.

Figure 4.10: The laptop, NI hardware and Canyon network switch inside the safe

4.6.1 Laptop

A powerful laptop was used on site for fast data-acquisition and analysis. The HP Probook 470 was used. The laptop had a quad core I7 2.2 GHz processor with a 6 Mb cache memory and 8 GB of RAM working with the Windows 7 operating system. An important aspect of this system was the software used for signal capturing and analysis in a Matlab environment and a fast computer was required.

4.6.2 The National Instruments (NI) hardware

The National Instruments (NI) data-acquisition system was used. Three important parameters were measured with sensors at the gearbox and were collected through the NI hardware. The three measured parameters were vibration with acceleration meters, temperature with thermocouples and current with current transformers. The layout of components is indicated in the hardware diagram shown in Figure 4.9.

4.6.3 The NI cDAQ 9188 chassis for NI modules

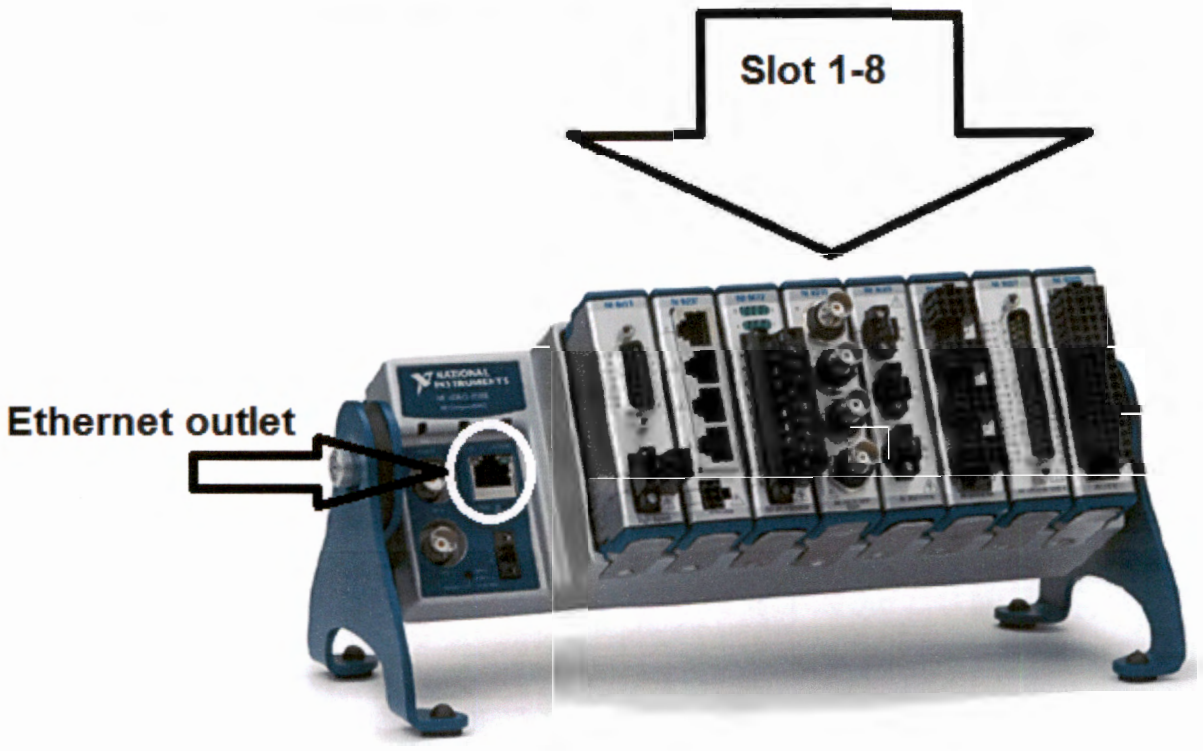

Figure 4.11: The NI cDAQ 9188 chassis

The NI compactDAQ 9188 eight-slot Ethernet chassis was used to locate and power the three modules as chosen for certain measurements as shown in Figure 4.11 (see also Figure 4.9). The three modules clipped into the chassis at slot 1 to 3. Five empty slots on the chassis remained open. Slot 1 contained the NI 9211 module for temperature, slot 2 contained the NI 9234 module for vibration measurements, and slot 3 contained the NI 9234 module for current measurements (see Paragraphs 4.6.4 and 4.6.5). The chassis powered the modules and connected to the computer via a Canyon network switch with an Ethernet cable (see Paragraph 4.6.6).

4.6.4 The NI 9211 module for temperature measurements

The NI 9211 module was chosen for temperature measurement and thermocouples coupled to this module as the input sensors (see also Figure 4.9). Four National Instruments type "J" thermocouples were used for the temperature measurements (see Paragraph 4.7.2).

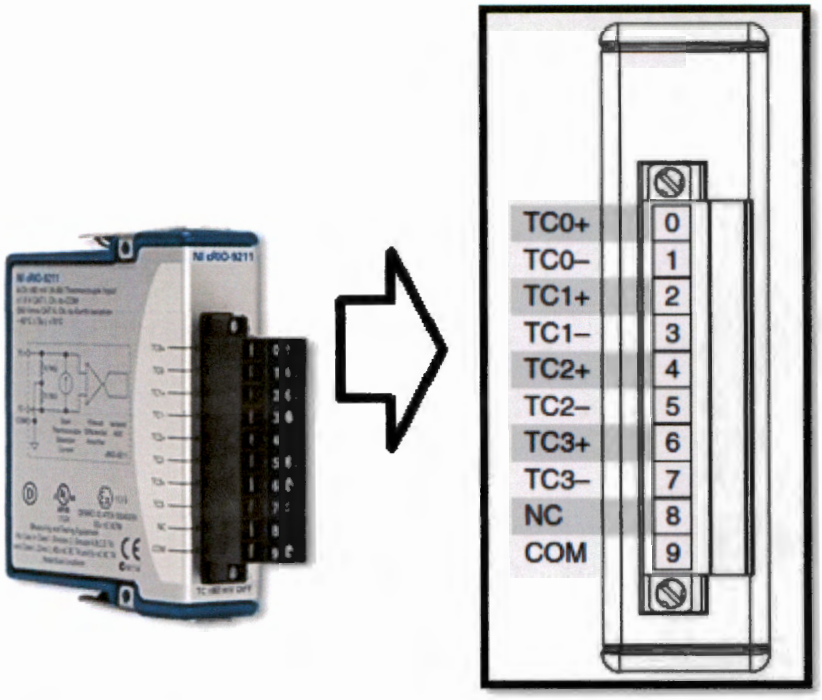

Figure 4.12: The NI 9211 Temperature module with its terminal assignment (right)

Four thermocouples were connected to the 10-screw-terminal detachable connector shown in Figure 4.12. Slots TC0 to TC3 were used for coupling the thermocouple wires. The positive (red) wire was connected to TC+ terminal and the negative (white) wire to the TC- terminal.

4.6.5 The NI 9234 module for vibration and current measurements

The NI 9234 module is a 4-Channel module with a ±5 V input range. It is a 24-Bit Software-Selectable IEPE and AC/DC Analog Input Module. The module has four BNC input ports for simultaneous analogue input. The NI 9234 module can sample at 51200 samples per second which calculates to a max rate of 12.8 Hz per channel. Two of these NI 9234 modules as shown in Figure 4.13 was chosen and used to transfer vibration measurements and current measurement data to the Matlab environment. Four channels on each of the modules connected to the four acceleration meters and two channels on the second module were connected to the two current transformers for data acquisition (see also Figure 4.9).

Figure 4.13: The NI 9234 AI module

4.6.6 The Canyon Network Switch

The Canyon 10/100 Mbps 5-Port Network Switch (NCP-D05PA) was used to connect the NI cDAQ 9188 chassis to the laptop and the Internet. The switch or router was needed because a laptop provided only one Ethernet input slot. But a connection between the laptop and the Internet was needed with an Ethernet cable, while the NI cDAQ 9188 chassis was connected to the laptop with an Ethernet cable. Three of the five input slots at the rear of this network switch were used for connection to the NI cDAQ 9188 chassis, the HP 470 laptop, and the Internet with three Ethernet cables respectively (see also Figures 4.9 and 4.14).

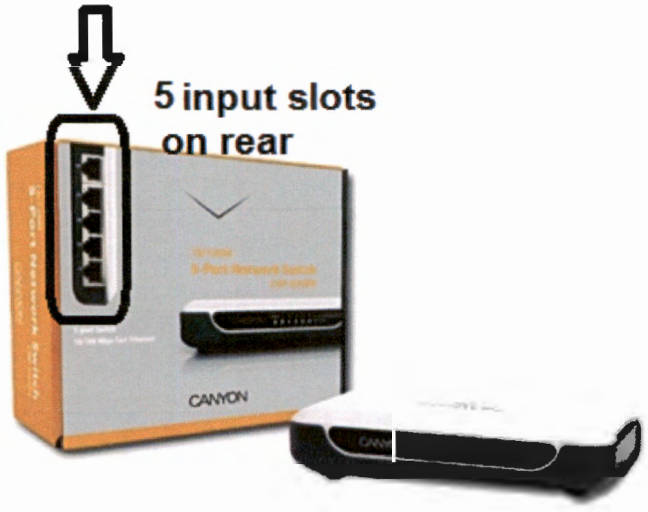

Figure 4.14: The Canyon Network Switch

4.7 Sensors at condition-monitoring system

4.7.1 Acceleration meters

The Dytran 3035B miniature IEPE piezoelectric acceleration meter with a sensitivity of 100 mV/g and mass of 2.5 gram is shown Figure 4.15. A 5-40 stud connected each acceleration meter to a mounting base. The base was glued with high strength superglue to a flat surface where measurements were taken on the gearbox. The unit is hermetically sealed and has a rugged stainless steel body. It can be used in high humidity and dirty environments. The cables used were 26 feet long 6056A26 Teflon insulated low noise mini coax cables with 5-44 to BNC connectors. Four acceleration meter sensors were coupled to the gearbox and the NI 9234 module (see also Figure 4.9). The acceleration meter drawing with dimensions is shown in Appendix A. Detailed characteristics of these acceleration meters are indicated in Appendix A.

Characteristics of the acceleration meters:

- Mass: 2.5 gram
- Sensitivity: 100 mV/g
- Range: 0.5 Hz – 10 kHz
- Resonance >45 kHz
- Temperature Range -60 to 225 degrees Fahrenheit

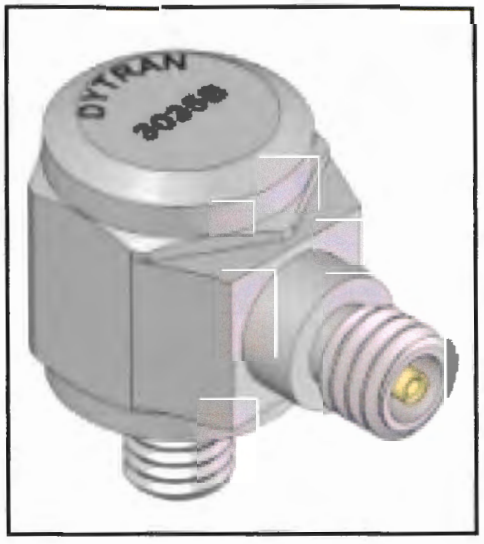

Figure 4.15: Dytran 3035B acceleration meter

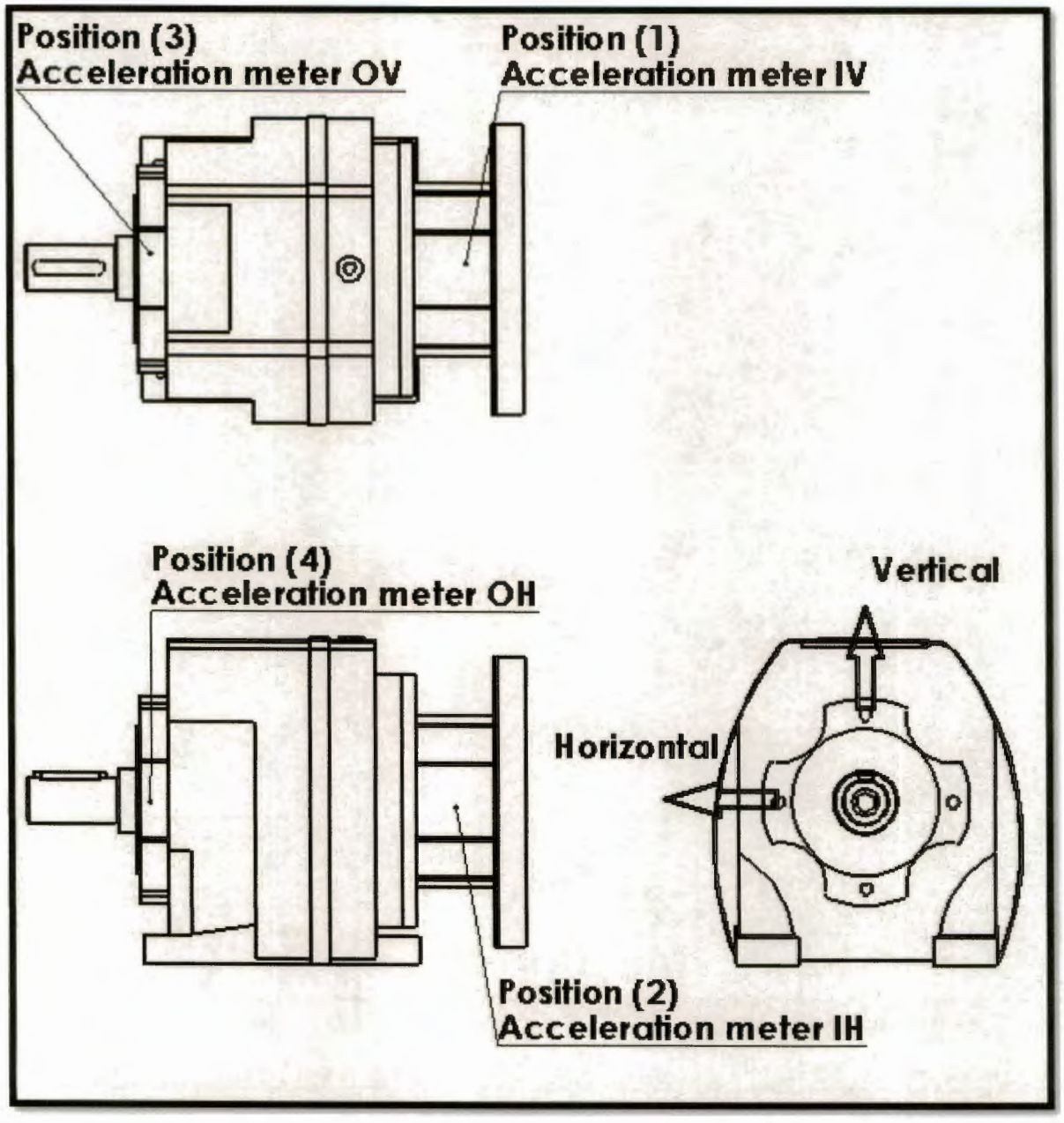

Figure 4.16: Acceleration meter positions

The acceleration meter positions are shown in Figure 4.16. At position 1, at the motor side or also the gearbox input shaft, the acceleration meter measured vibration in the vertical direction (IV). At position 2, vibration was measured in the horizontal direction at the input shaft (IH). At position 3, at the brake or output shaft of the gearbox, the acceleration meter measured the output shaft bearing vibration in the vertical direction (OV). At position 4, vibration was measured in the horizontal direction at the output shaft bearing (OH).

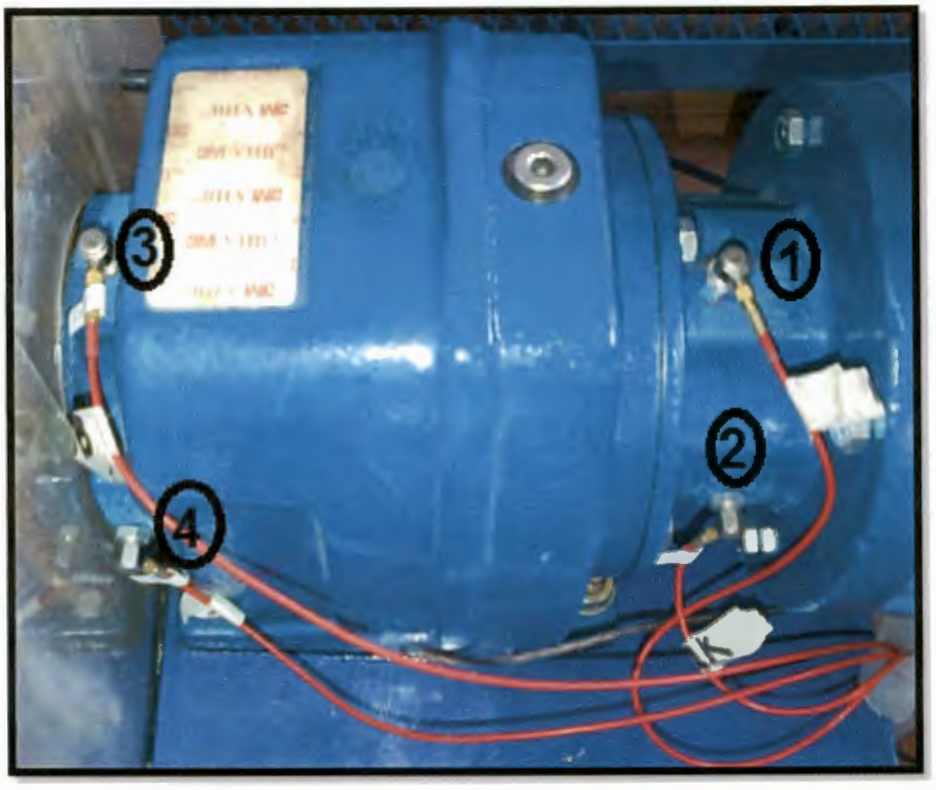

Figure 4.17: Acceleration meter positions 1 to 4 at the gearbox

The actual acceleration meter positions are shown in Figure 4.17. The motor is located at the right side (adjacent to position 1 and 2). The acceleration meter sensitivity magnitude was used in Program B to convert the electrical unit to an acceleration unit (m/s^2).

4.7.2 Thermocouples

Temperature was also measured at the gearbox. Gears and bearings with defects create heat from friction and temperature monitoring makes the system more secure. The National Instruments J-Type Thermocouple as shown in Figure 4.18 is a very versatile and cheap temperature transducer (also see Figure 4.9). It could measure in a temperature range from 0 to 750 C^{o} as indicated in Table 4.9. Four thermocouples, each with a two metre long cable were installed for temperature monitoring at the gearbox. The positions at the gearbox are at the input shaft bearing (Bearing A, see Figure 4.3), the output shaft bearing (Bearing F), the intermediate shaft bearing (Bearing C) and the temperature of the oil inside the gearbox.

Figure 4.18: The NI Type J thermocouple

The negative red wire was connected to the TC- terminal on the NI 9211 module and the white coloured, positive wire was connected to the TC+ terminal on the NI 9211 module as shown in Table 4.9 for the NI J type thermocouple. Program B required that the type of thermocouple of National Instruments be specified (thermocouple, "J" in this case) and this automatically allowed for the conversion of the electrical unit to the temperature unit (°C) with the interaction with the Measurement and Automation Explorer software (see Paragraph 3.4).

Table 4.9: The NI Thermocouple types

Type	Material		Color Code	Range (°C)	
Thermocouple Grade	Positive Wire	Negative Wire		Minimum	Maximum
J	Iron	Constantan	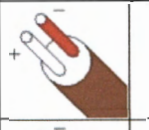	0	750
K	Chromel	Alumel		-200	1250
T	Copper	Constantan	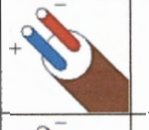	-200	350
E	Chromel	Constantan	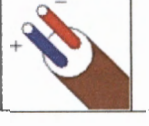	-200	900

4.7.3 Current transformers

The function of the dynamometer was to measure the load on an engine or motor. Electrical current was measured on this system and this measurement was mathematically converted to power and torque for the motor. A two watt meter method was used to calculate the applied load on the gearbox. Equations (2.26) and (2.27) indicate the equations used to

compute the power and torque magnitudes. To compute the power, voltage and current magnitudes were measured at two of the three phases of the input line of the motor. It was assumed that the voltage was constant throughout measurement and only measured it once and used as input throughout the test. From the plate on the motor the maximum power that the motor could create was computed and used to determine a theoretical efficiency. It was assumed that the efficiency value stayed the same throughout the load curve.

A split core CT234-30M-LC current transformer with a primary current of 30 amp nominal and 75 amp at maximum was used for current measurement as shown in Figure 4.19.

Figure 4.19: Current transformer at the input line of motor

The secondary current on the transformer was indicated as 0.01 amp. The current transformer was connected to the NI 9234 module in the chassis. Calibration was done before usage to plot the sensitivity of the current transformer. A known current was sent through a resistor and the voltage over the current transformer was measured. The current transformer was calibrated over a wide current range and made it possible to get the linearity and sensitivity of the modified current transformer.

The measured data from the calibration test are indicated in Table 4.10. It can be seen that the sensitivity was 531.89 mV/amp. The input range of the NI 9234 is +- 5 V and this made a current range between 0 and 9.5 amp possible as seen in Table 4.10. The maximum current

on the motor was indicated as 6.6 amp. It was evident that the current transformer was linear over the whole current range which gave an average slope of 0.531 Volt per amp. This sensitivity magnitude was used in Program B to convert the electrical unit to an electrical current unit (amp).

Table 4.10: Measurements for calibration procedure

Current [amp]	Potential difference [mV]	Slope [mV/amp]
0.1	54.7	547.00
0.2	108.8	544.00
0.3	162.3	541.00
0.4	216.7	541.75
0.5	270	540.00
1	529.8	529.80
1.5	818	545.33
2	1040	520.00
2.5	1321	528.40
3	1620	540.00
3.5	1881	537.43
4	2158	539.50
4.5	2437	541.56
5	2594	518.80
5.5	2889	525.27
6	3133	522.17
6.5	3420	526.15
7	3644	520.57
7.5	3912	521.60
8	4199	524.88
8.5	4467	525.53
9	4725	525.00
9.5	4983	524.53
10	5350	535.00
Average		531.89

The data from the calibration are graphically indicated as shown in Figure 4.20.

Paragraph 4.9, it was possible to pick the device up in Matlab by using the session-based code, "daq.getDevices" as Matlab code in Program B (see Chapter 3). The following output regarding data acquisition devices was given for the NI cDAQ 9188 chassis with the three NI modules clipped into the chassis (see Paragraph 4.8):

index	Vendor	Device ID	Description
1	ni	cDAQ9188-16D666AMod1	National Instruments NI 9234
2	ni	cDAQ9188-16D666AMod2	National Instruments NI 9211
3	ni	cDAQ9188-16D666AMod3	National Instruments NI 9234

For each module the Index, Vendor, Device ID and Description were indicated.

One of the biggest problems during this research study which was overcome was to solve data-acquisition and connection problems in a Matlab environment for the NI data-acquisition device. At the beginning of the study a 32-bit operating system at a HP Compaq nx 7400 laptop was used with Windows 7. The 2011a version of Matlab was initially used at the laptop to connect to a NI WLS 9163 single slot chassis. The legacy-based interface was used in Matlab for the data-acquisition code for this chassis. One module, namely the NI 9234, for vibration measurements, was clipped into the chassis. It was possible to connect to this device through the LAN at the North-West University and vibration signals were then collected in a Matlab environment. When the measured NI vibration data time signals were compared to corresponding signals obtained from a Diagnostic Instruments 2200 FFT Analyzer, it was found that the NI signals were totally inaccurate and the wave patterns also a bit different. This problem could initially not be solved, and it was decided that a new 64-bit Windows 7 operating system on a HP Probook 470 laptop linked to an alternative chassis namely a NI cDAQ 9188 eight slot chassis be used instead. This new equipment was tested, but a new problem was then experienced. Matlab could then not connect to the NI cDAQ 9188 chassis. The following Matlab error was then displayed:

No appropriate method, property, or field ChassisName for class daq.ni.DeviceInfo.

After weeks of several attempts to solve this problem it was decided to obtain the latest Matlab software. The R2014a version of Matlab with a research licence was then used. A technical assistant from Matlab indicated that codes related to previously connected NI devices were still stored in the NI Measurement and Automation Explorer software's memory as observed by the Matlab DAQ sub-routine code, although these devices were not connected. The code for a previously used NI device (NI WLS 9163 single-slot chassis) clashed with the NI cDAQ 9188 chassis device. After removing the codes related to previously connected NI devices, Matlab could connect to the NI cDAQ 9188 chassis. The integrity of measured vibration signal was investigated, and it was found that these data were accurate and reliable (Chapter 5, Paragraph 5.2). All problems that had been experienced were thus successfully solved.

The information described in Chapter 4 was used as input parameters at the computer programs described in Chapter 3. The experimental measurements and analysis are described in Chapter 5.

5. Experimental measurements and analysis

5.1 Introduction

The experimental phase had the purpose to test the developed condition-monitoring system. The experimental test setup for the gearbox as described in Chapter 4 was used for measured data collection. Three defects commonly seen in the industry on gearboxes were created at the gearbox in the laboratory. This environment was safe for personnel in the region during operational test conditions.

The input and output shaft bearings of the gearbox were monitored with acceleration meters in two directions, namely vertically and horizontally. The four measurement points for the acceleration meters are indicated as follows:

- IV = Input shaft (Bearing A) bearing measured in the vertical direction
- IH = Input shaft bearing (Bearing A) measured in the horizontal direction
- OV = Output shaft bearing (Bearing F) measured in the vertical direction
- OH = Output shaft bearing (Bearing F) measured in the horizontal direction

These abbreviations were used in different figures and tables in this Chapter. The acceleration meter positions are shown in Chapter 4 in Figures 4.16 and 4.17 (see also Figure 4.3).

5.2 Comparison of data from National Instruments system with Diagnostics Instruments Analyzer

The designed condition-monitoring system had to be tested to ensure that accurate data acquisition was done through the National Instruments hardware and Matlab. This was done by comparing data obtained from the National Instruments (NI) system with corresponding data obtained from a Diagnostic Instruments (DI) 2200 real time FFT Analyzer. The acceleration data were compared for corresponding time domain graphs and corresponding frequency domain graphs. These measurements were successively taken within a short time with the acceleration meter placed at the input shaft bearing (Bearing A) in the vertical direction.

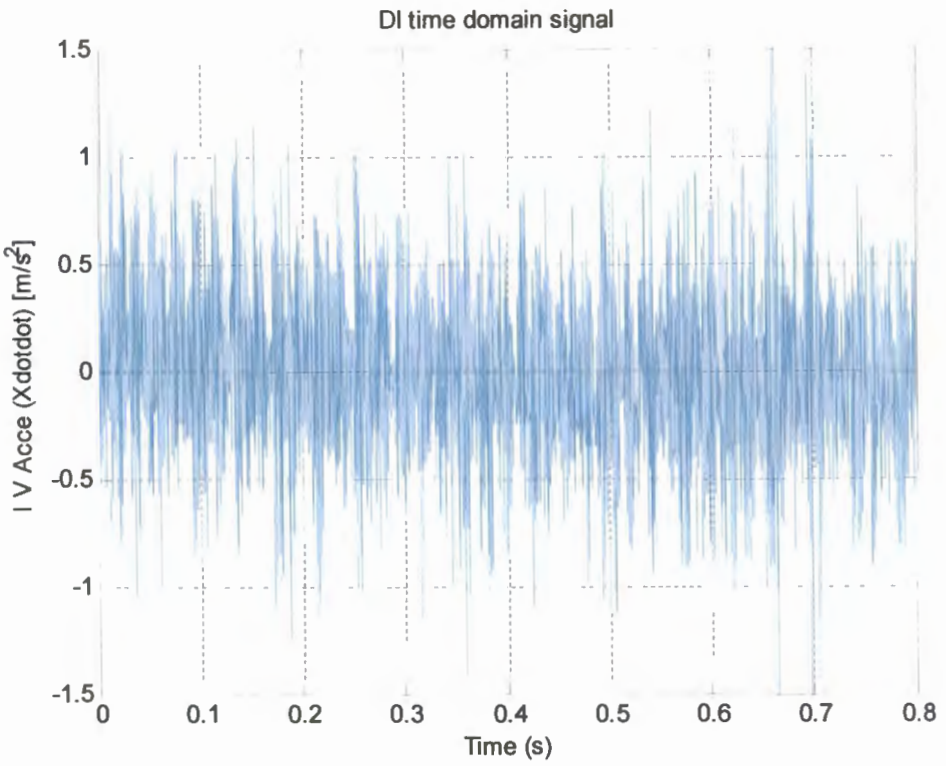

Figure 5.1: Time domain graph measured with Diagnostic Instruments FFT Analyser

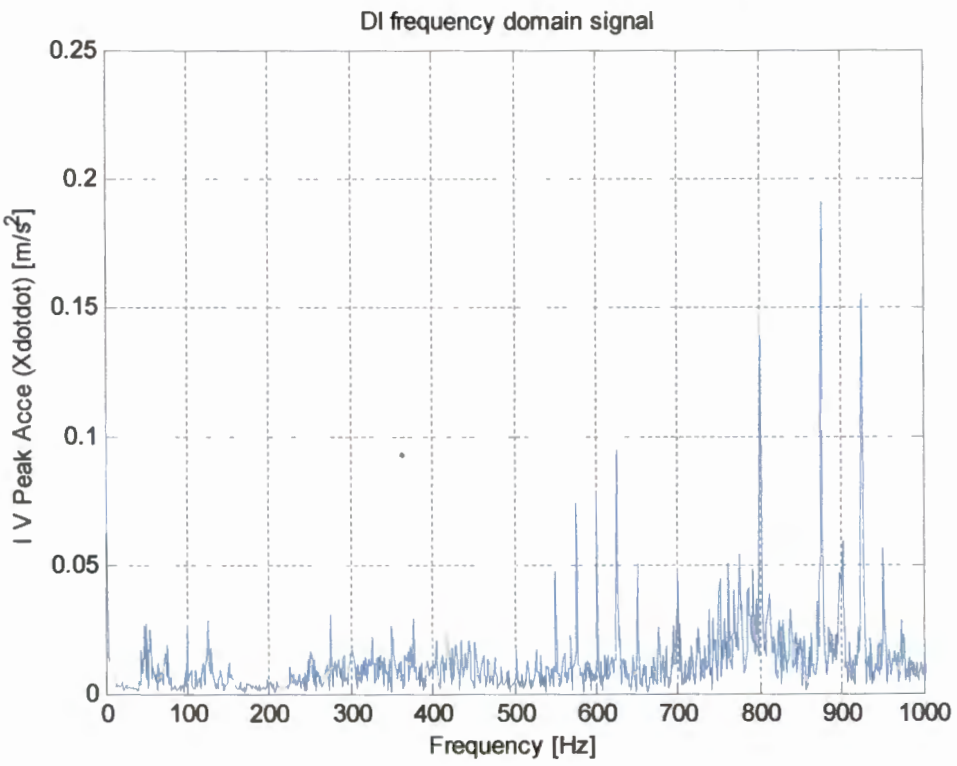

Figure 5.2: Frequency domain graph measured with Diagnostic Instruments FFT Analyser

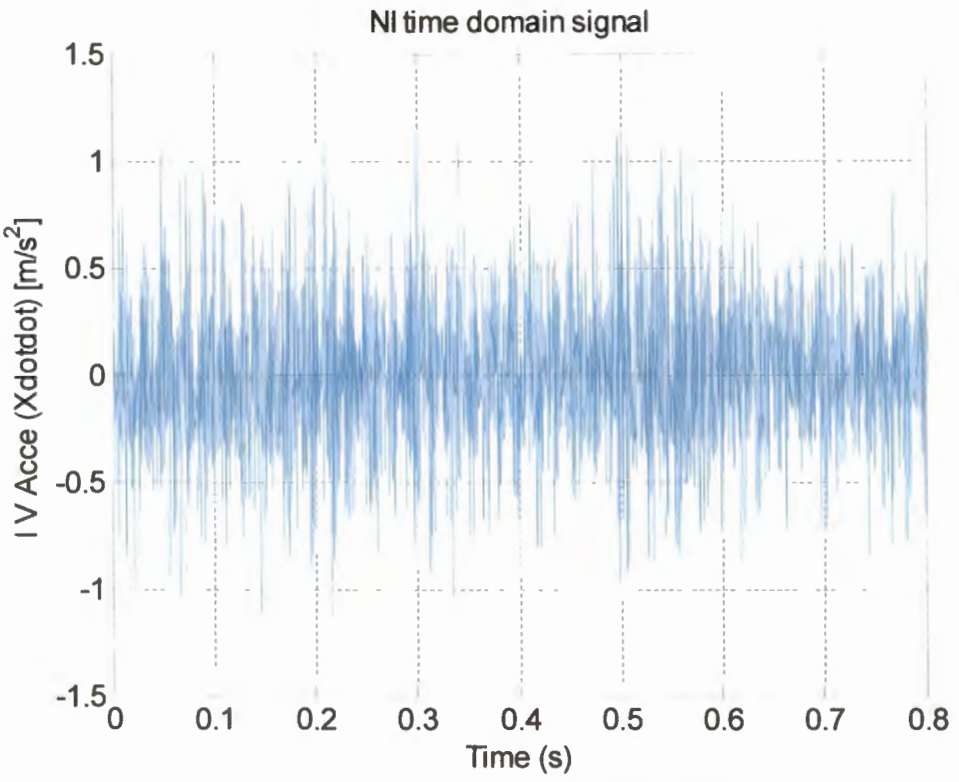

Figure 5.3: Time domain graph measured with National Instruments system

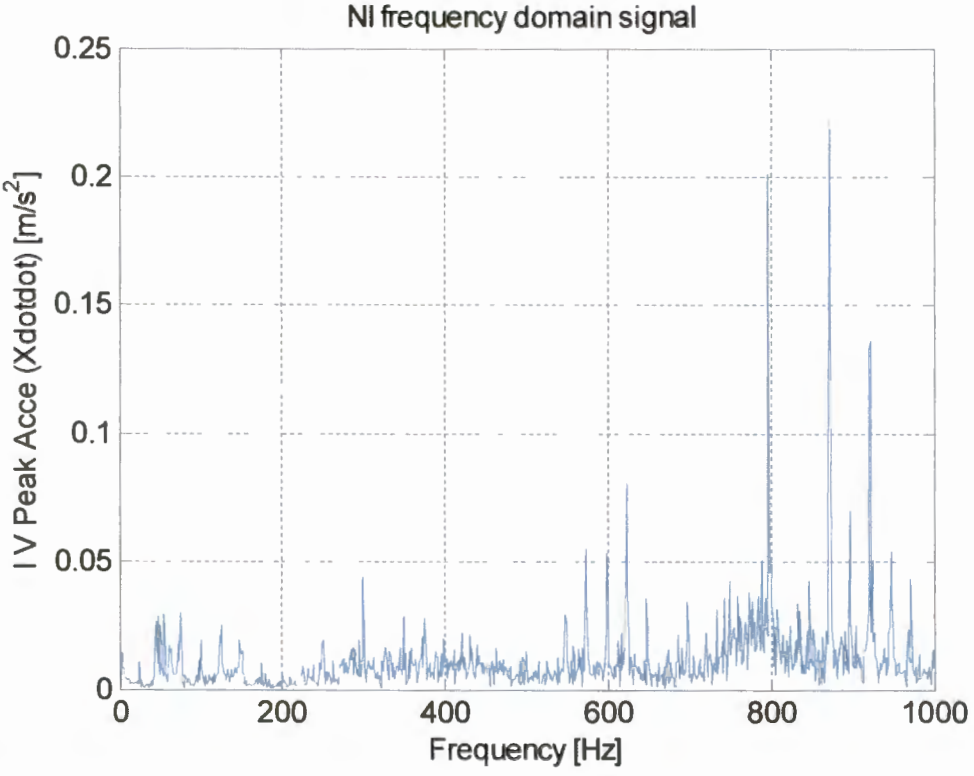

Figure 5.4: Frequency domain graph measured with National Instruments system

The time and frequency domain signals shown in Figures 5.1 and 5.2 were obtained from the Diagnostics Instruments 2200 FFT Analyzer. The time and frequency domain signals shown in Figures 5.3 and 5.4 were obtained from the National Instruments system coupled to a laptop, and constructed by Program B in the Matlab environment as developed in the study (see Chapters 3, Paragraph 3.3 and Chapter 4 for more details). It was found that these corresponding time and frequency domain signals corresponded very well (see Figures to 5.4). This proved that the National Instruments system linked to the laptop with the software developed was accurate and reliable.

Another important test was done to evaluate the integrity of the frequency domain signals. In this case the data of the time domain signal obtained from a measurement taken with the Diagnostics Instruments 2200 FFT Analyzer was imported to Program B in the Matlab environment as developed in the study. This time domain signal was then Fourier analysed and the frequency domain signal compared to the corresponding frequency domain signal provided by the Diagnostics Instruments 2200 FFT Analyzer. It was found that these corresponding frequency domain signals were almost perfectly the same. This proved that the underlying mathematical equations presented in Chapter 2, Paragraph 2.3.1 as well as the computer program developed (see Chapter 3, Paragraph 3.3) were effective, accurate and reliable.

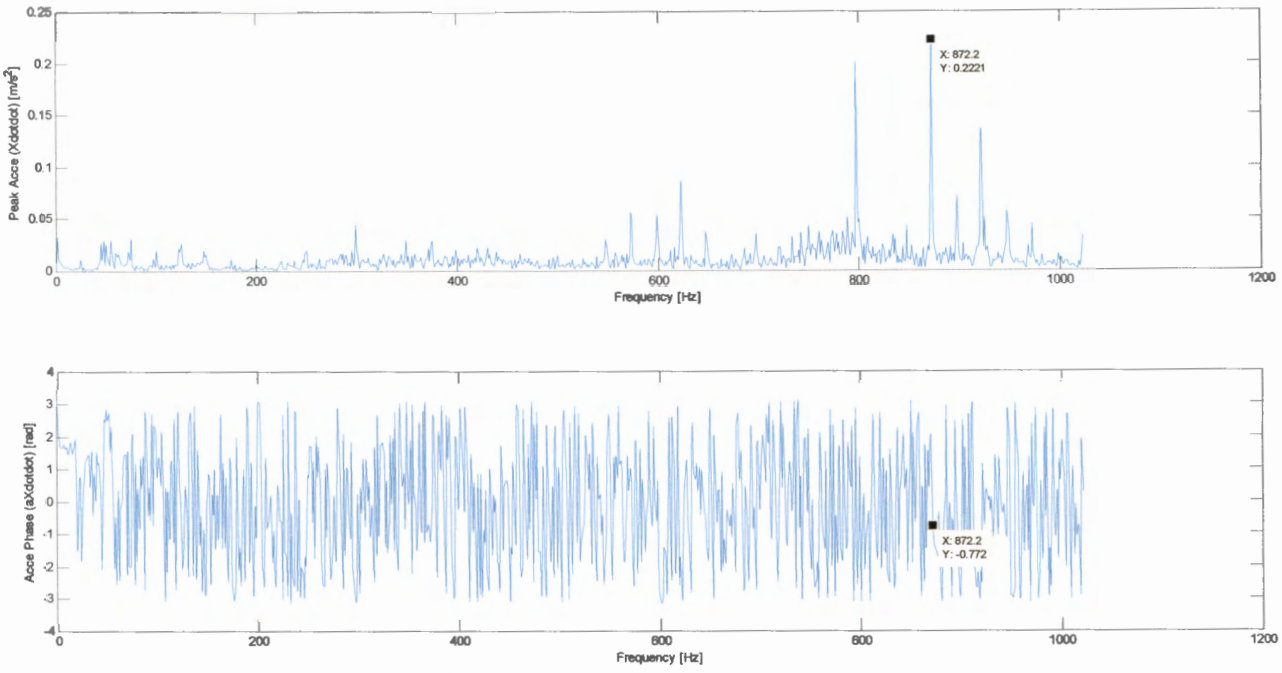

Figure 5.5: Frequency domain signals for acceleration amplitudes [m/s^2] and phase angles [rad] from the NI system

The frequency domain signals for acceleration amplitudes and corresponding phase angles obtained from the NI system and constructed by Program B in the Matlab environment are indicated in Figure 5.5 respectively. The frequency domain signals for velocity amplitudes and corresponding phase angles obtained from the NI system and constructed by Program B in the Matlab environment are indicated in Figure 5.6 respectively. Similar corresponding signals were obtained for measurements taken with the Diagnostics Instruments 2200 FFT Analyzer. Hand calculations regarding the integration from acceleration to corresponding velocity amplitudes as well as the 90^{o} ($\frac{\pi}{2}$ radians) phase angle difference between acceleration and corresponding velocity amplitudes confirmed that the integrity of these signals is trustworthy. This also proved that the underlying mathematical equations presented in Chapter 2, Paragraph 2.3.1 as well as the computer program developed (see Chapter 3, Paragraph 3.3) regarding velocity conversions and phase angles were effective, accurate and reliable.

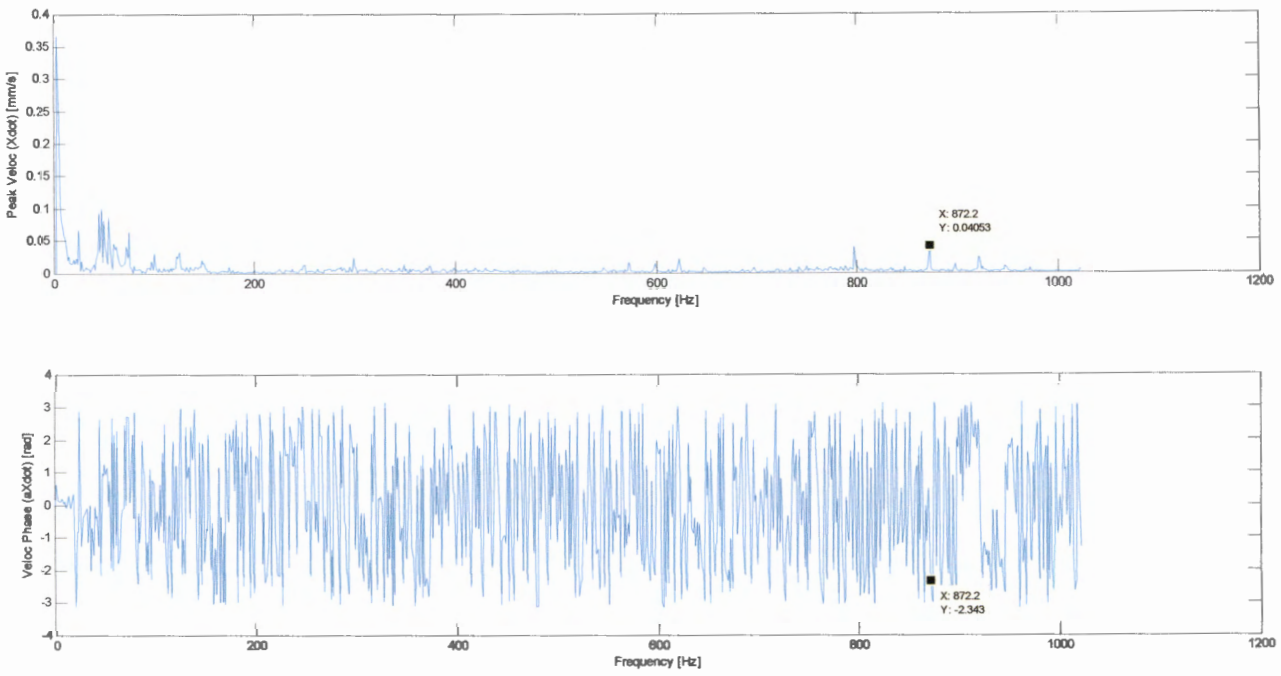

Figure 5.6: Frequency domain signals for velocity amplitudes [mm/s] and phase angles [rad] from the NI system

5.3 Defects created at the gearbox

5.3.1 Misalignment defect

A misalignment defect was created at the gearbox. This was done by finally using 0.5 mm shims as spacers at two different positions at the gearbox flange nearest to the input shaft as shown in Figure 5.7. Wynn's high temperature gasket maker (-62 to 260 degrees Celsius) was effectively used to avoid oil leaks.

Figure 5.7: Spacer position for misalignment at the input shaft

An approximate increase of 367 % in the overall vibration acceleration magnitude was obtained for measurements taken at the input shaft bearing (Bearing A) in the vertical direction, after this misalignment defect was created. In addition an approximate increase of 277 % in the overall vibration acceleration magnitude was obtained for measurements taken at the input shaft bearing (Bearing A) in the horizontal direction, after this misalignment defect was created.

5.3.2 Gear defect

Gear 1 with 39 teeth is located on the input shaft (see Figure 4.3 in Chapter 4). The running speed was 25 Hz. A pencil grinder was used to create damage at this Gear 1 as shown in Figure 5.8. The groove induced was approximately 1 mm wide and 1 mm deep at only one gear tooth and this damage is shown in Figures 5.9 and 5.10.

Figure 5.8: Pencil grinder and cutting disc used at the cutting setup

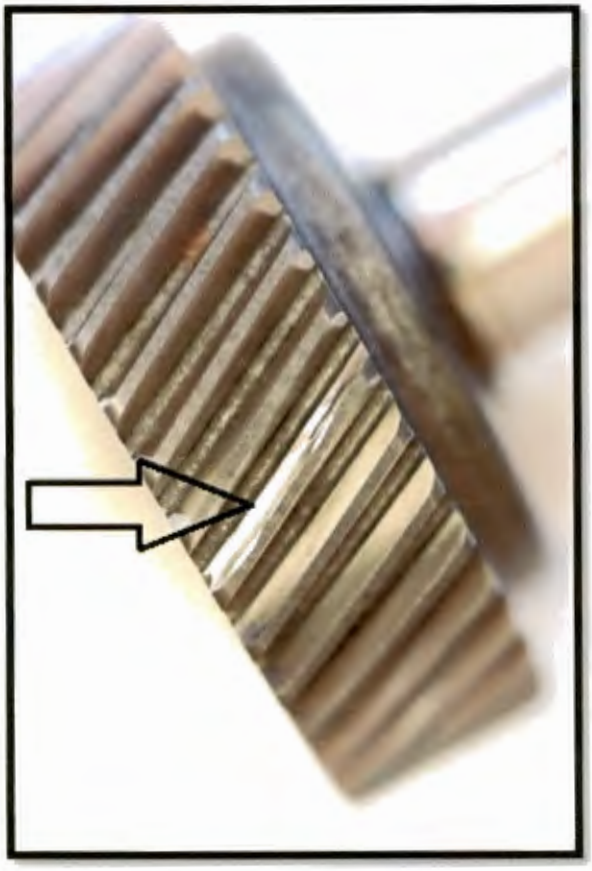

Figure 5.9: Gear with defect at one tooth

Figure 5.10: Gear with defect at one tooth

5.3.3 Bearing defect

Bearing A on the input shaft was chosen to create damage as a bearing defect (see Figure 4.3 in Chapter 4). The bearing number was 6008/2RS-1 C3. The defect at the inner ring was enlarged on the photo for a better view as shown in Figure 5.11. A diamond graphing tip was used in the pencil grinder so that a groove could be created as damage between the bearing rollers at the inner race (see Figure 5.12). The groove was approximately 1 mm deep and 1 mm wide with a circular shape.

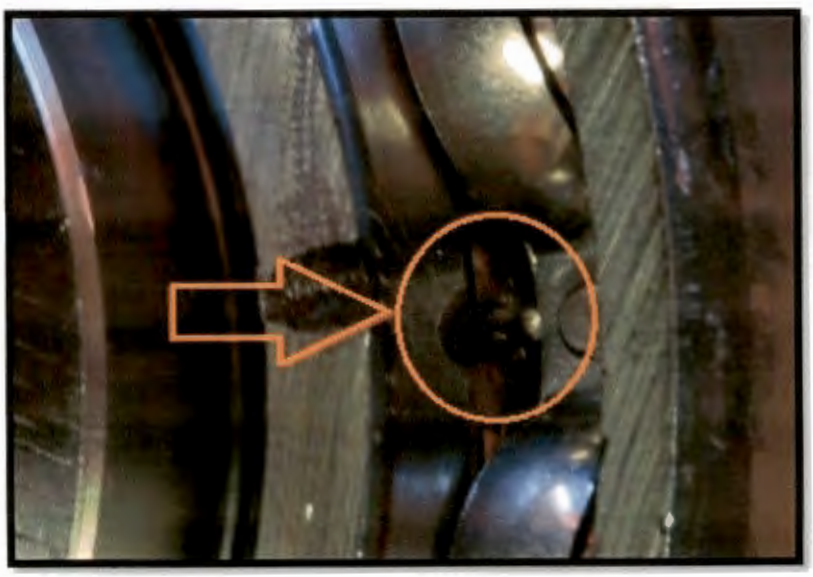

Figure 5.11: Bearing defect

Figure 5.12: Diamond engraving tip encircled

5.3.4 Test procedure

The total test was done over a 48-hour period, when the gearbox was running. The test was done as follows:

- 12 hours without load
- 2 hours under lower load with disc brake
- 2 hours under higher load with disc brake
- 12 hours without load
- 2 hours under lower load with disc brake
- 2 hours under higher load with disc brake
- 16 hours without load

The time schedule under load conditions and without load for different hour numbers is indicated in Table 5.1. The hour numbers were necessary to allow easy reference regarding the measured data described in this Chapter. The hydraulic power pack was activated at the disc brake for load. The condition-monitoring system was programmed to take a reading every half hour. This resulted in 96 data points over the 48-hour test period as used for trends for the condition of the gearbox. Temperature, current and vibration data was collected for the analysis.

Table 5.1: Test schedule for the 48-hour test

Time	Hour number	Without load	Lower load	Higher load
6:00 AM	1			
7:00 AM	2			
8:00 AM	3			
9:00 AM	4			
10:00 AM	5			
11:00 AM	6			
12:00 PM	7			
1:00 PM	8			
2:00 PM	9			
3:00 PM	10			
4:00 PM	11			
5:00 PM	12			
6:00 PM	13			
7:00 PM	14			
8:00 PM	15			
9:00 PM	16			
10:00 PM	17			
11:00 PM	18			
12:00 AM	19			
1:00 AM	20			
2:00 AM	21			
3:00 AM	22			
4:00 AM	23			
5:00 AM	24			
6:00 AM	25			
7:00 AM	26			
8:00 AM	27			
9:00 AM	28			
10:00 AM	29			
11:00 AM	30			
12:00 PM	31			
1:00 PM	32			
2:00 PM	33			
3:00 PM	34			
4:00 PM	35			
5:00 PM	36			
6:00 PM	37			
7:00 PM	38			
8:00 PM	39			
9:00 PM	40			
10:00 PM	41			
11:00 PM	42			
12:00 AM	43			
1:00 AM	44			
2:00 AM	45			
3:00 AM	46			
4:00 AM	47			
5:00 AM	48			

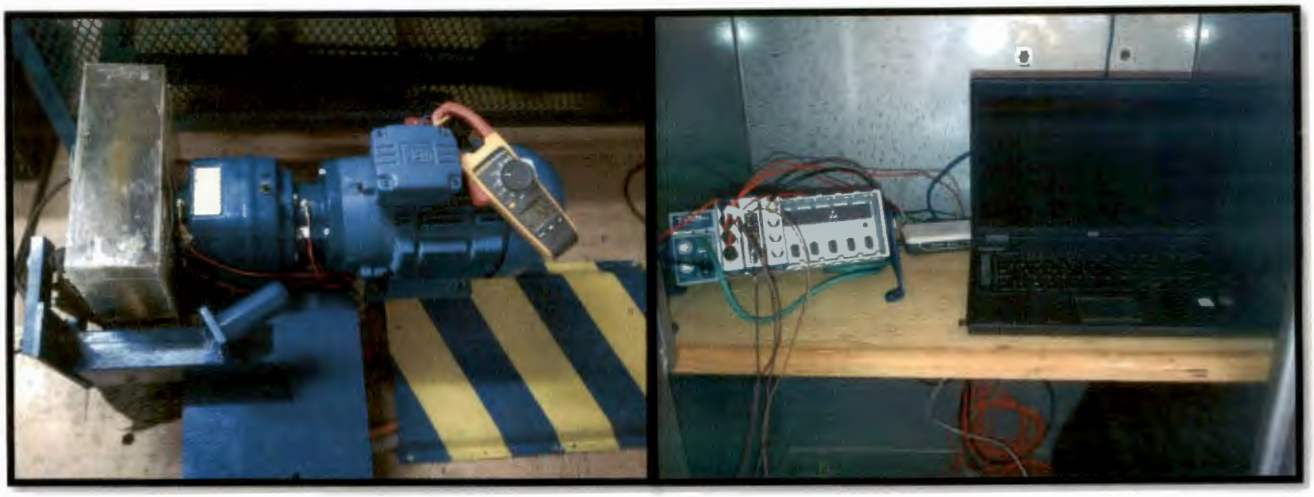

Figure 5.13: Test setup: gearbox with sensors and instrumentation with the laptop

The test setup in the laboratory with the gearbox, sensors, instrumentation and laptop is shown in Figure 5.13. The instrumentation and laptop for data acquisition were located in the safe adjacent to the gearbox in the laboratory. The load on the gearbox was verified with a Multimeter during the load condition periods during the test.

5.4 Results

5.4.1 Monitoring output screens

The continuous data collected through all the sensors and other instrumentation at the gearbox were captured by the Matlab program and two output screens were shown while the program was running. The data at these two output screens as shown in Figures 5.14 and 5.15 were updated after every data-acquisition interval. For the 48-hour test a total of 96 data sets were updated, thus the data –acquisition interval was chosen and set at every 30 minutes. A host computer away from the laboratory was able to access the remote computer in the laboratory through TeamViewer, by using the Internet. Monitoring of the gearbox in the laboratory was thus done via the Internet during the 48-hour test. Trends of measured data indicated a change in the condition of the machine which could be observed during real time on the host computer screen. In order to identify the sources that influenced this change in condition, further analysis of signals were carried out as explained in Paragraphs 5.6.1 and 5.6.2. The continuous Internet condition monitoring system was thus successfully tested for the gearbox in the laboratory, via the University Wifi Internet connection.

The first output screen contained trends of the measured parameters. For every data-acquisition point a value was plotted on the specific graph as trend. This provided a good comparison in magnitude of the specific measured parameter as function of time. These measured parameters include electrical current, power, torque, % of full load, four different overall vibration accelerations, four different overall vibration velocities and also four different temperatures as indicated in Table 5.2. The different trends are indicated in Figure 5.14 for the first output screen at hour number 48 of the 48-hour test (also see Table 5.1).

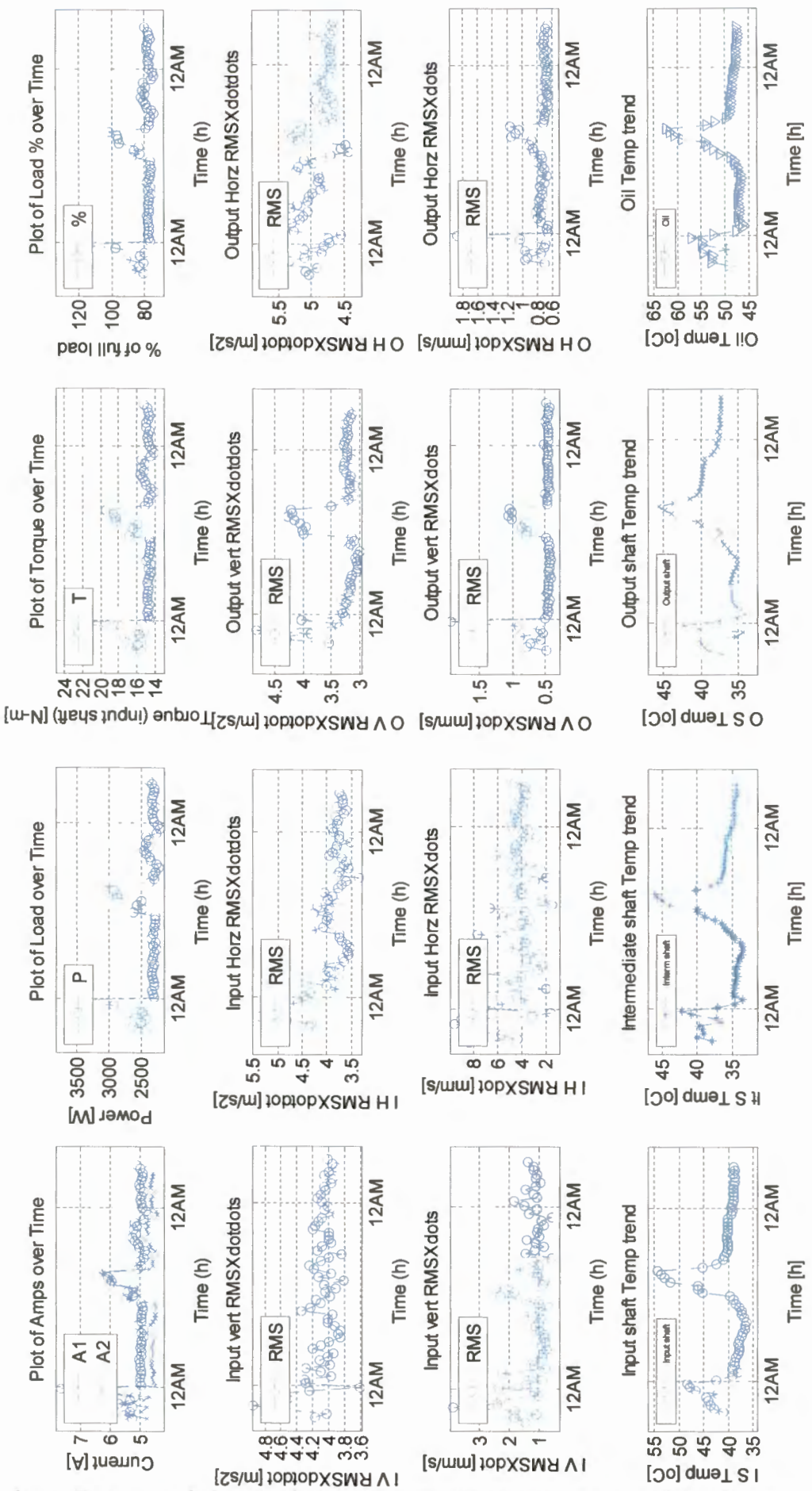

Figure 5.14: Trends for the first output screen at hour number 48 of the test

Table 5.2: Trends at the first output screen

1. Current [A]	2. Power [W]	3.Input shaft Torque [Nm]	4. % of full load power.
5. Input shaft vertical direction overall acceleration [m/s^2]	6. Input shaft horizontal direction overall acceleration [m/s^2]	7. Output shaft vertical direction overall acceleration [m/s^2]	8. Output shaft horizontal direction overall acceleration [m/s^2]
9. Input shaft vertical direction overall velocity [mm/s]	10. Input shaft horizontal direction overall velocity [mm/s]	11. Output shaft vertical direction overall velocity [mm/s]	12. Output shaft horizontal direction overall velocity [mm/s]
13. Input shaft temp [°C]	14. Intermediate shaft temp [°C]	15. Output shaft temp [°C]	16. Oil temp [°C]

The second output screen contained different vibration signals with the last updated signals shown on this screen. The four positions of the vibration sensors at the gearbox are described in Chapter 4. The twelve measured vibration time and frequency domain signals as constructed by the Matlab program for the different positions and directions at the gearbox are indicated in Table 5.3. The different vibration signals are indicated in Figure 5.15 for the second output screen at hour number 12 of the 48-hour test.

Table 5.3: Vibration signals at the second output screen

1. Input shaft vertical direction time vs. acceleration	2. Input shaft horizontal direction time vs. acceleration	3. Output shaft vertical direction time vs. acceleration	4. Output shaft horizontal direction time vs. acceleration
5. Input shaft vertical direction frequency vs. acceleration	6. Input shaft horizontal direction frequency vs. acceleration	7. Output shaft vertical direction frequency vs. acceleration	8.Output shaft horizontal direction frequency vs. acceleration
9. Input shaft vertical direction frequency vs. velocity.	10. Input shaft horizontal direction frequency vs. velocity.	11. Output shaft vertical direction frequency vs. velocity.	12. Output shaft horizontal direction frequency vs. velocity.

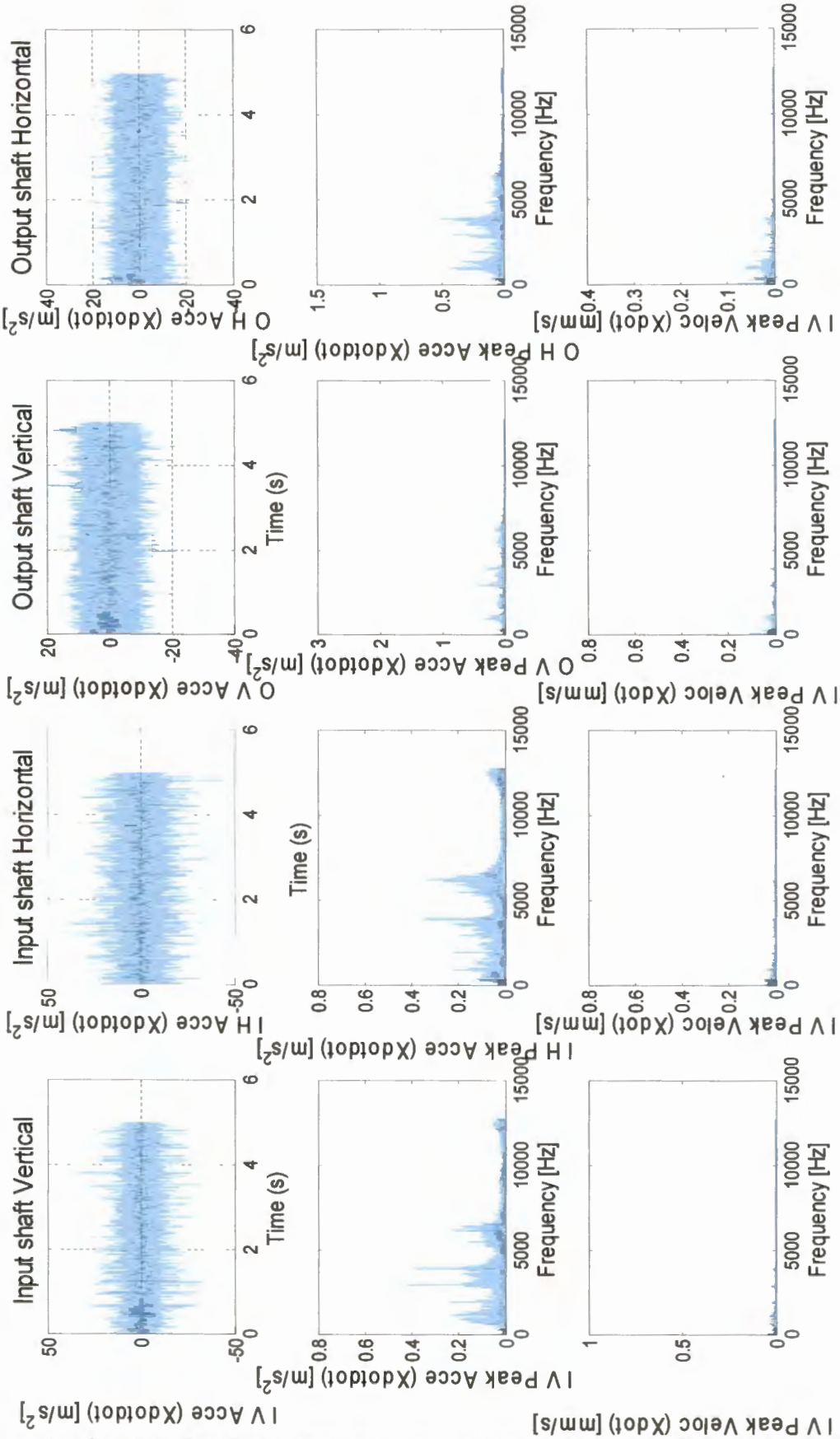

Figure 5.15: Vibration signals for second output screen at hour number 12 of the test

5.4.2 Current, power and torque data

The measured electrical current magnitudes at two input lines were used to compute the power used by the gearbox. The torque on the input shaft was also compute and trended over the 48-hour test. Trends for current, load and torque magnitudes over the total 48-hour test period are indicated in Figure 5.16 to Figure 5.18. An alarm was implemented for load. In the case when the alarm value was exceeded it triggered the warning sound at the laptop.

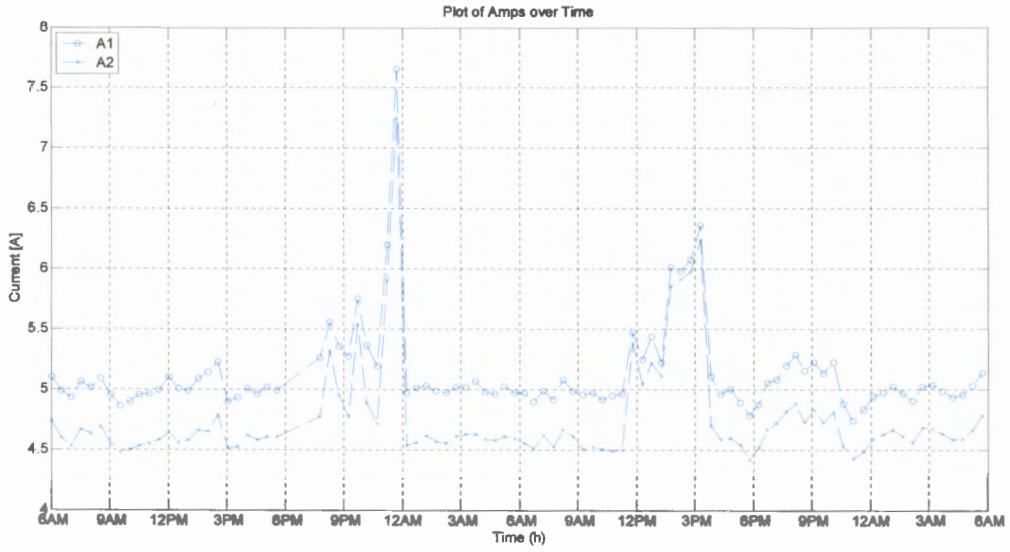

Figure 5.16: Current trend [A]

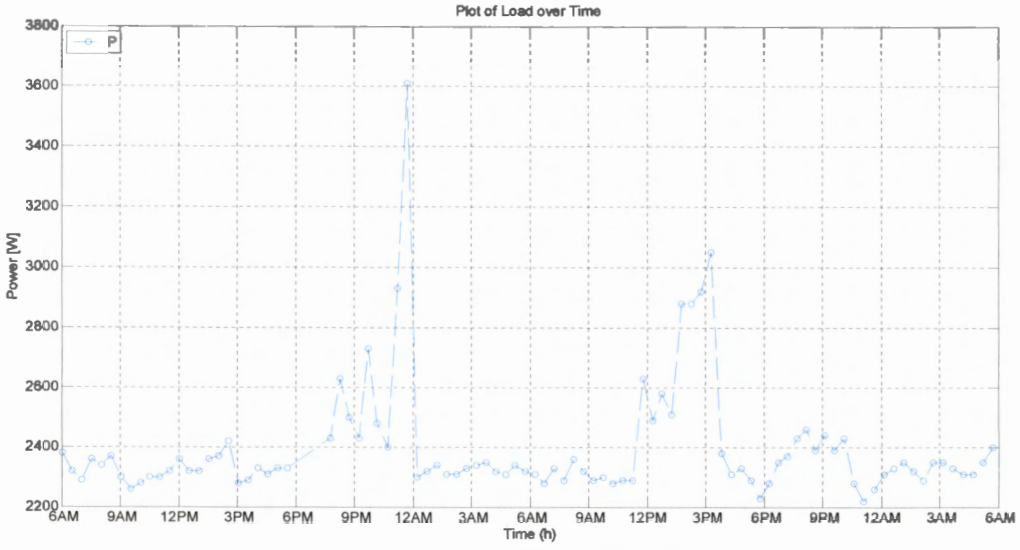

Figure 5.17: Power trend [W]

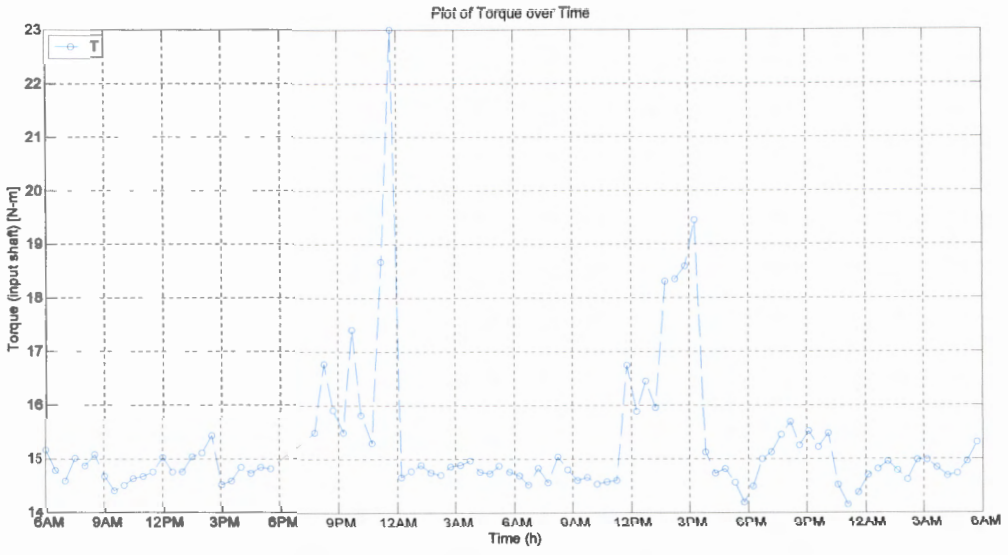

Figure 5.18: Torque trend of the input shaft [Nm]

5.4.3 Temperature

The trends for the four different temperature sensors (see Chapter 4 for the locations at the gearbox) over the total 48-hour test are indicated in Figures 5.19 to 5.22.

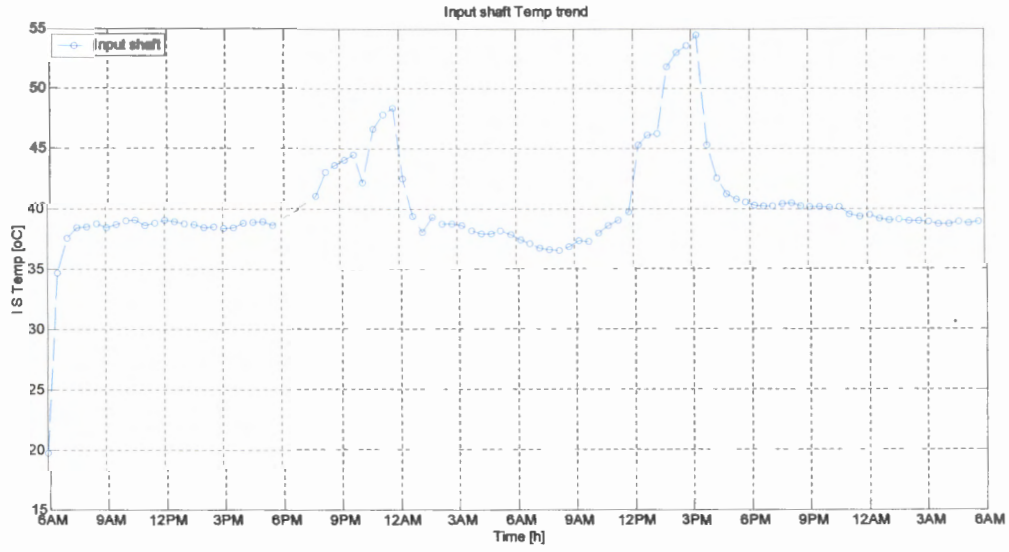

Figure 5.19: Temperature trend for the input shaft [°C]

The test started with a relatively cold gearbox at 6 am on Saturday 9 August. The two spikes observed in the trend indicate the two load phases during the test. This indicated the load at the gearbox when more heat was created. These spikes can be seen throughout the measured signals.

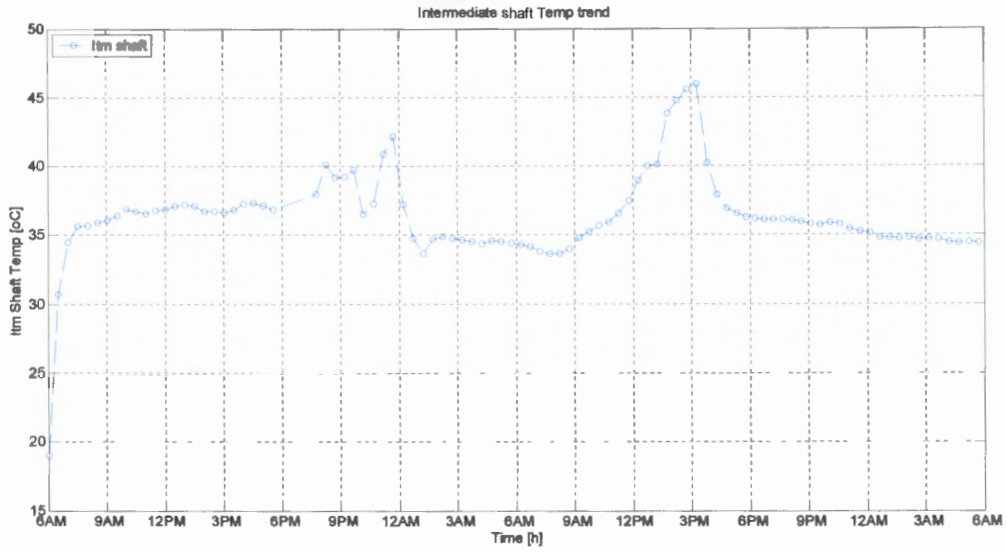

Figure 5.20: Temperature trend for the intermediate shaft [°C]

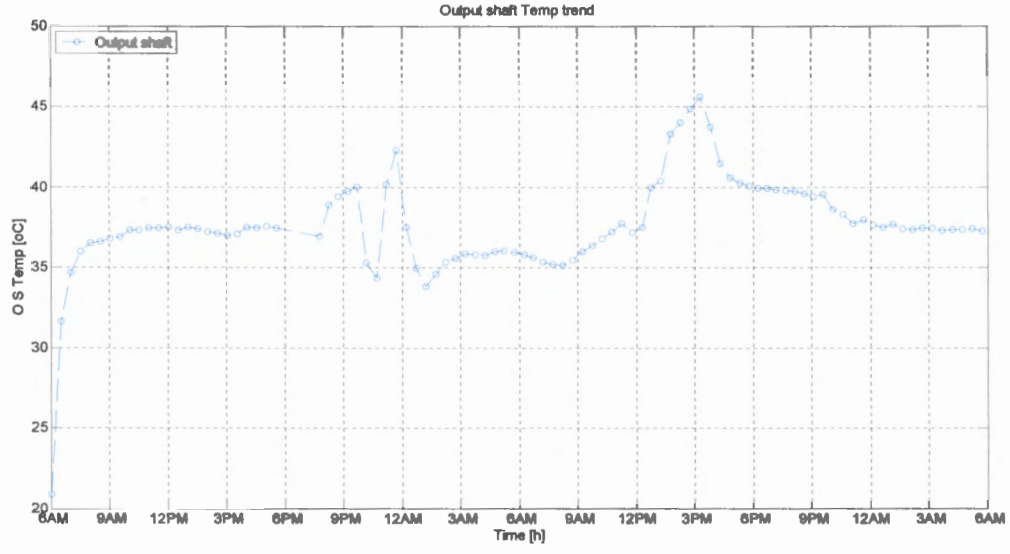

Figure 5.21 : Temperature trend for the output shaft [°C]

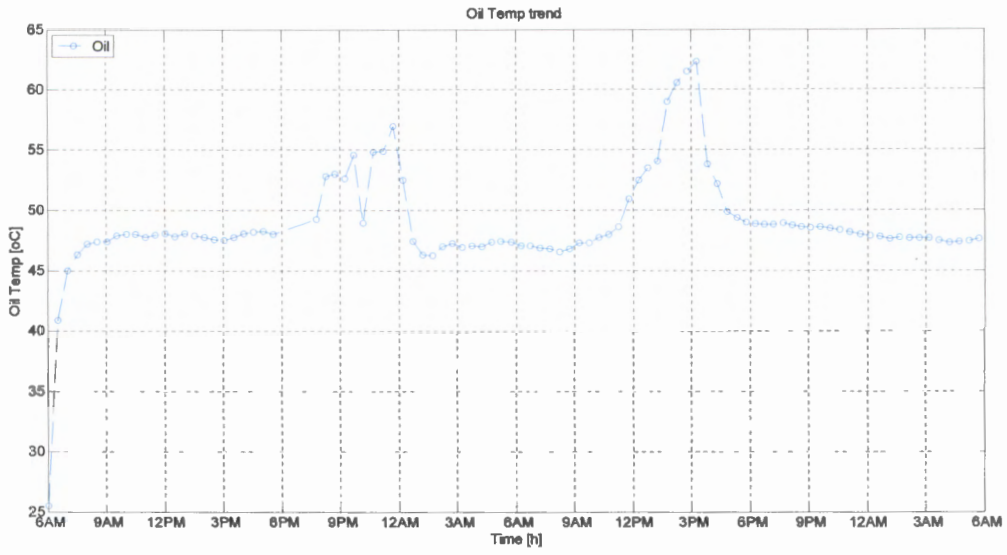

Figure 5.22: Temperature trend for the oil [°C]

5.4.4 Overall RMS acceleration

The Root Mean Square acceleration values were computed with the Matlab program for each of the 96 data points over the 48-hour test, for each of the four time-domain signals obtained from the four acceleration meters. The RMS acceleration trends for the four different vibration sensors (see Chapter 4 for the locations and directions at the gearbox) over the total 48-hour test are indicated in Figures 5.23 to 5.26. The larger values at some of these trends corresponded to the larger load conditions applied at the gearbox.

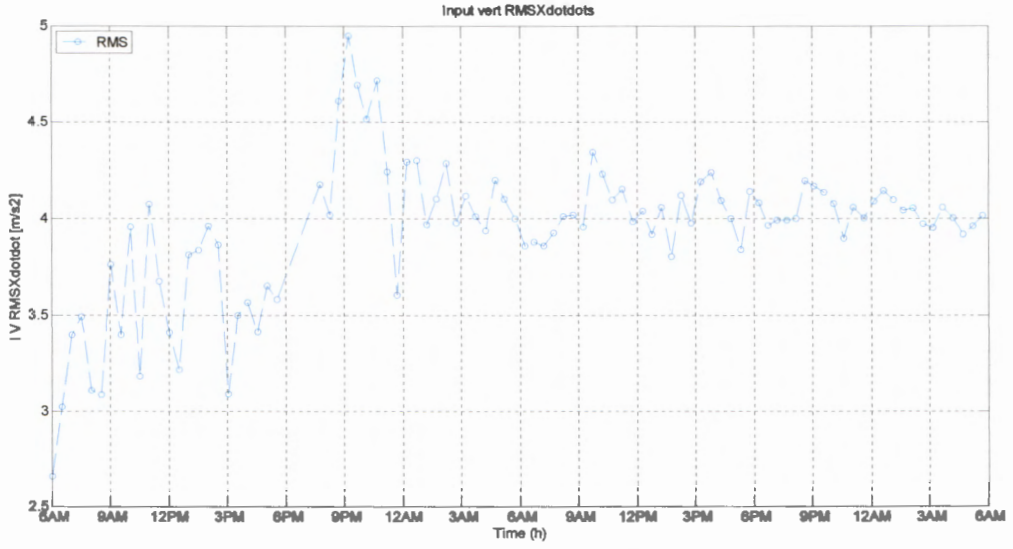

Figure 5.23: Overall RMS acceleration trend, input shaft bearing, vertical direction [m/s^2]

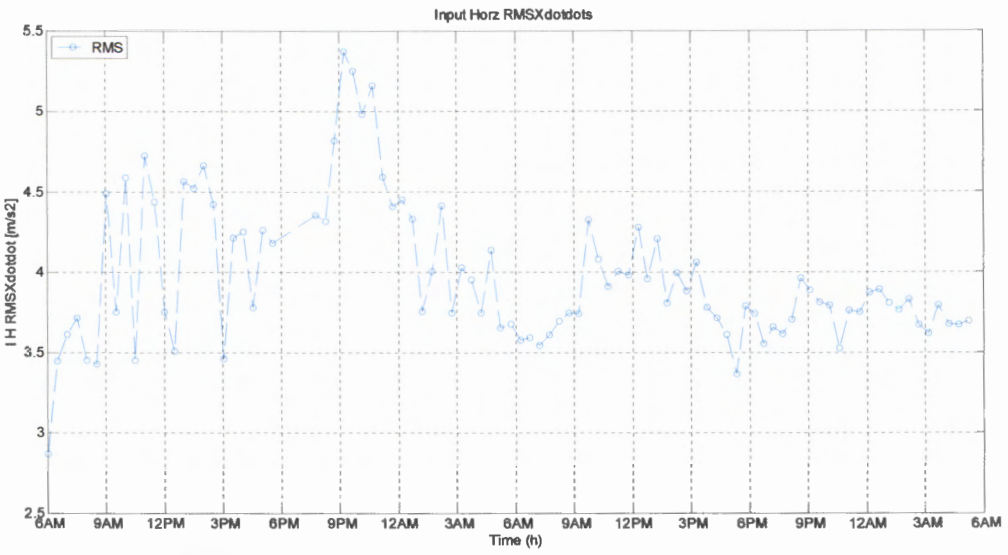

Figure 5.24: Overall RMS acceleration trend, input shaft bearing, horizontal direction [m/s^2]

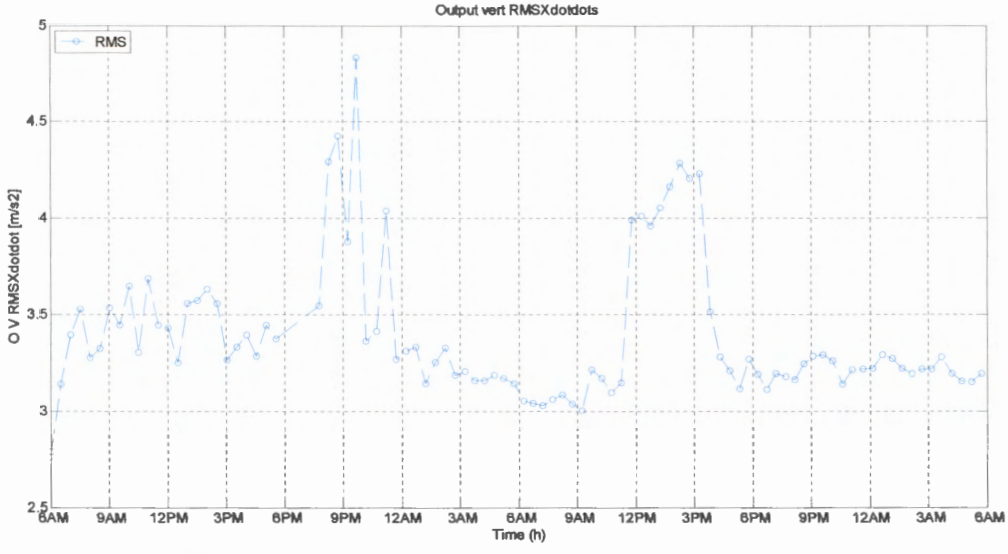

Figure 5.25: Overall RMS acceleration trend, output shaft bearing, vertical direction [m/s^2]

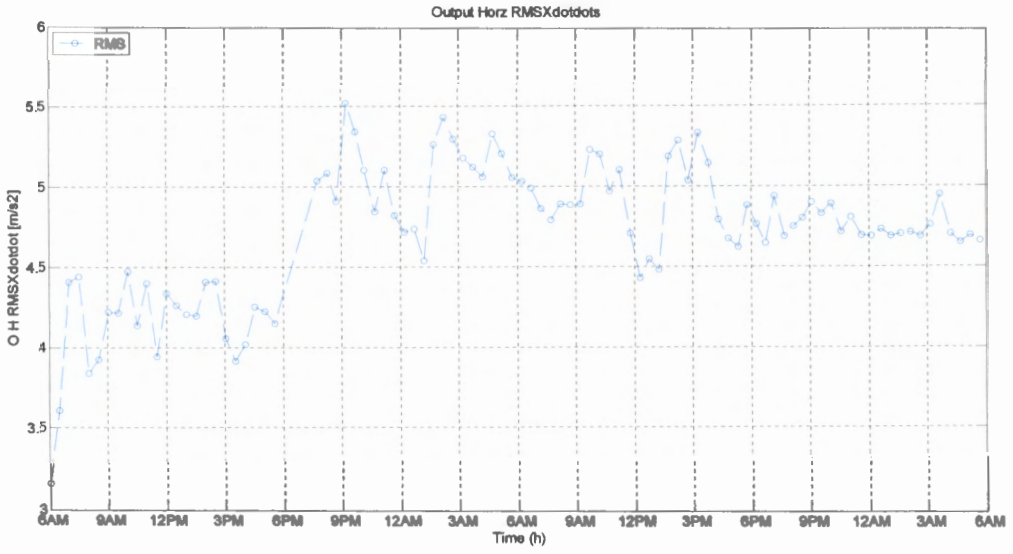

Figure 5.26: Overall RMS acceleration trend, output shaft bearing, horizontal direction [m/s^2]

5.4.5 Overall RMS velocity

Similarly to the overall RMS acceleration trends as described in the previous Paragraph, the corresponding RMS velocity trends were obtained and indicated in Figures 5.27 to 5.30.

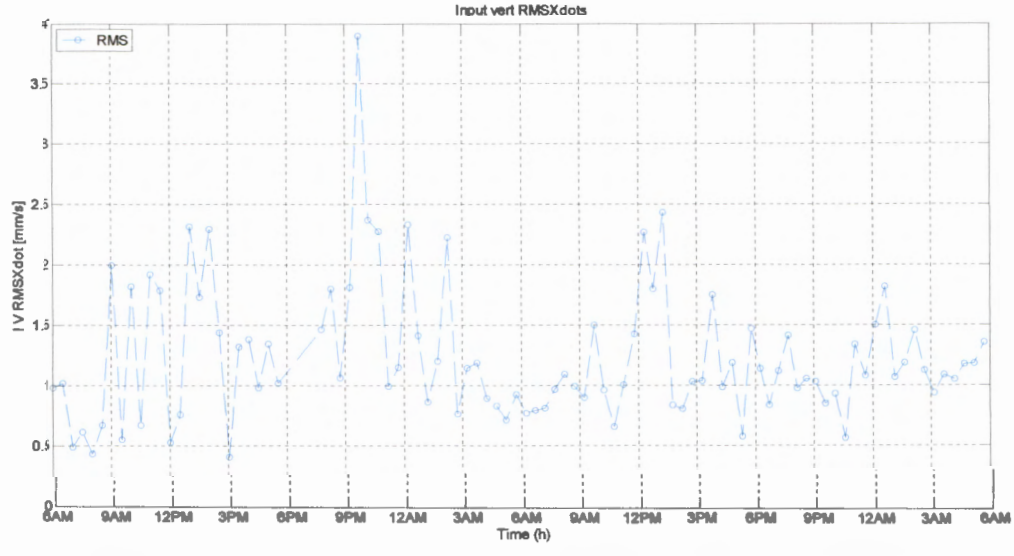

Figure 5.27: Overall RMS velocity trend, input shaft bearing, vertical direction [mm/s]

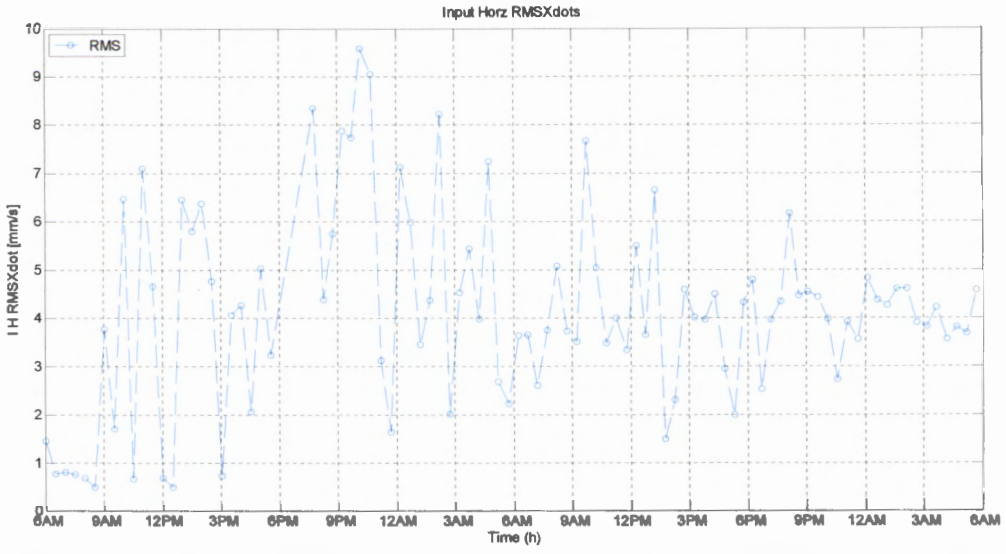

Figure 5.28: Overall RMS velocity trend, input shaft bearing, horizontal direction [mm/s]

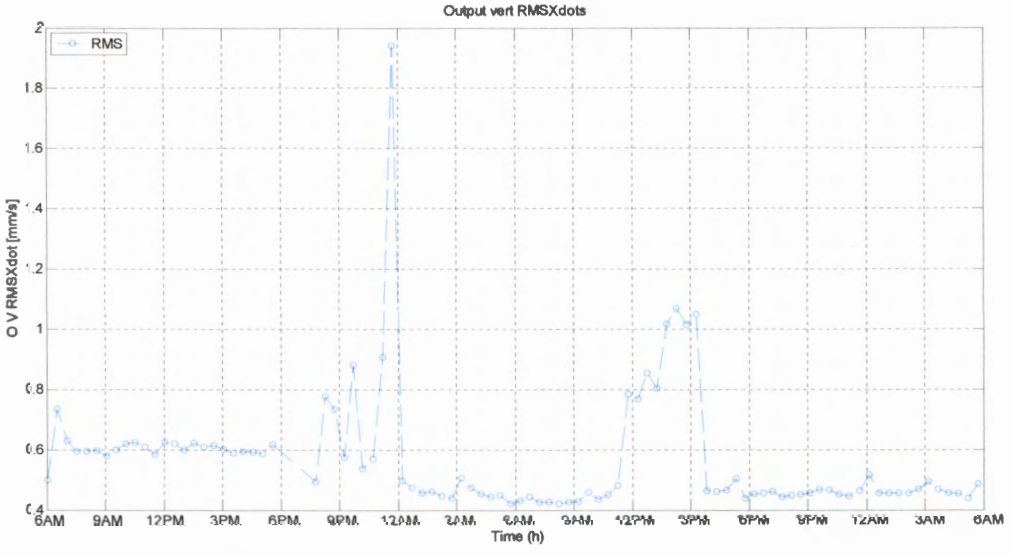

Figure 5.29: Overall RMS velocity trend, output shaft bearing, vertical direction [mm/s]

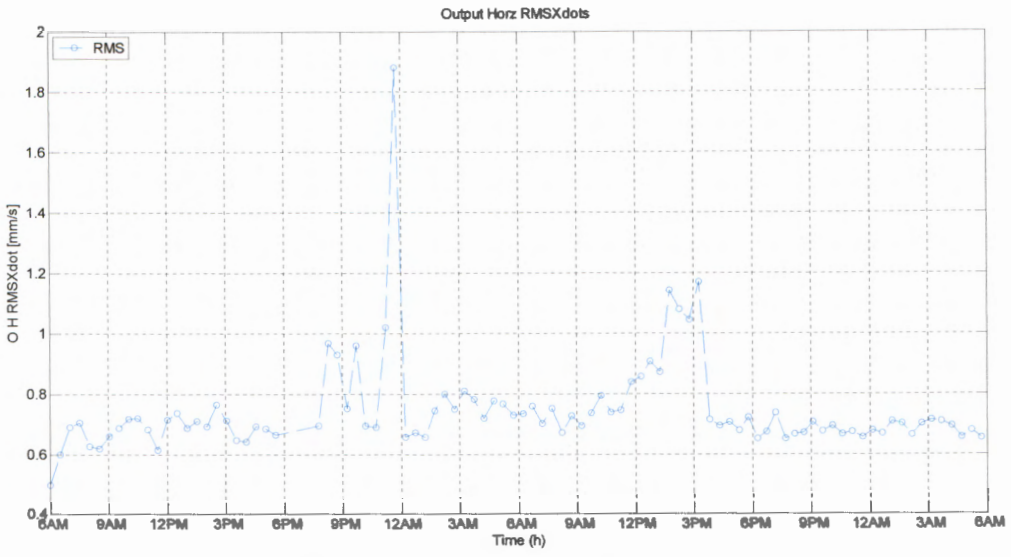

Figure 5.30: Overall RMS velocity trend, output shaft bearing, horizontal direction [mm/s]

5.5 Frequency domain waterfalls

5.5.1 Acceleration frequency waterfall graphs

The measured acceleration frequency domain signals were saved as 96 data sets over the 48-hour test period, for each of the four acceleration meters respectively. Every vibration measurement was taken for five seconds with a rate of 25000 samples per second. The Piezo crystal measurements were taken in mV and were converted to m/s^2. The 5 second time domain signal was converted by the Matlab program into the frequency domain with the maximum frequency at 12.5 kHz. This was done for all four acceleration meter inputs in the computer program developed.

The acceleration frequency domain waterfall graph for the input shaft bearing (Bearing A, see Figure 4.3) in the vertical direction is shown in Figure 5.31. It should be kept in mind that all three the defects induced at the gearbox are closest to the input shaft bearing (see Paragraph 5.3.3 for more information regarding these defects induced). The increase in the amplitudes below 5 kHz over time is clearly observed in Figure 5.31. The largest and most dominant amplitudes are clearly observed in this frequency domain waterfall graph, and this revealed important information regarding specific problems that developed over time, and the deterioration in the condition of the gearbox over time. The analysis regarding the

presence of the amplitudes at certain frequencies is described later in this Chapter. This graph as a three-dimensional representation of data thus provided the history at the input shaft bearing in the vertical direction regarding gearbox condition over the 48-hour test. Similar information regarding gearbox condition is observed in Figure 5.32 to 5.34, but for the data collected at the specific bearings and directions as mentioned in the figure subscripts below each of these figures.

The acceleration frequency domain waterfall graph for the input shaft bearing in the vertical direction is shown in Figure 5.31.

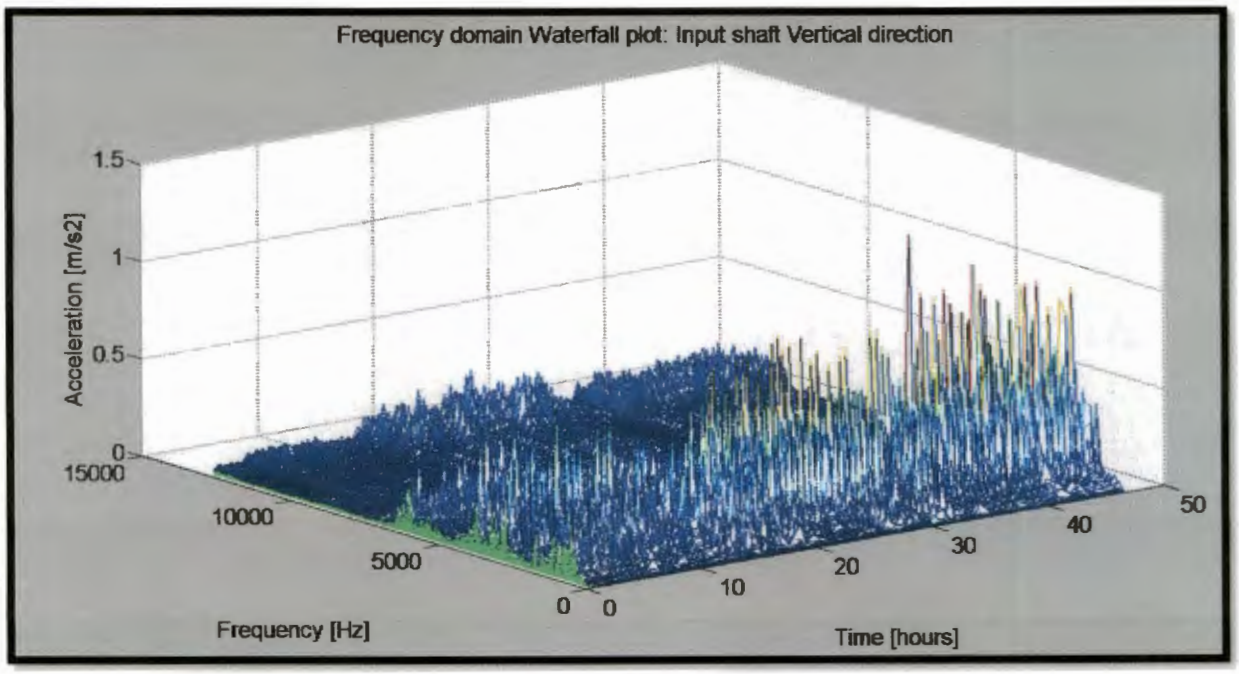

Figure 5.31: Frequency domain acceleration waterfall graph, input shaft bekaring, vertical direction

Significant increases in amplitudes at frequencies above 10000 Hz as function of time are also observed in Figure 5.32. The analysis regarding the presence of these amplitudes at certain frequencies is described later in this Chapter.

The acceleration frequency domain waterfall graph for the input shaft bearing in the horizontal direction is shown in Figure 5.32.

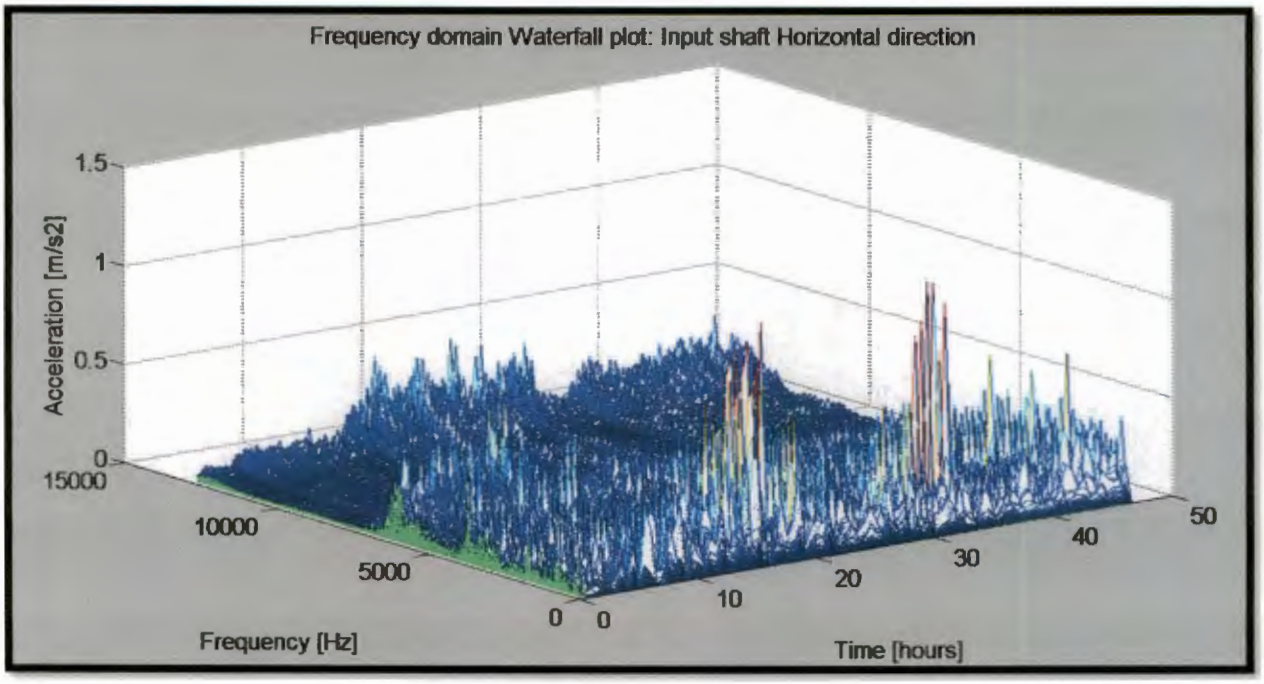

Figure 5.32: Frequency domain acceleration waterfall graph, input shaft bearing, horizontal direction.

The acceleration frequency domain waterfall graph for the output shaft bearing in the vertical direction is shown in Figure 5.33.

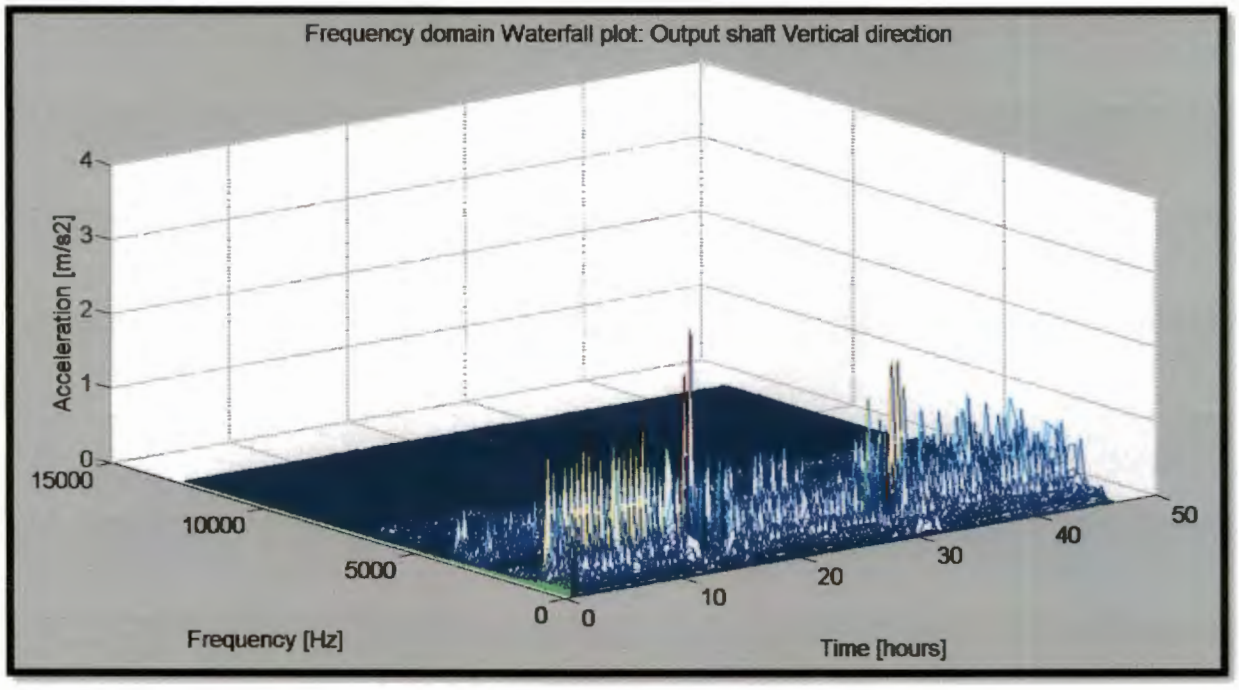

Figure 5.33: Frequency domain acceleration waterfall graph, output shaft bearing, vertical direction

The acceleration frequency domain waterfall graph for the output shaft bearing in the horizontal direction is shown in Figure 5.34.

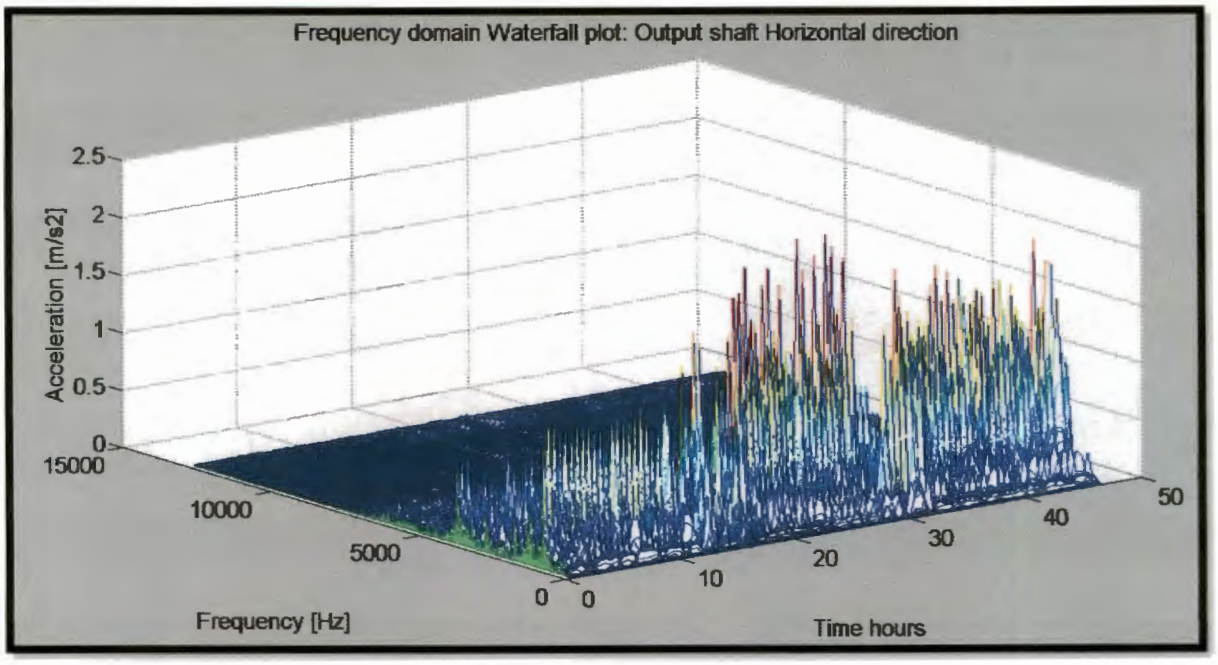

Figure 5.34: Frequency domain acceleration waterfall graph, output shaft bearing, horizontal direction

These typical three dimensional waterfall graphs provide a lot of information of the 48 hour test. This is very useful, because the most dominant amplitudes that developed over time at certain frequencies as affected over 48 hours could immediately be observed. Two dimensional frequency response graphs were then extracted at specific times and were then thoroughly analysed. The analysis entailed the presence of amplitudes at their different frequencies as explained in Paragraphs 5.6 and 5.7.

5.5.2 Velocity frequency waterfall graphs

Similarly to the acceleration frequency domain waterfall graphs as described in the previous paragraph, frequency domain waterfall graphs were obtained for velocity as shown in Figure 5.35 to Figure 5.38. Similar advantages regarding observation in a quick glance of gearbox condition over the total 48-hour test as described in Paragraph 5.5.1 are here also applicable. Instead of acceleration as the response parameter used in the graphs indicated in Paragraph 5.5.1 velocity was used as the response parameter in these four frequency

domain waterfall graphs. The presence of amplitudes at certain frequencies, also the larger and most dominant frequencies are described later in Chapter 5. The frequency domain velocity waterfall graphs revealed fewer large visible amplitudes at different frequencies in general, than that of the corresponding acceleration graphs. Acceleration is thus a more sensitive parameter to monitor machine condition, when compared to velocity. Velocity is however the preferred parameter regarding condition monitoring ISO standards (Reliability direct, 2014).

The velocity frequency domain waterfall graph for the input shaft bearing in the vertical direction is shown in Figure 5.35.

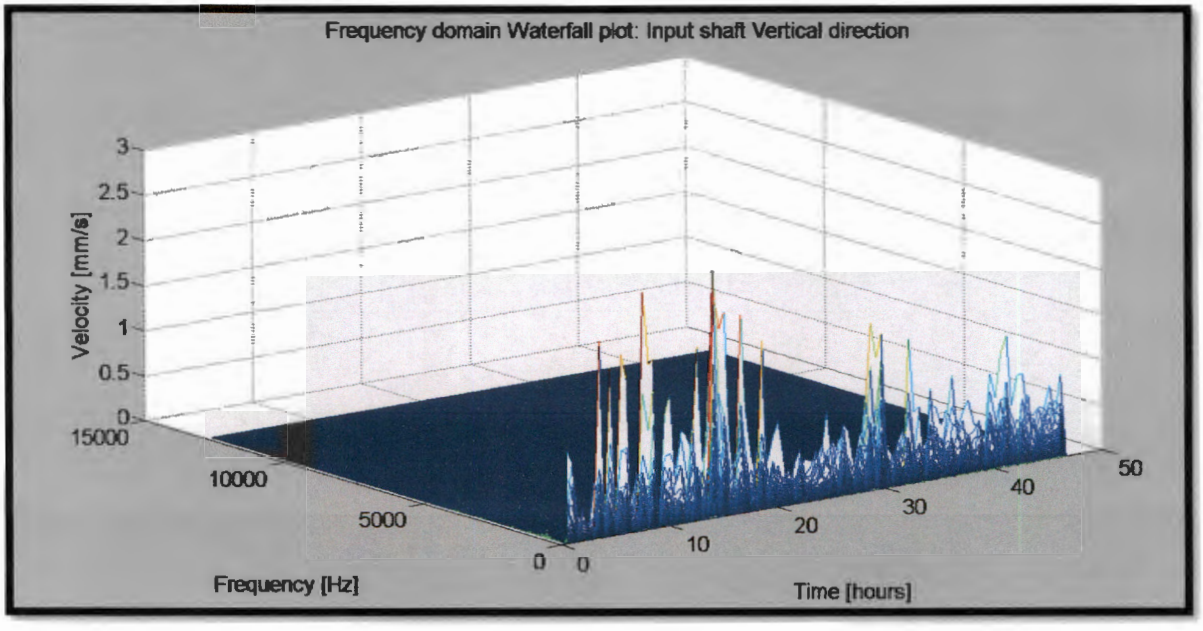

Figure 5.35: Frequency domain velocity waterfall graph, input shaft bearing, vertical direction

The velocity frequency domain waterfall graph for the input shaft bearing in the horizontal direction is shown in Figure 5.36.

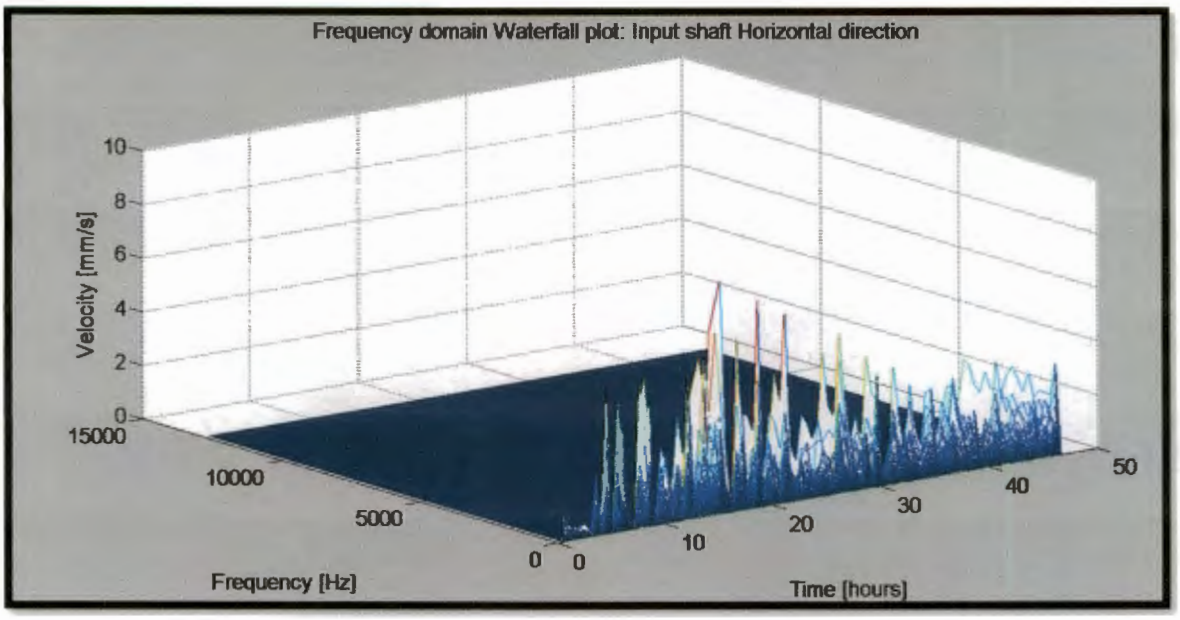

Figure 5.36: Frequency domain velocity waterfall graph, input shaft bearing, horizontal direction

The velocity frequency domain waterfall graph for the output shaft bearing in the vertical direction is shown in Figure 5.37.

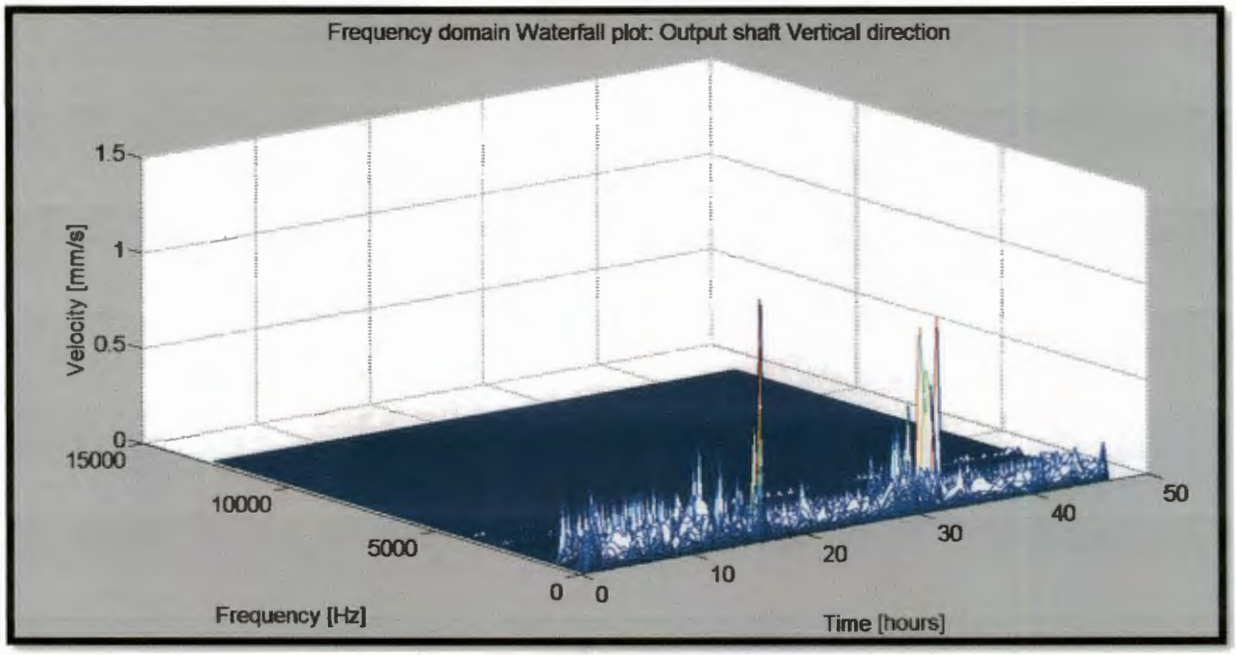

Figure 5.37: Frequency domain velocity waterfall graph, output shaft bearing, vertical direction

The velocity frequency domain waterfall graph for the output shaft bearing in the horizontal direction is shown in Figure 5.38.

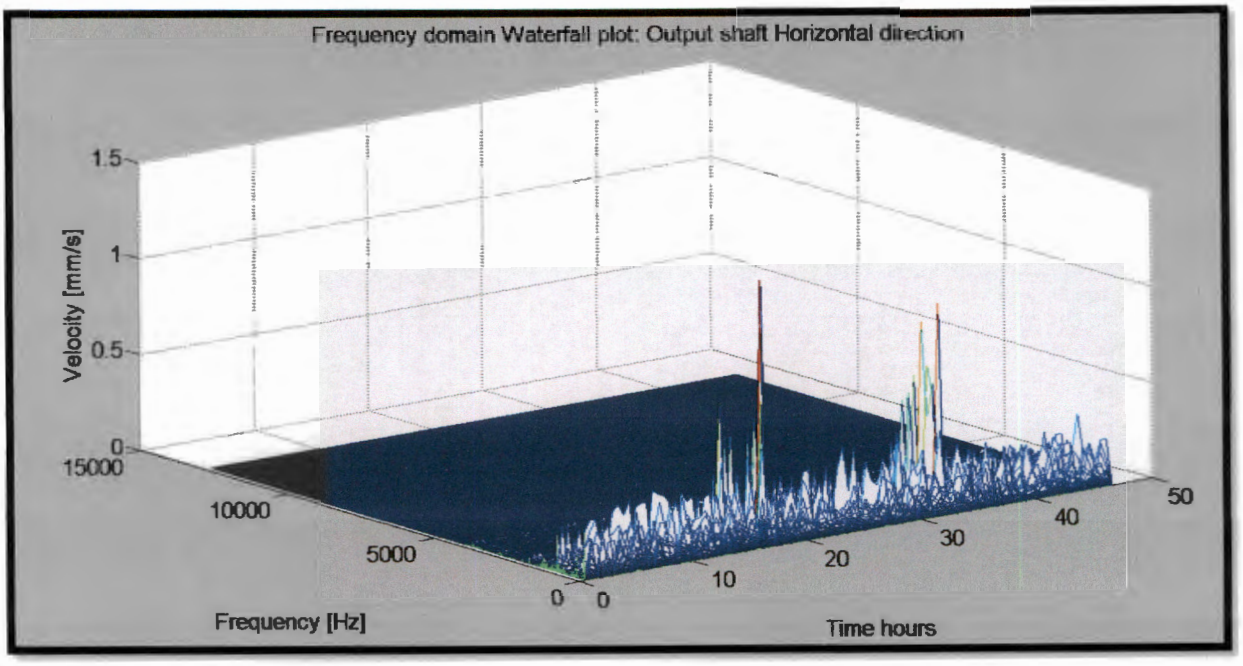

Figure 5.38: Frequency domain velocity waterfall graph, output shaft bearing, horizontal direction

5.6 Defect deviation

Vibration signals as observed at the increasing stages of wear were used for comparison. No indication of wear could be observed in the measured vibration signals of the new gearbox, because there was no wear. Vibration measurements were taken at the beginning of the 48-hour test (directly after certain defects were created), and then also every half an hour during the 48-hour test period. The vibration signals contained signs of wear at Bearing A as well as gear pair 1, for the increasing stages of wear.

Each gear pair and each ball bearing has its own unique defect frequency values. Each of these values was evaluated to determine which gear pair or which bearing was damaged. In the case of a bearing, the specific location of the damage at the bearing could be identified and this is related to the specific bearing defect frequency value.

The frequency domain acceleration signals obtained from the four acceleration meters (see Figures 4.16 and 4.17 in Chapter 4 for their specific positions and directions at the gearbox) are shown in Figure 5.39, but are here applicable to the new gearbox, before the beginning of the 48-hour test.

The frequency domain acceleration signals obtained from the four acceleration meters (see Figures 4.16 and 4.17 in Chapter 4 for their specific positions and directions at the gearbox) are shown in Figure 5.40 but are here applicable to the beginning of the 48-hour test. When these corresponding acceleration frequency domain signals are compared to those in Figure 5.39, it was found that the amplitudes at the gear mesh frequency of the first gear pair increased rapidly. It should be kept in mind that a small defect was created at the input shaft gear (Gear 1, see Figure 4 .3) of this gear pair as described in Paragraph 5.3.2. Amplitudes at harmonics of this gear mesh frequency also increased rapidly. These amplitudes are indicated in Table 5.4 to Table 5.7 for the different acceleration meter positions and directions respectively. In addition the presence and increase of certain bearing defect frequencies were also observed, with reference to Table 5.8 to 5.11 regarding the magnitudes of specific bearing defect frequencies.

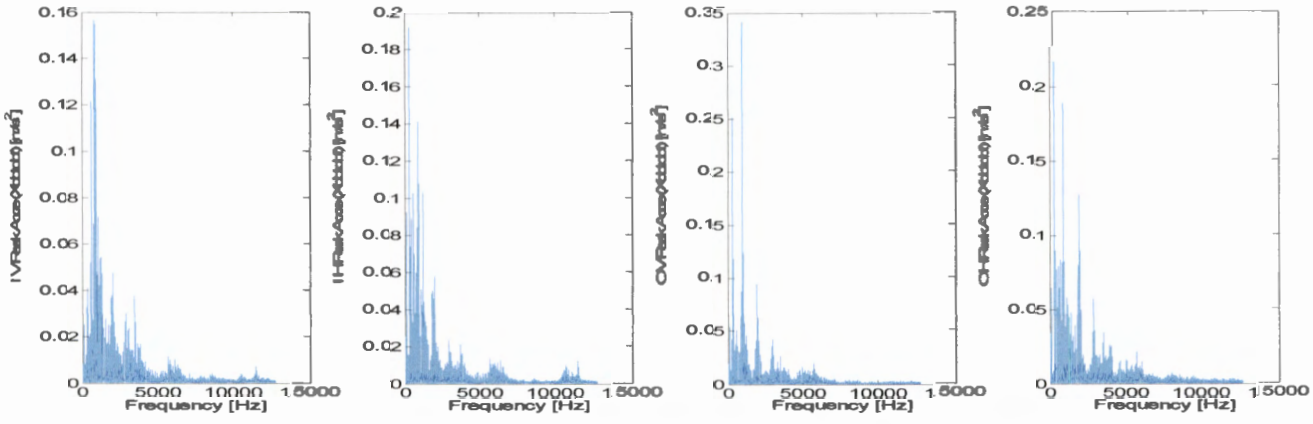

Figure 5.39: Frequency domain graphs at a new gearbox

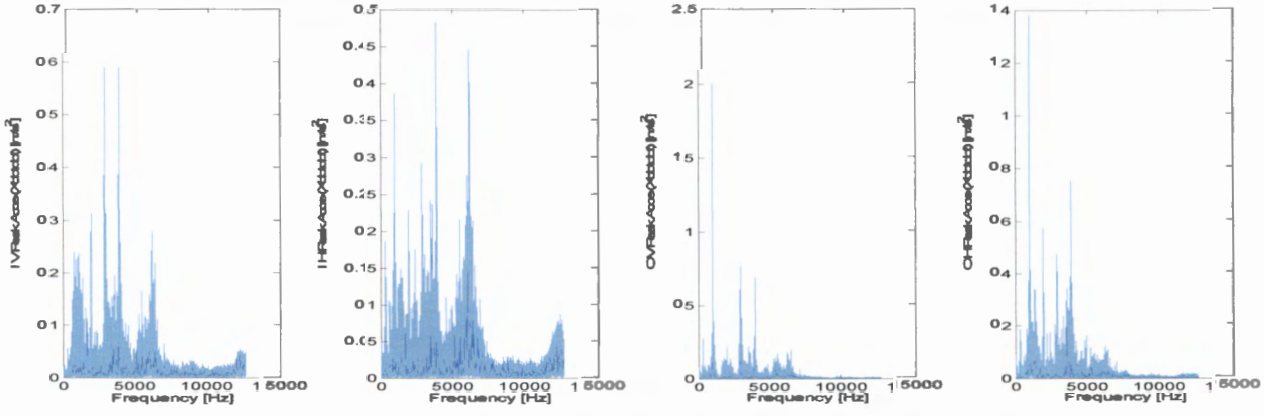

Figure 5.40: Frequency domain graphs at the beginning of the 48-hour test

The frequency domain acceleration signals obtained from the four acceleration meters (see Chapter 4 for their specific positions and directions at the gearbox) are shown in Figure 5.41 but are here applicable to the end of the 48-hour test. When the corresponding acceleration frequency domain signals shown in Figure 5.39 are compared to those in Figure 5.41 it was found that the amplitudes at the gear-mesh frequency of the first gear pair differed significantly. Amplitudes at harmonics of this gear mesh frequency also differed significantly. These amplitudes are indicated in Table 5.4 to Table 5.7 for the different acceleration meter positions and directions respectively. During the 48-hour test the misaligned gear teeth experienced wear and this could be the reason for the changes in amplitudes of gear mesh frequency and its harmonics. In addition, mainly the inner race defect frequency of the bearing at the input shaft (Bearing A, see Figure 4.3) and its harmonics drastically increased because of the increase in wear at this bearing. It should be kept in mind that a small defect was created at this bearing as described in Paragraph 5.3.3. The amplitudes at all the bearing defect frequencies are indicated in Table 5.8 to 5.11

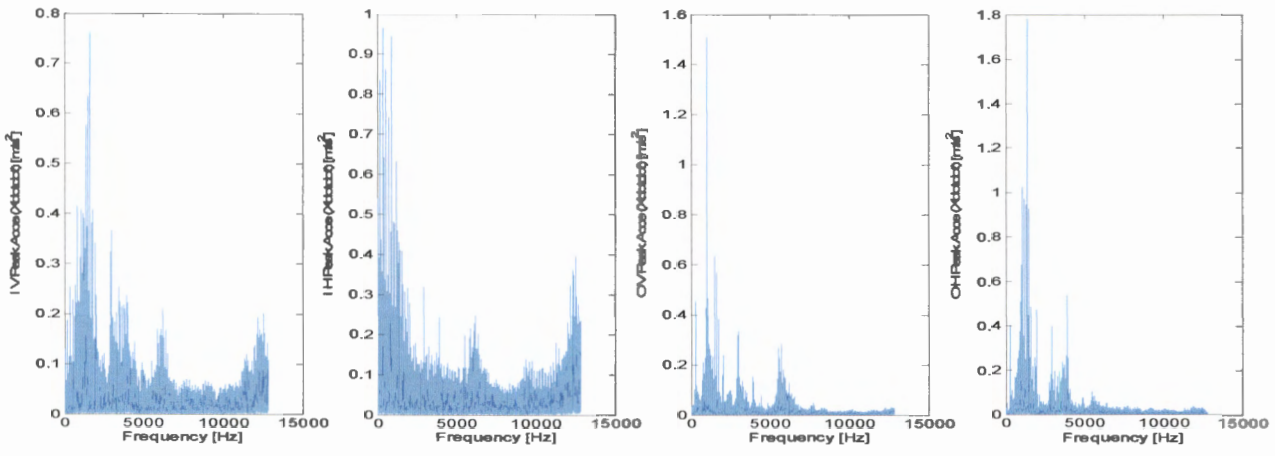

Figure 5.41: Frequency domain graphs at the end of the 48-hour test

The frequency domain acceleration signals obtained from the four acceleration meters (see Chapter 4 for their specific positions and directions at the gearbox) are shown in Figure 5.42, but are here applicable to a time during the test when load was applied, at hour number 32 (see also Table 5.1 and Paragraph 5.3.4). It was observed that amplitudes at the gear mesh frequency of the first gear pair and also some of its harmonics were significantly affected. In

addition, the amplitudes at the inner race bearing defect frequency of the bearing at the input shaft (Bearing A) as well as its harmonics were also significantly affected. It was also observed that the random frequencies in the frequency range between 10 000 and 12 000 Hz increased rapidly for the signal taken at the input shaft bearing (Bearing A) in the horizontal direction (this was also observed in the waterfall graph as shown in Figure 5.32). This phenomenon observed is related to the increase in damage at the inner race and the dynamic overloading of this bearing.

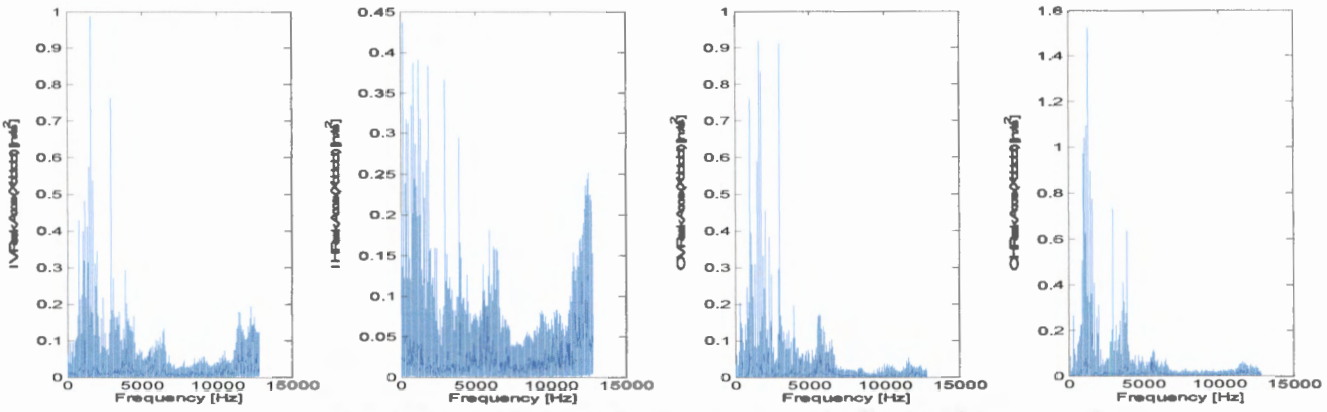

Figure 5.42: Frequency domain graphs during load [hour 32]

5.6.1 Gear defect vibration values

Acceleration amplitudes at the gear mesh frequency and five orders for the first gear pair are indicated in Table 5.4 for vibration measurements taken at the input shaft bearing in the vertical direction. This was done for vibration measurements taken at a new gearbox, at the beginning and also at the end of the 48-hour test respectively. These measured frequency values coincided with the predicted corresponding values (see Chapter 4, Table 4.5).

Table 5.4: Acceleration amplitudes at gear mesh frequencies for first gear pair [m/s^2]

Input shaft bearing, vertical direction, IV						
Order	**X 1**	**X 2**	**X 3**	**X 4**	**X 5**	**X 6**
f_{gm1} **[Hz]**	**972.4**	**1944.8**	**2917.2**	**3889.6**	**4862**	**5834.4**
New gearbox	0.065	0.032	0.030	0.006	0.005	0.004
At the beginning of the 48-hour test	0.172	0.279	0.413	0.387	0.017	0.092
At the end of the48-hour test	0.227	0.250	0.765	0.290	0.050	0.067

Acceleration amplitudes at the gear mesh frequency and five orders for the first gear pair are indicated in Table 5.5 for vibration measurements taken at the input shaft bearing in the

horizontal direction. This was done for vibration measurements taken at a new gearbox, at the beginning and also at the end of the 48-hour test respectively. These measured frequency values coincided with the predicted corresponding values (see Chapter 4, Table 4.5).

Table 5.5: Acceleration amplitudes at gear mesh frequencies for first gear pair [m/s^2]

Input shaft bearing, horizontal direction, IH						
Order	**X 1**	**X 2**	**X 3**	**X 4**	**X 5**	**X 6**
f_{gm1} **[Hz]**	**972.4**	**1944.8**	**2917.2**	**3889.6**	**4862**	**5834.4**
New gearbox	0.108	0.046	0.023	0.006	0.007	0.003
At the beginning of the 48-hour test	0.388	0.220	0.223	0.483	0.043	0.131
At the end of the48-hour test	0.287	0.069	0.366	0.295	0.059	0.125

Acceleration amplitudes at the gear mesh frequency and five orders for the first gear pair are indicated in Table 5.6 for vibration measurements taken at the output shaft bearing (Bearing F) in the vertical direction. This was done for vibration measurements taken at a new gearbox, at the beginning and also at the end of the 48-hour test respectively. These measured frequency values coincided with the predicted corresponding values (see Chapter 4, Table 4.5).

Table 5.6: Acceleration amplitudes at gear mesh frequencies for first gear pair [m/s^2]

Output shaft bearing, vertical direction, OV						
Order	**X 1**	**X 2**	**X 3**	**X 4**	**X 5**	**X 6**
f_{gm1} **[Hz]**	**972.4**	**1944.8**	**2917.2**	**3889.6**	**4862**	**5834.4**
New gearbox	0.342	0.087	0.023	0.098	0.007	0.005
At the beginning of the 48-hour test	2.009	0.126	0.468	0.292	0.102	0.035
At the end of the48-hour test	0.763	0.243	0.912	0.166	0.074	0.099

Acceleration amplitudes at the gear mesh frequency and five orders for the first gear pair are indicated in Table 5.7 for vibration measurements taken at the output shaft bearing in the horizontal direction. This was done for vibration measurements taken at a new gearbox, at the beginning and also at the end of the 48-hour test respectively. These measured frequency values coincided with the predicted corresponding values (see Chapter 4, Table 4.5).

Table 5.7: Acceleration amplitudes at gear mesh frequencies for first gear pair [m/s^2]

Output shaft bearing, horizontal direction, OH						
Order	**X 1**	**X 2**	**X 3**	**X 4**	**X 5**	**X 6**
f_{gm1} **[Hz]**	**972.4**	**1944.8**	**2917.2**	**3889.6**	**4862**	**5834.4**
New gearbox	0.046	0.128	0.028	0.014	0.007	0.003
At the beginning of the 48-hour test	1.381	0.577	0.351	0.754	0.149	0.076
At the end of the48-hour test	0.886	0.187	0.734	0.427	0.085	0.062

From Tables 5.4 to 5.7 it is clear that corresponding amplitudes differed significantly which proved changes regarding gear teeth wear and alignment as changes in mechanical condition.

5.6.2 Bearing-defect vibration values

Acceleration amplitudes at the four different bearing defect frequencies and five orders for Bearing A are indicated in Table 5.8 for vibration measurements taken at the input shaft bearing in the vertical direction (see also Chapter 2). This was done for vibration measurements taken for the gearbox when new and at the beginning and the end of the 48-hour test respectively. These measured frequency values coincided with the predicted corresponding values (see Chapter 4, Table 4.7). The increase in amplitude magnitudes over time during the 48-hour test indicates more damage, as clearly observed for the ball-pass frequency at the inner race of Bearing A (see Table 5.8). The amplitudes at the harmonics were also affected. Values for the harmonics of the fundamental-train frequency f_{ft} and harmonics of the fundamental ball-spin frequency f_{bs} were not listed in Tables 5.8 to 5.11, because amplitudes at these frequencies were not clearly observed in the corresponding measured frequency domain signals. This indicated that no severe defect was present on the ball or cage of Bearing A. The fundamental values of these frequencies were however observed in the measured corresponding frequency domain signals, and thus indicated in Tables 5.8 to 5.11.

Table 5.8: Bearing defect frequency acceleration amplitudes [m/s^2]

Bearing A: 6008/2RS1-C3 input shaft bearing, vertical direction, IV						
Order	**X 1**	**X 2**	**X 3**	**X 4**	**X 5**	**X 6**
f_{ft} **[Hz]**	**10.64**	-	-	-	-	-
New gearbox	0.0005746	-	-	-	-	-
At the beginning of the 48-hour test	0.00563	-	-	-	-	-
At the end of the 48-hour test	0.01819	-	-	-	-	-
f_{bpo} **[Hz]**	**127.63**	**255.26**	**382.89**	**510.52**	**638.14**	**765.77**
New gearbox	0.02515	0.01208	0.01006	0.01538	0.1215	0.02248
At the beginning of the 48-hour test	0.01321	0.01665	0.03122	0.02478	0.1014	0.2405
At the end of the 48-hour test	0.0395	0.03626	0.05278	0.04163	0.06212	0.08727
f_{bpi} **[Hz]**	**171.63**	**343.26**	**514.89**	**686.52**	**858.16**	**1029.79**
New gearbox	0.004565	0.04109	0.01635	0.02728	0.1548	0.04216
At the beginning of the 48-hour test	0.01003	0.02893	0.05746	0.1158	0.1929	0.0758
At the end of the 48-hour test	0.09409	0.09512	0.09716	0.1702	0.03086	0.2502
f_{bs} **[Hz]**	**82.97**	-	-	-	-	-
New gearbox	0.0005606	-	-	-	-	-
At the beginning of the 48-hour test	0.003972	-	-	-	-	-
At the end of the 48-hour test	0.01575	-	-	-	-	-

Acceleration amplitudes at the four different bearing-defect frequencies and five orders for Bearing A are indicated in Table 5.9 for vibration measurements taken at the input shaft bearing in the horizontal direction (see also Chapter 2). This was done for vibration measurements taken at a new gearbox, at the beginning and also at the end of the 48-hour test respectively. These measured frequency values coincided with the predicted corresponding values (see Chapter 4, Table 4.7). The increase in amplitude magnitudes over time during the 48-hour test indicates more damage as clearly observed for the ball-pass frequency at the inner race of Bearing A (see Table 5.9). The amplitudes at the harmonics were also affected.

Table 5.9: Bearing defect frequency acceleration amplitudes [m/s^2]

Bearing A: 6008/2RS1-C3 input shaft bearing , horizontal direction, IH						
Order	**X 1**	**X 2**	**X 3**	**X 4**	**X 5**	**X 6**
f_{ft} **[Hz]**	**10.64**	-	-	-	-	-
New gearbox	0.0002624	-	-	-	-	-
At the beginning of the 48-hour test	0.005073	-	-	-	-	-
At the end of the 48-hour test	0.02871	-	-	-	-	-
f_{bpo} **[Hz]**	**127.63**	**255.26**	**382.89**	**510.52**	**638.14**	**765.77**
New gearbox	0.09237	0.01508	0.01762	0.03105	0.06356	0.01828
At the beginning of the 48-hour test	0.03133	0.05513	0.1124	0.03243	0.06488	0.09818
At the end of the 48-hour test	0.1005	0.07414	0.08185	0.0371	0.08621	0.1009
f_{bpi} **[Hz]**	**171.63**	**343.26**	**514.89**	**686.52**	**858.16**	**1029.79**
New gearbox	0.008281	0.07395	0.02458	0.02506	0.1412	0.01316
At the beginning of the 48-hour test	0.02361	0.03648	0.02258	0.05425	0.0965	0.01362
At the end of the 48-hour test	0.4369	0.3171	0.3128	0.3345	0.3869	0.2357
f_{bs} **[Hz]**	**82.97**	-	-	-	-	-
New gearbox	0.0002359	-	-	-	-	-
At the beginning of the 48-hour test	0.00816	-	-	-	-	-
At the end of the 48-hour test	0.05231	-	-	-	-	-

Acceleration amplitudes at the four different bearing-defect frequencies and five orders for Bearing A are indicated in Table 5.10 for vibration measurements taken at the output shaft bearing in the vertical direction (see also Chapter 2). This was done for vibration measurements taken at a new gearbox, at the beginning and also at the end of the 48-hour test respectively. These measured frequency values coincided with the predicted corresponding values (see Chapter 4, Table 4.7).

Table 5.10: Bearing defect frequency acceleration amplitudes [m/s^2]

Bearing A: 6008/2RS1-C3 output shaft bearing, vertical direction, OV						
Order	**X 1**	**X 2**	**X 3**	**X 4**	**X 5**	**X 6**
f_{ft} **[Hz]**	**10.64**	-	-	-	-	-
New gearbox	0.000264	-	-	-	-	-
At the beginning of the 48-hour test	0.002018	-	-	-	-	-
At the end of the 48-hour test	0.000872	-	-	-	-	-
f_{bpo} **[Hz]**	**127.63**	**255.26**	**382.89**	**510.52**	**638.14**	**765.77**
New gearbox	0.05392	0.03557	0.0313	0.02873	0.03625	0.02466
At the beginning of the 48-hour test	0.03758	0.07839	0.02917	0.06399	0.03613	0.04547
At the end of the 48-hour test	0.06064	0.06039	0.1164	0.04261	0.07697	0.08284
f_{bpi} **[Hz]**	**171.63**	**343.26**	**514.89**	**686.52**	**858.16**	**1029.79**
New gearbox	0.01249	0.1188	0.02105	0.01318	0.06533	0.058
At the beginning of the 48-hour test	0.01482	0.03603	0.03711	0.09101	0.1292	0.1262
At the end of the 48-hour test	0.03126	0.07084	0.07697	0.07383	0.07072	0.162
f_{bs} **[Hz]**	**82.97**	-	-	-	-	-
New gearbox	0.001343	-	-	-	-	-
At the beginning of the 48-hour test	0.0009557	-	-	-	-	-
At the end of the 48-hour test	0.0008287	-	-	-	-	-

Acceleration amplitudes at the four different bearing-defect frequencies and five orders for Bearing A are indicated in Table 5.11 for vibration measurements taken at the output shaft bearing in the horizontal direction (see also Chapter 2). This was done for vibration measurements taken at a new gearbox, at the beginning and also at the end of the 48-hour test respectively. These measured frequency values coincided with the predicted corresponding values (see Chapter 4, Table 4.7). The damaged bearing was thus clearly and successfully identified through vibration signal analysis.

Table 5.11: Bearing-defect frequency acceleration amplitudes [m/s^2]

Bearing A: 6008/2RS1-C3 output shaft bearing, horizontal direction, OH						
Order	**X 1**	**X 2**	**X 3**	**X 4**	**X 5**	**X 6**
f_{ft} **[Hz]**	**10.64**	-	-	-	-	-
New gearbox	0.0007702	-	-	-	-	-
At the beginning of the 48-hour test	0.0008811	-	-	-	-	-
At the end of the 48-hour test	0.0009937	-	-	-	-	-
f_{bpo} **[Hz]**	**127.63**	**255.26**	**382.89**	**510.52**	**638.14**	**765.77**
New gearbox	0.06482	0.008725	0.02835	0.03898	0.04818	0.01947
At the beginning of the 48-hour test	0.01802	0.04287	0.1008	0.02039	0.04315	0.1918
At the end of the 48-hour test	0.0181	0.01504	0.0825	0.05462	0.07299	0.1319
f_{bpi} **[Hz]**	**171.63**	**343.26**	**514.89**	**686.52**	**858.16**	**1029.79**
New gearbox	0.002963	0.09018	0.03219	0.08378	0.1023	0.02022
At the beginning of the 48-hour test	0.008518	0.03745	0.03692	0.05471	0.1683	0.3162
At the end of the 48-hour test	0.02253	0.06008	0.02175	0.08338	0.2276	0.2411
f_{bs} **[Hz]**	**82.97**	-	-	-	-	-
New gearbox	0.0005037	-	-	-	-	-
At the beginning of the 48-hour test	0.001208	-	-	-	-	-
At the end of the 48-hour test	0.0005263	-	-	-	-	-

5.7 High-frequency energy

The high frequency region between 6 and 12 kHz could be used for enveloping analysis regarding the gears and bearings. The frequency domain signal for the input shaft bearing in the horizontal direction is shown in Figure 5.43 for the new gearbox, before defects were created and thus before the 48-hour test. The frequency domain signal for the input shaft bearing in the horizontal direction is shown in Figure 5.46, taken at the end of the 48-hour test. When these two signals were compared, it was found that the presence of many random types of amplitude at various frequencies in the frequency range between 6 to 12 kHz was observed. The presence of the amplitudes in this frequency range represented the enveloping energy. A typical measured frequency domain signal with a spectrum range from 0 to 12.5 kHz contained many visible amplitudes (see Figures 5.43 and 5.46).

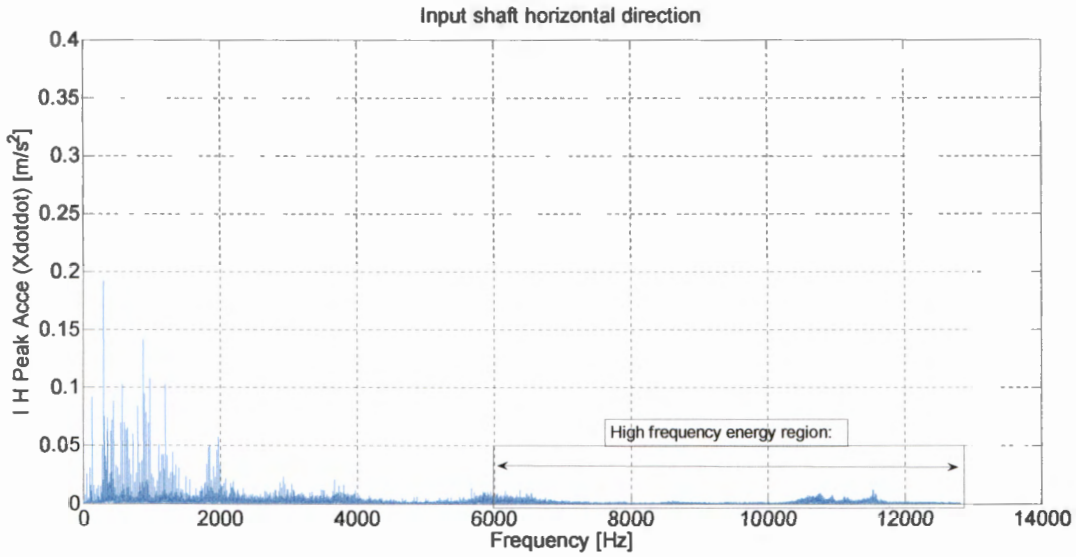

Figure 5.43: Frequency domain graph at a new gearbox, input shaft bearing, horizontal direction

The frequency domain signal shown in Figure 5.43 was used to construct a zoom view for the lower frequency range, with a maximum frequency around 1100 Hz, as indicated in Figure 5.44. The presence of amplitudes at the bearing inner race defect frequency and its harmonics were investigated as part of thorough signal analysis to monitor defect and wear progression, and indicated in this graph. It should be kept in mind that this signal was obtained at the input shaft bearing in the horizontal direction, for the new gearbox, before defects were created and thus before the 48-hour test.

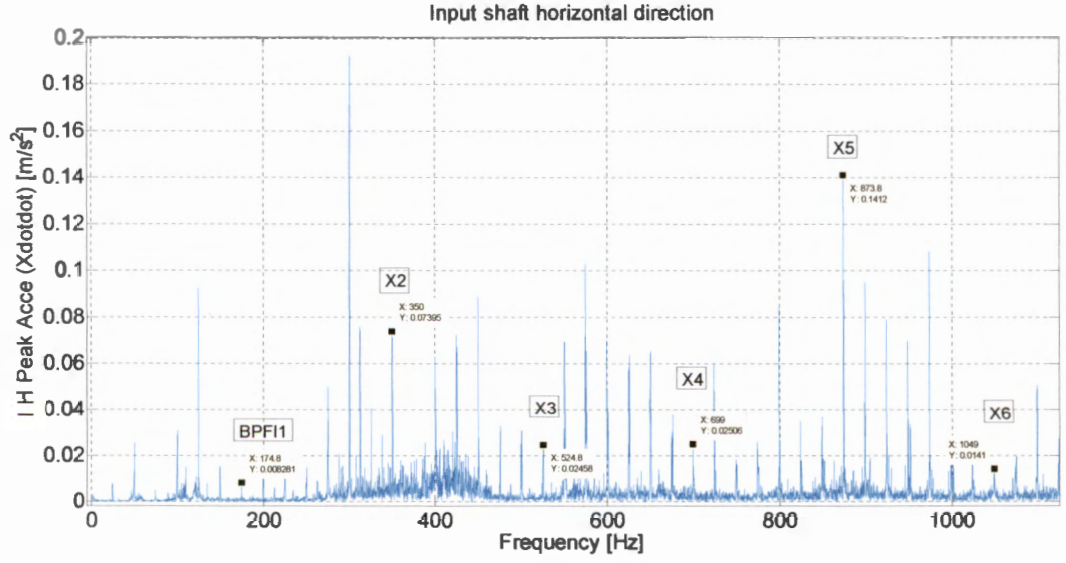

Figure 5.44: Inner race ball pass frequency of Bearing A f_{bpi} (see Figure 4.3), in frequency domain graph between 0 – 1200 Hz, at a new gearbox

The frequency domain signal shown in Figure 5.43 was used to construct a zoom view for the lower frequency range, with a maximum frequency around 6200 Hz, as indicated in Figure 5.45. The presence of amplitudes at the first gear pair gear mesh frequency and its harmonics were investigate, and indicated in this graph. It should be kept in mind that this signal was obtained at the input shaft bearing in the horizontal direction, for the new gearbox, before defects were created and thus before the 48-hour test.

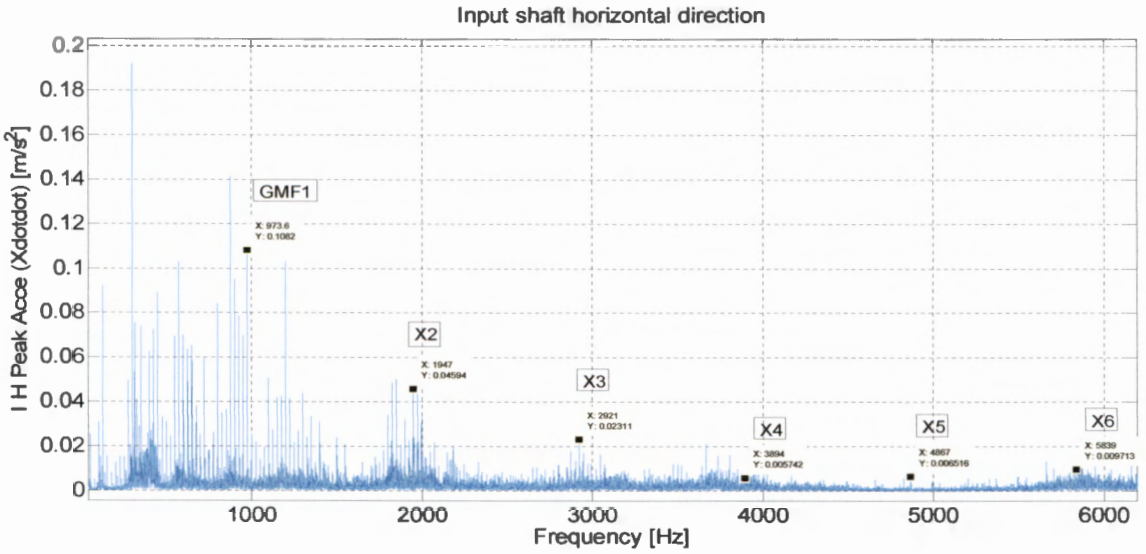

Figure 5.45: Gear mesh frequency of gear pair 1 f_{gm1} (see Figure 4.3), in frequency domain graph between 0 – 6200 Hz, at a new gearbox

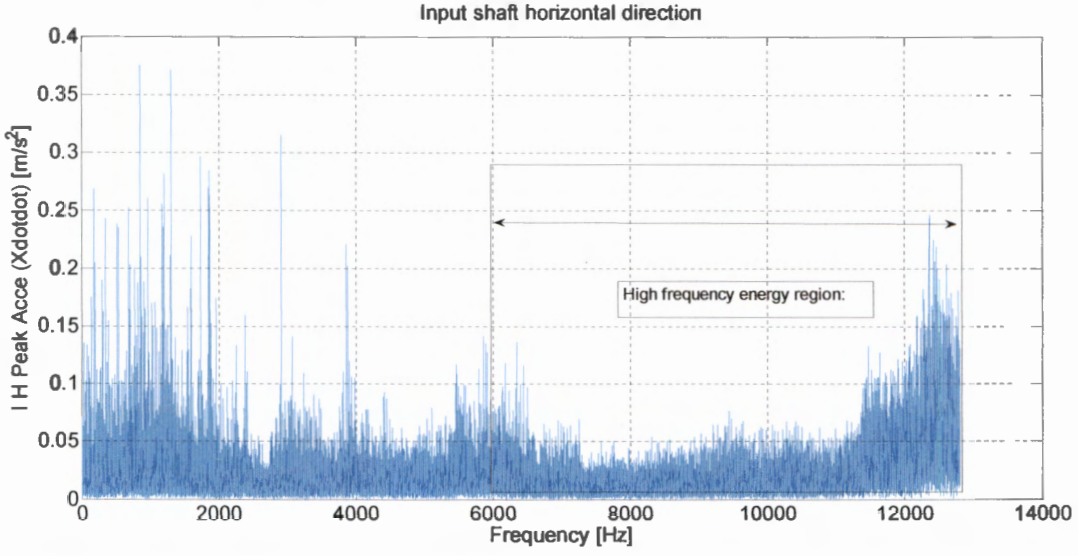

Figure 5.46: Frequency domain graph at the end of the 48-hour test, input shaft bearing, horizontal direction

The frequency domain signal shown in Figure 5.46 was used to construct a zoom view for the lower frequency range, with a maximum frequency around 1200 Hz, as indicated in Figure 5.47. The presence of amplitudes at the bearing inner race defect frequency and its harmonics were investigated, and indicated in this graph. It should be kept in mind that this signal was obtained at the input shaft bearing in the horizontal direction, for the signal taken at the end of the 48-hour test.

The fundamental ball pass frequency of the inner race of Bearing A and also its harmonics are observed and indicated in Figure 5.47, which is a zoom view of Figure 5.46. This was a good indication that the defect at a certain bearing could be detected. The exact location of the defect at Bearing A could also be detected after analysis of an acceleration frequency domain signal. This indicated that the defect was located at the inner ring of Bearing A and that the bearing had a large defect at the inner ring, because these measured frequencies corresponded with the theoretical computed bearing defect inner race frequency and its harmonics. When Figure 5.47 is analysed in detail, it revealed that the amplitudes relate to bearing defect frequencies, gear defect frequencies, and also shaft speeds of the input, intermediate and output shafts of the gearbox. The harmonics of these frequencies were also observed on Figure 5.47

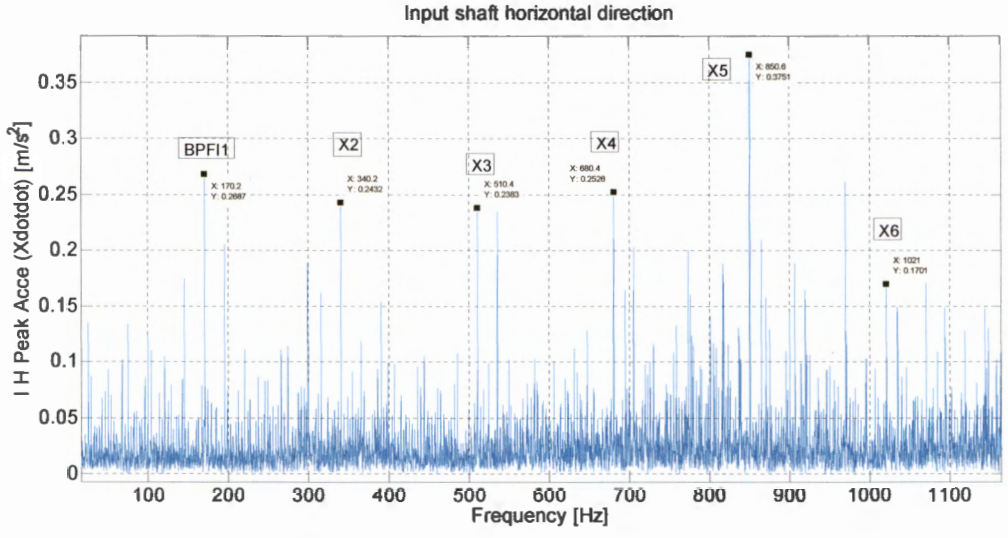

Figure 5.47: Inner race ball pass frequency of Bearing A f_{bpi} (see Figure 4.3), in frequency domain graph between 0 – 1200 Hz, at the end of the 48-hour test

The frequency domain signal shown in Figure 5.46 was used to construct a zoom view for the lower frequency range, with a maximum frequency around 6500 Hz, as indicated in Figure 5.48. The presence of amplitudes at the first gear pair gear mesh frequency and its harmonics were investigated, and indicated in this graph. It should be kept in mind that this signal was obtained at the input shaft bearing in the horizontal direction, for the signal taken at the end of the 48-hour test.

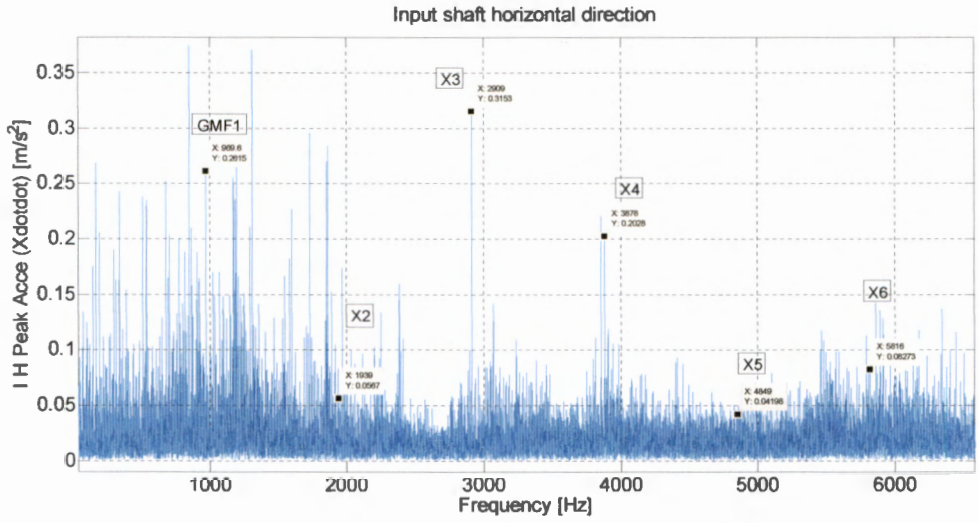

Figure 5.48: Gear mesh frequency of gear pair 1 f_{gm1} (see Figure 4.3), in frequency domain graph between 0 – 6500 Hz, at the end of the 48-hour test

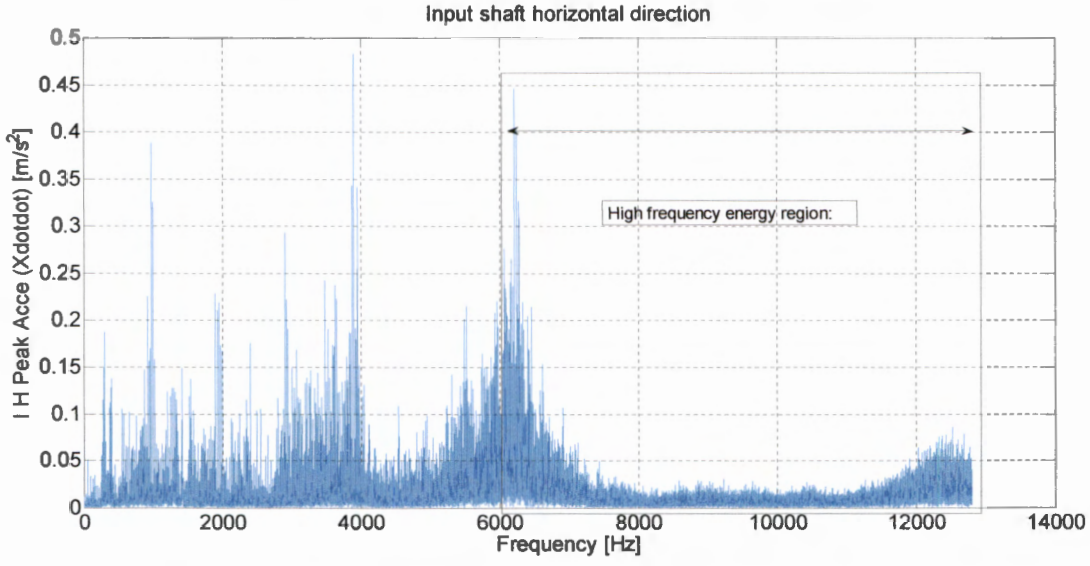

Figure 5.49: Frequency domain graph at the beginning of the 48-hour test, input shaft bearing, horizontal direction

The frequency domain signal for the input shaft bearing in the horizontal direction is shown in Figure 5.49, at the beginning of the 48-hour test. The frequency domain signal shown in Figure 5.49 was used to construct a zoom view for the lower frequency range, with a maximum frequency around 1150 Hz, as indicated in Figure 5.50. The presence of amplitudes at the bearing inner race defect frequency and its harmonics were investigated, and indicated in this graph. It should be kept in mind that this signal was obtained at the input shaft bearing in the horizontal direction, for the signal taken at the beginning of the 48-hour test.

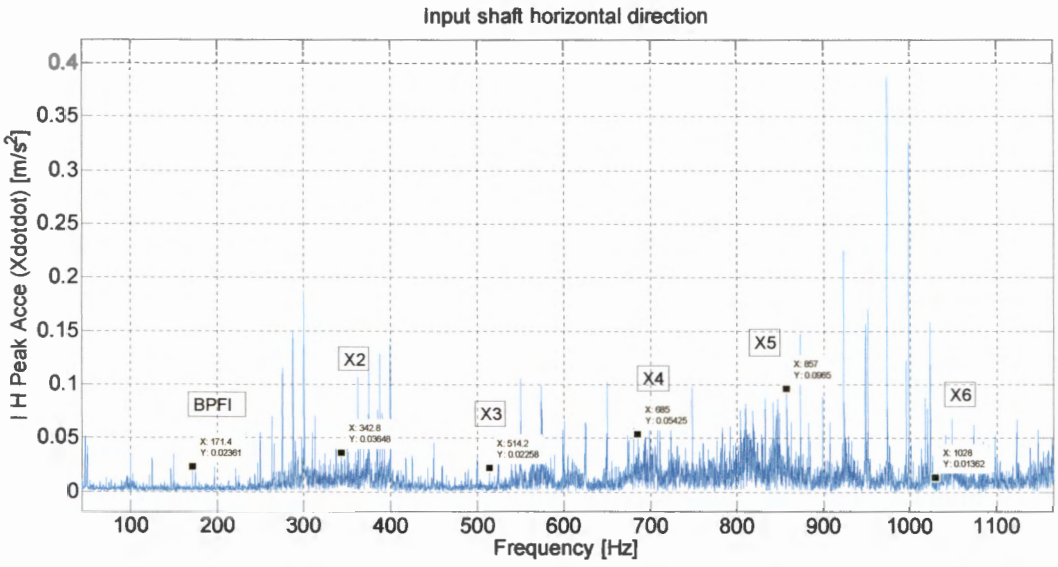

Figure 5.50: Inner race ball pass frequency of Bearing A f_{bpi} (see Figure 4.3), in frequency domain graph between 0 – 1200 Hz, at the beginning of the 48-hour test

The frequency domain signal shown in Figure 5.49 was used to construct a zoom view for the lower frequency range, with a maximum frequency around 7200 Hz, as indicated in Figure 5.51. The presence of amplitudes at the first gear pair gear mesh frequency and its harmonics were investigated, and indicated in this graph. It should be kept in mind that this signal was obtained at the input shaft bearing in the horizontal direction, for the signal taken at the beginning of the 48-hour test.

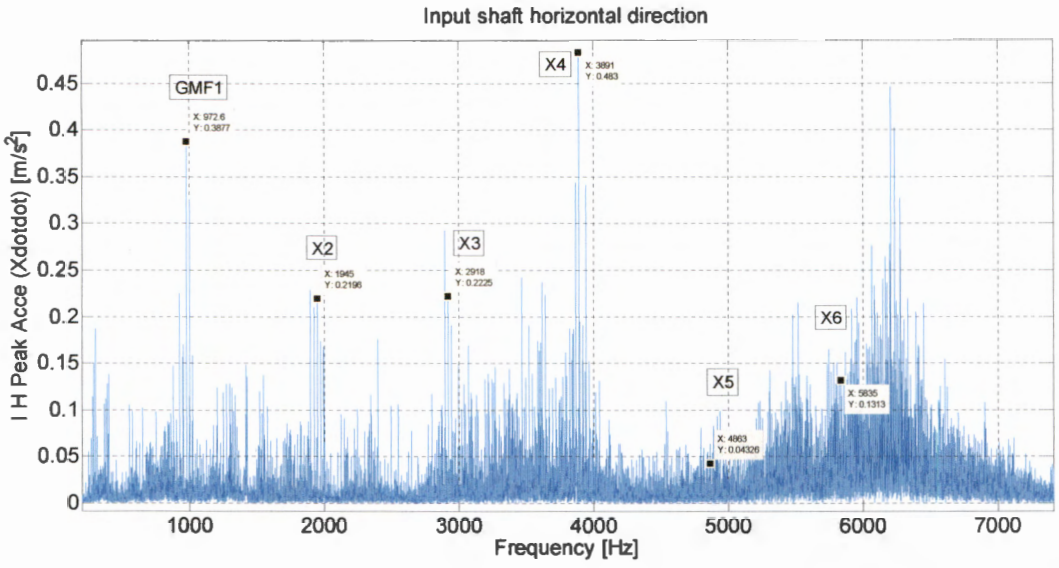

Figure 5.51: Gear mesh frequency of gear pair 1 f_{gm1} (see Figure 4.3), in frequency domain graph between 0 – 7200 Hz, at the beginning of the 48-hour test

It was found that amplitudes at the bearing inner race defect frequency and its harmonics increased and reached a maximum at the end of the 48-hour test, as indicated in Table 5.12, for the vibration measurements taken at Bearing A in the horizontal direction. It was found that amplitudes at the gear mesh frequency and its harmonics of the first gear pair changed, without any drastic increase or decrease at the end of the 48-hour test, as indicated in Table 5.13, for the vibration measurements taken at Bearing A in the horizontal direction. It is thus strongly suspected that the enveloping energy in the frequency range between 6 and 12 kHz represents the damage at the bearing with the defect which increased over time during the 48-hour test.

Table 5.12: Bearing A inner race defect frequency f_{bpi} acceleration amplitudes [m/s^2]

Input shaft bearing horizontal direction, IH						
Order	**X 1**	**X 2**	**X 3**	**X 4**	**X 5**	**X 6**
f_{bpi} **[Hz]**	**171.63**	**343.26**	**514.89**	**686.52**	**858.16**	**1029.79**
New gearbox	0.0082	0.0739	0.0245	0.0250	0.1412	0.0131
At the beginning of the 48-hour test	0.0236	0.0364	0.0225	0.0542	0.0965	0.0136
At the end of the 48-hour test	0.4369	0.3171	0.3128	0.3345	0.3869	0.2357

Table 5.13: Gear mesh defect frequency for first gear pair f_{gm1} acceleration amplitudes [m/s^2]

Input shaft bearing horizontal direction, IH						
Order	**X 1**	**X 2**	**X 3**	**X 4**	**X 5**	**X 6**
f_{gm1} [Hz]	**972.4**	**1944.8**	**2917.2**	**3889.6**	**4862**	**5834.4**
New gearbox	0.108	0.046	0.023	0.006	0.007	0.003
At the beginning of the 48-hour test	0.388	0.220	0.223	0.483	0.043	0.131
At the end of the 48-hour test	0.287	0.069	0.366	0.295	0.059	0.125

It was possible to clearly distinguish between gear wear and ball bearing wear. Some of the calculated bearing and gear pair defect frequencies, listed in Tables 5.12 and 5.13, were observed in the measured frequency domain signals. The presence of amplitudes at these frequencies indicated that a defect was present at the component associated with the particular defect frequency. The change in wear at the bearing and gears, were observed in the variation in magnitudes of the amplitudes of the defect frequencies. Bearing and gear wear were thus easily identified and thus clearly separated. Failure of either the bearing or the gear could be predicted by the analysis of measured frequency domain signals.

5.8 Time signal analysis

Time signal analysis could be a useful tool in gearbox condition monitoring, but it is often not used to its full potential. The time domain signal for the input shaft bearing in the horizontal direction is shown in Figure 5.52, for the signal taken at the beginning of the 48-hour test. The time domain signal shown in Figure 5.52 was used to construct a zoom view for the smaller time range, as indicated in Figure 5.53. The presences of repetitive spikes in the signal were investigated. This signal revealed information of spikes with the periodic time between repetitive spikes indicated on this graph. It was found that the inverse of this periodic time corresponded to the damaged bearing inner race defect frequency around 172 Hz.

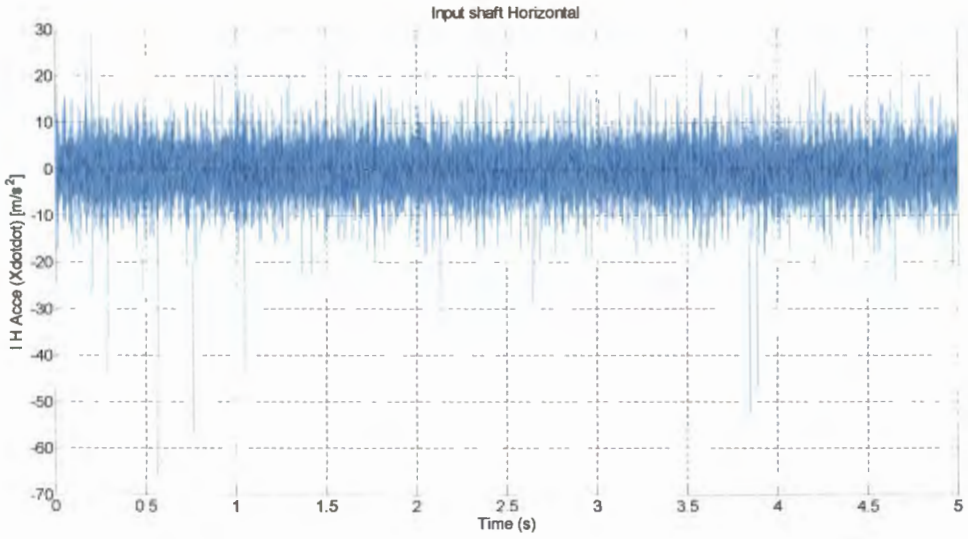

Figure 5.52: Time signal measured at beginning of the 48-hour test, input shaft bearing, horizontal direction

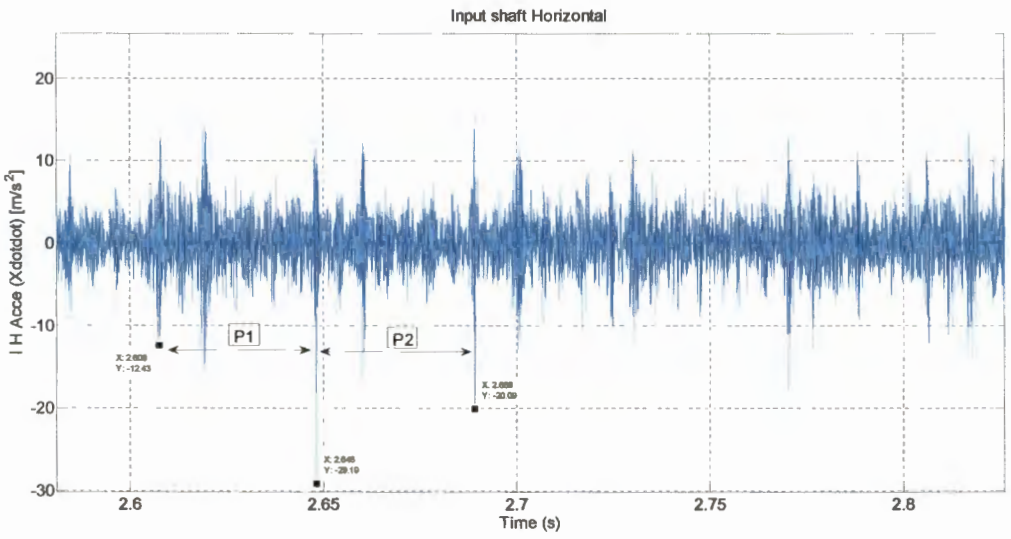

Figure 5.53: Detail view of the time signal at the beginning of the 48-hour test

The time domain signal for the input shaft bearing in the horizontal direction is shown in Figure 5.54, for the signal taken at the end of the 48-hour test. The time domain signal shown in Figure 5.54 was used to construct two different zoom views for smaller time ranges, as indicated in Figure 5.55 and Figure 5.56. The presences of repetitive spikes in these signals were investigated. These signals revealed information of spikes with the periodic time between repetitive spikes indicated on these graphs. It was found that the inverse of this periodic time corresponded to the damaged bearing inner race defect frequency around 172 Hz.

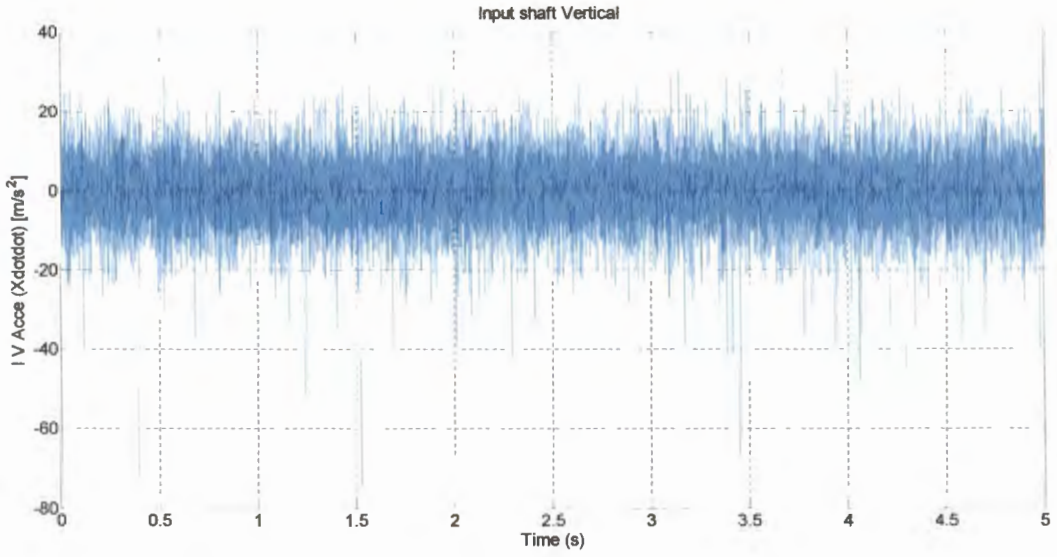

Figure 5.54: Time signal measured at end of the 48-hour test, input shaft horizontal

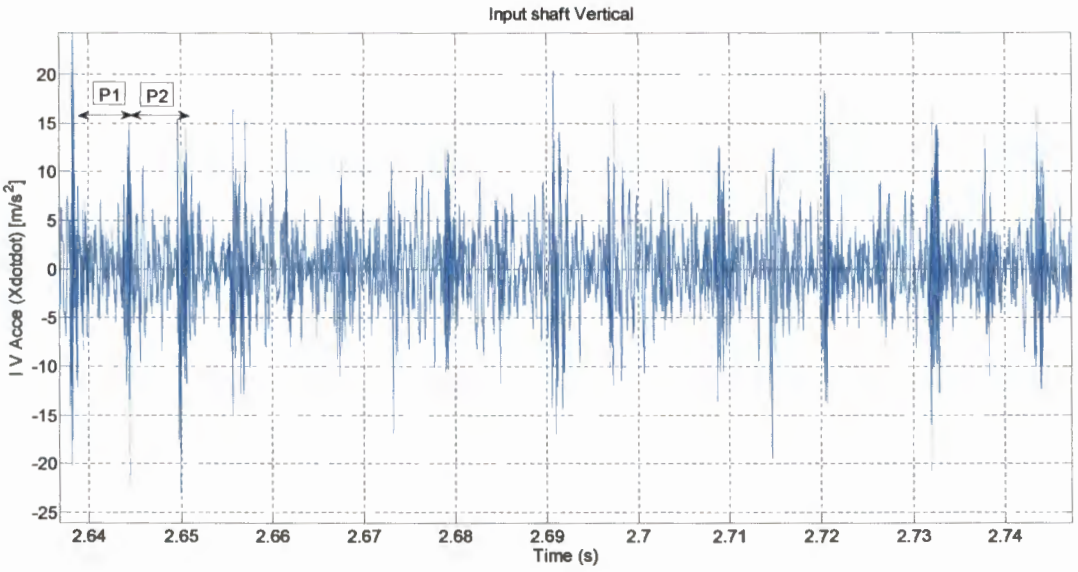

Figure 5.55: Detail view of the time signal at the end of the 48-hour test

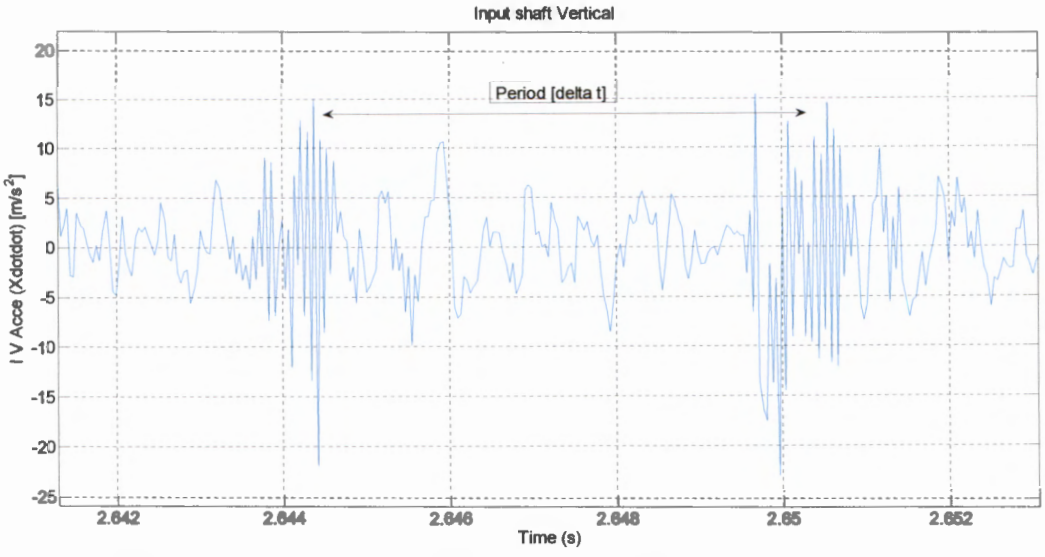

Figure 5.56: Detail view 2 of the time signal at the end of the 48-hour test

5.9 Visual inspection of defects

5.9.1 Bearings

After the 48-hour test period the gearbox was disassembled for a visual inspection of all the gears and bearings. Bearings and gears were pressed out and cleaned for inspection. Each bearing was cut open with a wire cutter in the mechanical workshop. These six bearings are shown in Figure 5.57.

Figure 5.57: Opened bearings

The inspection of the bearings did not show any visual sign of defects, except for the input shaft bearing (Bearing A, see Chapter 4, Figure 4.3) shown in Figure 5.58. The test period of 48-hours was too short for the other bearings to be damaged. Bearing A, with the defect on the bottom left corner is shown in more detail. The increased damage during the 48-hour test was observed as additional spalling marks at the inner race near the initial defect as shown in Figure 5.58 as indicated with the arrow and circle.

The outer race of Bearing A shown in Figure 5.59 was also inspected and small (almost invisible) spalling marks could be observed as an indication of initial damage as a result of surface fatigue.

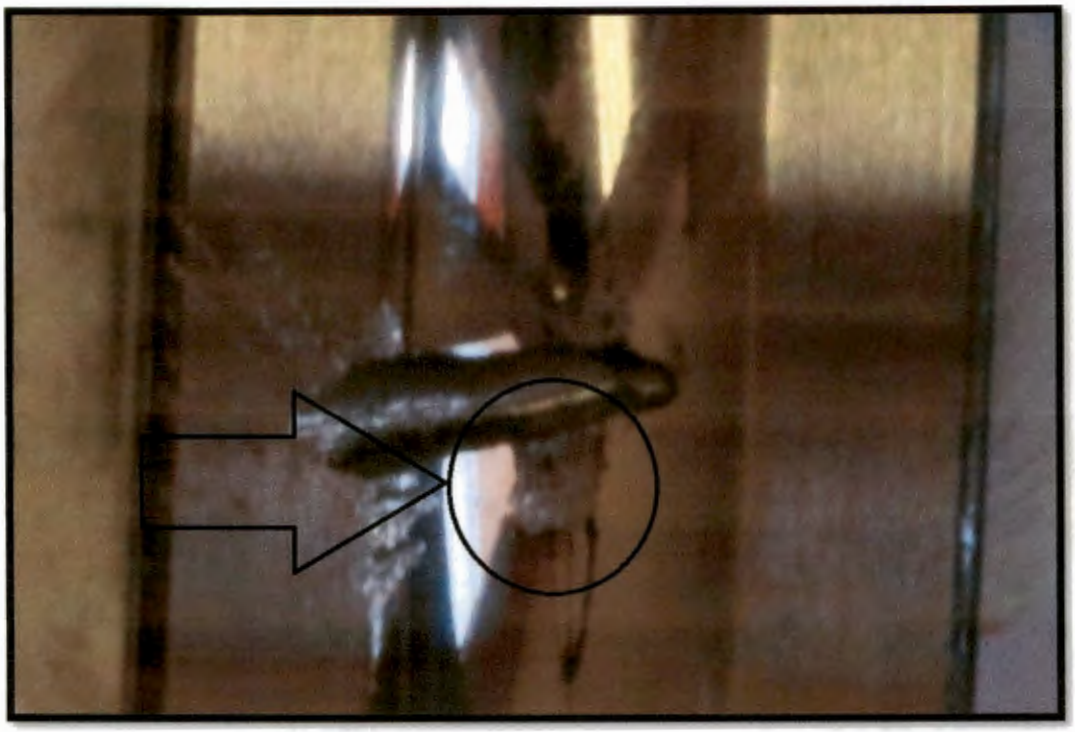

Figure 5.58: Defect on Bearing A inner race after 48-hour test (see also Figure 4.3)

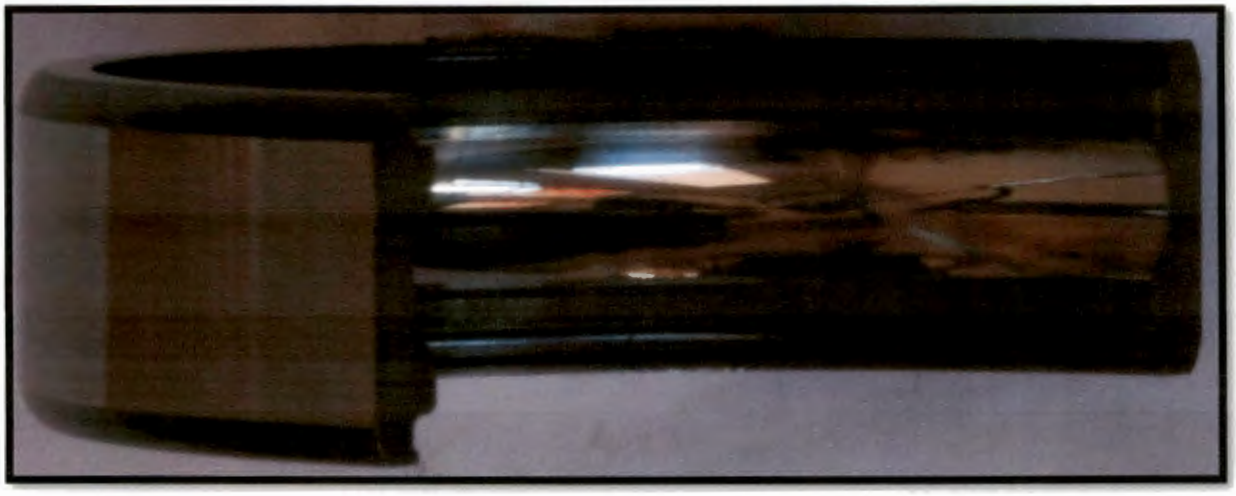

Figure 5.59: Outer race of Bearing A (see also Figure 4.3)

5.9.2 Gears

Inspection was done of all four gears (gear pair 1 is shown in Figure 5.60, and gear pair 2 shown in Figure 5.61) after the 48-hour test.

Figure 5.60: Gear pair 1 (see also Figure 4.3)

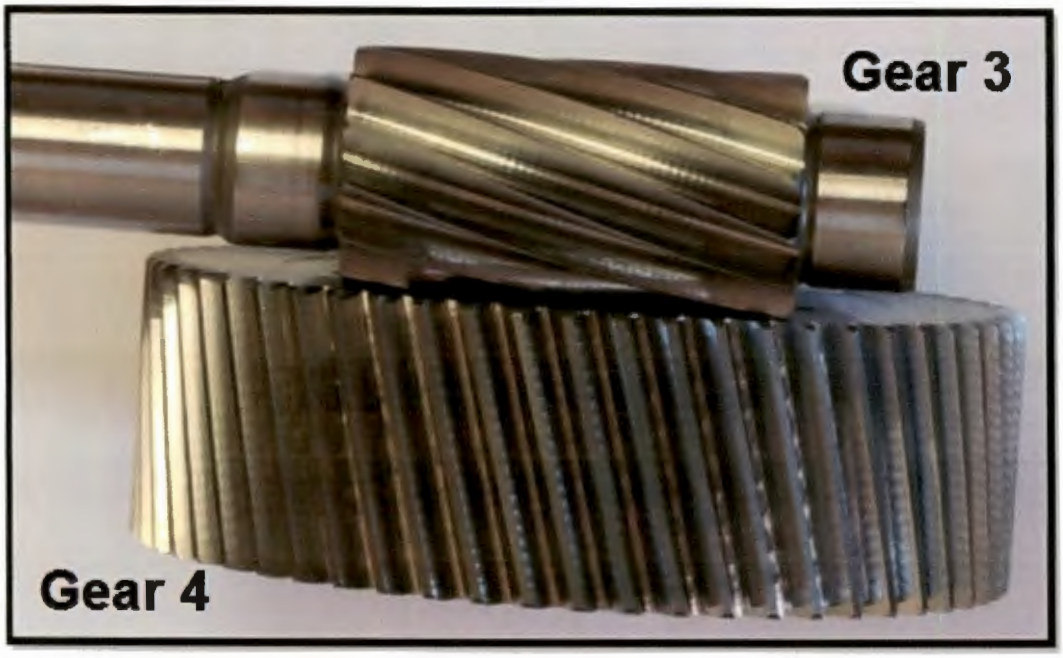

Figure 5.61: Gear pair 2 (see also Figure 4.3)

The inspection of gear pair 1 revealed clear pitting marks on the bottom between the gear teeth of Gear 2 as shown in Figure 5.62. The misalignment defect created (see Chapter 5) pushed the teeth of Gear 1 deeper into Gear 2 and this induced the damage marks observed as shown in Figure 5.62. On the rear face of the teeth on Gear 1, scuffing marks were observed as caused by the misalignment. The teeth of Gear 2 were in contact on the rear of the teeth of Gear 1, as shown in Figure 5.63. Gear 1 with the initial defect as created (see Chapter 5) is shown in Figure 5.64. No pitting marks could be observed from the human inspection done at gear pair 2.

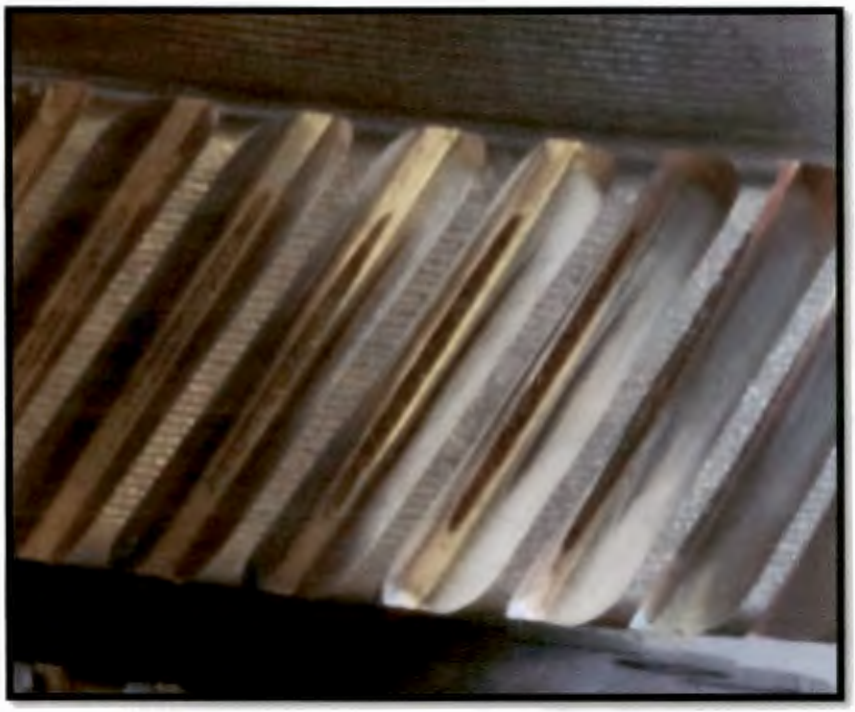

Figure 5.62: Damage at Gear 2 (see also Figure 4.3)

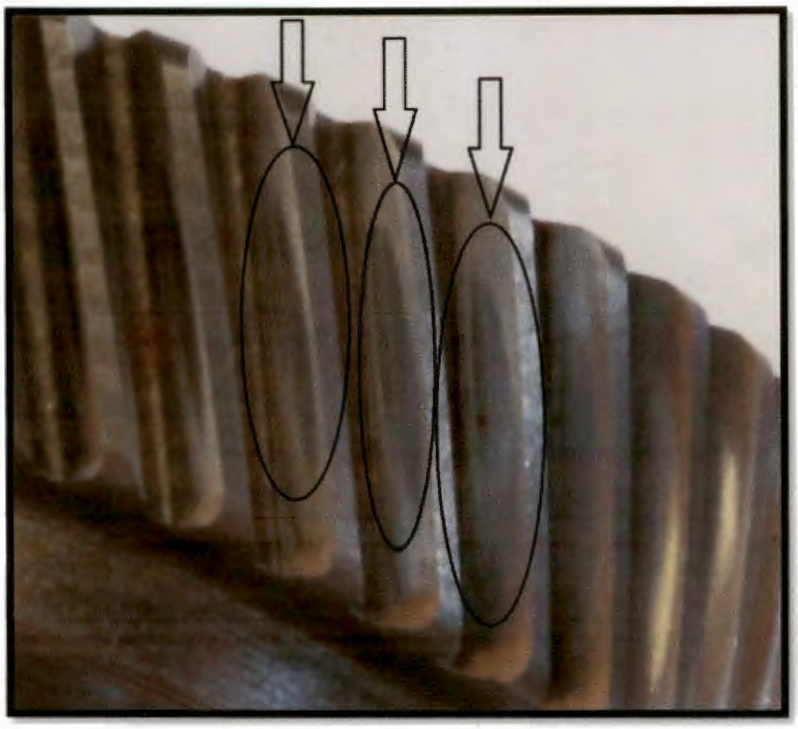

Figure 5.63:Damage at Gear 1 (see also Figure 4.3)

Figure 5.64: Impact of 48-hour test on defect induced at Gear 1 (see also Figure 4.3)

The measured data and analysis are described in Chapter 5. A cost breakdown of the experimental equipment used during this study was important to proof a cost effective condition monitoring system, as next described in Chapter 6.

6. Cost-effectiveness of the condition-monitoring system

A cost-effective condition-monitoring system (see Chapter 4 for more information and pictures shown in Figures 4.9 to 4.19) was built, and the total cost (VAT included) for this system is indicated in Table 6.1. Reliable and accurate components were chosen and linked together to create a unique system with relatively low-cost hardware and software that interacted effectively. Quotations for all the condition-monitoring system components are included in Appendix B and the overall cost breakdown indicated in Table 6.1. Quotations obtained for other typical condition-monitoring systems indicated enormously larger costs.

Table 6.1: Cost layout of condition-monitoring system

Component:	Unit Price	QTY	Total
NI cDAQ-9188 chassis for NI modules, CompactDAQ chassis (8 Slot ENET)	R 18 890.00	1	R 18 890.00
NI 9211 module for temperature measurements, 4-Ch ±80 mV, 14 S/s, 24-Bit TC and Diff AI	R 4 470.00	1	R 4 470.00
NI J-Type Thermocouples Wire, Fiberglass	R 380.00	4	R 1 520.00
NI 9234 module for vibration and current measurements	R 22 520.00	2	R 45 040.00
Matlab software, commercial individual license	R 77 633.16	1	R 77 633.16
Dytran acceleration meters, 50g range, 100mV/g and mini coax cables	R 4 426.75	4	R 17 707.00
HP 470 Laptop Windows 7	R 14 263.00	1	R 14 263.00
TeamViewer software commercial use	R 4 579.00	1	R 4 579.00
Canyon network switch	R 475.00	1	R 475.00
		Total	**R 184 102.16**

The conclusions and recommendations are described in Chapter 7.

7. Conclusions and recommendations

This study made a meaningful contribution to address typical huge industrial problems regarding unexpected gearbox failures, which often result in unnecessary maintenance costs, and also occasionally extremely large production losses. A cost-effective continuous condition-monitoring system for a gearbox was developed. A laboratory test setup was built where the condition-monitoring system sensors were attached to a gearbox. These sensors were then connected to instrumentation, and the instrumentation linked to a laptop. The monitoring system measured vibration and temperature at brief time intervals, and these parameters were effectively used as early warnings when problems started and developed over time. In addition, electrical current was also measured for changing power and torque which was then also determined for the gearbox regarding different applied loading conditions. It was possible to monitor these measured parameters during real time when the gearbox was running in the laboratory via a host computer located away from the laboratory using the Internet. The condition monitoring system developed proved that it could be effectively and reliably used at industrial applications for rotational machines.

A mathematical model was developed to describe all the different defect frequencies for each of the ball bearings in the gearbox. This model also described the gear-mesh frequencies for the gears in the gearbox. This mathematical model was implemented in a computer program, and the information obtained used in the analysis of measured data regarding possible damage to the bearings and gears.

The condition-monitoring system comprised feasible electronic hardware linked to appropriate sensors and also to a computer. A second computer program was written so that the measured parameters could be captured and indicated. In addition, a second mathematical model was developed to convert measured time-domain acceleration data into the frequency domain by using a series of Fourier coefficient amplitudes at certain frequencies and corresponding phase angles. This frequency domain acceleration data (amplitudes at certain frequencies and corresponding phase angles) were then mathematically converted to frequency domain velocity data, and also converted to frequency domain displacement data. In addition, this model made it possible to also express the time domain signals obtained from the corresponding frequency domain signals

for velocity and displacement respectively. The time domain signals for acceleration, velocity and displacement made it possible to mathematically express single overall RMS vibration magnitudes for each of these three parameters respectively. This model was then also implemented in this computer program.

The computer programs were both implemented in a Matlab environment. By using certain input parameters for the bearings and for the gears respectively as characterised, the first program computed bearing-defect frequencies and gear-mesh frequencies. This was regarded as necessary because amplitudes at these frequencies normally represent wear. The second computer program made it possible to capture measured acceleration data obtained from instrumentation, and time-domain signals were then constructed for each of the four acceleration meter inputs. The program constructed trends and graphs for the measured time and frequency domain vibration signals. The corresponding velocity and displacement frequency domain signals were then computed and constructed. The corresponding phase angle signals were also computed and constructed for acceleration, velocity and displacement respectively. By using Matlab's extensive graphical capabilities, trends for these frequency domain signals were constructed as three-dimensional waterfall plots. The program then also computed time-domain data for velocity and displacement and also constructed these corresponding time-domain signals. By using corresponding time-domain signal data, the program then also computed the overall RMS magnitudes for acceleration, velocity and displacement respectively. This computer program also captured measured temperature and electrical current data obtained from instrumentation. The measured electrical current magnitudes were used to compute changing power and torque, and corresponding trends were also constructed. Trends for temperature were also constructed. Alarm settings were programmed for certain measured parameters.

This system was developed, built and thoroughly tested to ensure accuracy and reliability of the measured data. A test setup was built in the laboratory for the experimental phase of this work. A small gearbox linked to an electrical motor with a brake at the output shaft for loading purposes was used. Instrumentation coupled to a laptop and connected to the Internet was part of this test setup.

Extensive time and frequency domain signal analysis was done for a broad range of frequencies up to 12500 Hz. The vibration signal analysis was very effective to clearly distinguish between ball bearing wear and tear on gear teeth for different stages of wear.

The pinion (Gear 1, see Chapter 4, Figure 4.3) at the input shaft of the gearbox was slightly damaged with a pencil grinder at one tooth only, and at the beginning of the 48-hour test period the amplitude at the gear mesh frequency in the frequency domain signal was significantly larger compared to when it was not damaged. The overall vibration magnitude was then also larger. The input shaft was also slightly misaligned when the 48-hour test period started, but the misalignment effect improved over time as the wear then increased at the meshing gear pair (Gear 1 and Gear 2) and became more worn in. This was revealed when the gearbox was opened after the 48-hour test period and the wear then inspected. The vibration signals thus effectively indicated a decrease in amplitude at this gear-mesh frequency over time during the 48-hour test.

The ball bearing (Bearing A, see Chapter 4, Figure 4.3) at the input shaft of the gearbox was also slightly damaged with a pencil grinder at one point on the inner race, and at the beginning of the 48-hour test period the amplitude at the inner race defect frequency in the frequency domain signal was significantly larger compared to when it was not damaged. The overall vibration magnitude was then also larger. The input shaft was also slightly misaligned when the 48-hour test period started to deliberately increase the dynamic fluctuating load on the bearings. The gearbox was opened after the 48-hour test and the wear then inspected on the inner race of this bearing. The visual inspection revealed significantly wear on the inner race of this bearing which increased from the initial induced small damage mark over the 48-hour test period. The amplitude at the inner race defect frequency and its harmonics increased over time during the 48-hour test period, which thus effectively indicated increasing wear at the inner race over time during the 48-hour test. Many small random amplitudes in the higher frequency range between 8000 and 12500 Hz were clearly observed, which increased drastically when corresponding frequency domain signals at the beginning and at the end of the 48-hour test were compared. These amplitudes were small for a vibration measurement taken before the bearing was damaged, but became significantly larger at the beginning of the 48-hour test. This observation confirmed the presence of vibration enveloping energy as repetitive events in the higher frequency range,

which also indicated increasing wear at the inner race over time during the 48-hour test. The time signal analysis also revealed very useful information regarding the bearing wear as previously described.

Loading was applied with a brake for a certain time during the 48-hour test, and the trends for electrical current, power, torque and temperature magnitudes then significantly increased as observed. The many small random amplitudes in the higher frequency range between 8000 and 12500 Hz which represent bearing wear also increased drastically during loading as clearly observed in the three-dimensional frequency domain waterfall graph.

The measured parameters namely vibration, temperature, electrical current, power and torque were made available on the Internet. The main advantage here was that the gearbox condition could be observed by other people, even in a different town or country compared to where the gearbox was actually installed and used. For example, vibration signal analysis could thus be done by experts in this field far away from where the gearbox was running, so that specific problems could be identified at an early stage.

It could be considered to rather use a Direct Current electrical motor as dynamometer instead of the hydraulic brake system that was used in this study at the test setup. Minor problems such as occasional shuttering of the disc pads and effective cooling could then be overcome, but will then be much more expensive.

It is recommended that the technology developed in this study should be used for condition monitoring of rotating machines where white metal bearings are installed such as big fans and generators at electrical power stations. Acceleration meters will then be replaced by Eddy current probes to measure relative displacement. Future work regarding vibration signal analysis should be done for different loading conditions.

REFERENCES

ÅKERBLOM, M. 2001. Gear Noise and Vibration [Elektronisk resurs] : A Literature Survey.

http://kth.diva-portal.org/smash/get/diva2:139878/FULLTEXT01.pdf. Date of access: 15 Mei 2013.

ALEXEJ, V. & NATALIA, A. Diagnostics of Gearing and Geared Couplings Using Envelope Spectrum Methods. http://www.vibrotek.com/article.php?article=articles/

AMARNATH, M. & KRISHNA, I.R.P. 2013. Detection and diagnosis of surface wear failure in a spur geared system using EEMD based vibration signal analysis. *Tribology International,* 61(0):224-234.

ANTONI, J. & RANDALL, R.B. 2002. Differential Diagnosis of Gear and Bearing. Faults *Journal of Vibration and Acoustics,* 124(2):165.

BARTELMUS, W. & ZIMROZ, R. 2009. A new feature for monitoring the condition of gearboxes in non-stationary operating conditions *Mechanical Systems and Signal Processing,* 23(5):1528 - 1534.

BASARABA, B.M. & ARCHER, J.E. 1995. IPT's Rotating Equipment Handbook IPT Publishing and Training.

BLOCH, H.P. & GEITNER, F.K. 1997. Machinery failure analysis and troubleshooting. Houston, Tex.: Gulf Pub. Co.

DALPIAZ, G., RIVOLA, A. & RUBINI, R. 2008. Gear Fault Monitoring: Comparison of Vibration Analysis Techniques CNR - Italian National Research Council.

DAVIES, A.J. 1998. Handbook of condition monitoring: techniques and methodology. London: Chapman & Hall.

DE SMIDT, M.R., HEYNS, P.S. & STANDER, C.J. 2009. Internal vibration monitoring of a planetary gearbox. *International Journal of Vibration and Control*. Submitted: 2009-07-23

DUNTON, T. An introduction to time waveform analysis. www.unitechinc.com/pdf/. Date of access: 1 April 2013.

EWINS, D.J. 2000. Modal Testing, theory, practice and application. 2nd ed. England: Research Studies Press.

GANERIWALA, S. 2010. Review of techniques for bearing and gearbox diagnostics. Presentation at IMAC Conference Jacksonville. 3 February 2010.

HEYNS, P.S., NEL, C.B. & SNYMAN, J.A. 1994. Optimisation of engine mounting configurations. Proceedings. ISMA19. Tools for Noise and Vibration Analysis. Volume II. Katholieke Universiteit Leuven, Belgium, September 1994.

JENA, D.P., PANIGRAHI, S.N. & KUMAR, R. 2013. Gear fault identification and localization using analytic wavelet transform of vibration signal. *Measurement,* 46(3):1115-1124.

KAR, C. & MOHANTY, A.R. 2006. Monitoring gear vibrations through motor current signature analysis and wavelet transform. *Mechanical Systems and Signal Processing,* 20(1):158-187.

GANERIWALA, S. 2010. Vibration analysis of rolling element bearings with various defects under the action of an unbalanced force. *Mechanical Systems and Signal Processing, 20(8):1967-1991.*

LIMMER, J.D. 1997. Improved methods of vibration measurement, gear fault detection and bearing fault detection for gearbox diagnostics. Rensselaer Polytechnic Institute.

LITVIN, F.L., FUENTES, A. & HAYASAKA, K. 2006. Design, manufacture, stress analysis, and experimental tests of low-noise high endurance spiral bevel gears. *Mechanism and Machine Theory,* 41(1):83-118.

LOUTAS, T.H., SOTIRIADES, G., KALAITZOGLOU, I. & KOSTOPOULOS, V. 2009. Condition monitoring of a single-stage gearbox with artificially induced gear cracks utilizing on-line vibration and acoustic emission measurements. *Applied acoustics, 70(9):*1148-1159.

LOUTFI, M.Y. 2011. Online condition monitoring network for critical equipment at Holcim's STE. Genevieve plant. Paper presented at the 2011 IEEE-IAS/PCA 53rd Cement Industry Technical Conference; 2011, pp. 1 - 11.

MAHALUNGKAR, S. & INGRAM, M. 2004. Online and manual (offline) vibration monitoring of equipment for reliability centered maintenance. Paper presented at the Cement Industry

Technical Conference, 2004. IEEE-IAS/PCA, 25-30 April 2004. Available: http://ieeexplore.ieee.org/xpls/abs_all.jsp?arnumber=1309871&tag=1. Date of access: [4/23/2013, 2013].

Nel, C.B. 2000. Optimisation of engine mount systems at front-wheel-drive vehicles for multiple operational conditions. *ISMA25*. Katholieke Universiteit Leuven, Belgium, September 2000.

NEL, C.B. 2007. Design analysis of a rubber mount system for a push type centrifuge. *Proceedings*. ICSV 14. Cairns, Australia, July 2007.

Nel, C.B. 2009. Analysis of a vibration isolation system for a circulation pump. *Proceedings of IRF'2009, 3rd International Conference on Integrity, Reliability and Failure*, University of Porto, Porto, Portugal, July 2009.

NILSSON, J.W. & RIEDEL, S.A. 2011. Electric Circuits. 9th Ed. New Jersey: Pearson.

OZTURK, H., YESILYURT, I. & SABUNCU, M. 2010. Investigation of effectiveness of some vibration-based techniques in early detection of real-time fatigue failure in gears. *Shock & Vibration*, 17(6):741-757.

PAEZ T.L. & PIERSOL A.G. 2010. Harris' shock and vibration handbook. 6th ed. NY: McGraw-Hill.

PAN, M., LI, P. & CHENG, Y. 2008. Remote online machine condition-monitoring system. *Measurement*, 41(8):912-921.

PRYOR, T. 2011. Time waveform analysis (In the beginning). Vibration Institute 2011 Annual Meeting Proceedings, pp. 23-39.

RAFIEE, J., ARVANI, F., HARIFI, A. & SADEGHI, M.H. 2007. Intelligent condition monitoring of a gearbox using artificial neural network. *Mechanical systems and signal processing. 21(4):1746-1754.*

RAFIEE, J., RAFIEE, M.A. & TSE, P.W. 2010. Application of mother wavelet functions for automatic gear and bearing fault diagnosis. *Expert systems with applications*, 37(6):4568-4579.

RANDALL, R.B. & SAWALHI, N. 2011. A new method for separating discrete components from a signal. *Sound and vibration,* 45 (5):6-9.

RAO, S.S. 1990. Mechanical vibrations *r*eading. Massachusetts: Addison-Wesley.

RELIABILITY DIRECT. 2014. Vibration severity. http://www.reliabilitydirectstore.com/

ProductDetails.asp?ProductCode=RDI%20VI-1. Date of access: 31 Oct. 2014.

Rockwell Automation. 2005. Condition monitoring: misused and misunderstood. Available: http://www.ferret.com.au/c/Rockwell-Automation/Condition-monitoring-misused-and-misunderstood-n678999 . Date of access: 18 Mar. 2013.

SKF. 1999. Frequently asked questions about SEE (Spectral Emitted Energy) Technology. *SKF application note.*

SKF. 1999. SEE vs. traditional vibration. *SKF application note.*

SKF. 1999. What are Enveloping and SEE? *SKF application note.*

SKF. 2000. Early warning fault detection in rolling element bearings using microlog Enveloping. *SKF application note.*

SKF. Acceleration Enveloping-It works! *Revolutions,* 7(3):1-14.

SMITH, J.M. 1983. Gears and their vibration a basic approach to understanding gear noise. New York & Basel: Dekker; London & Basingstoke: Macmillan.

STANDER, C.J. & HEYNS, P.S. 2000. Fault detection on gearboxes operating at varying speed and load. *Comadem 2000*, Houston, 3-8 December: pp. 1011-1020.

STANDER, C.J. & HEYNS, P.S. 2001. Fault detection on gearboxes operating under fluctuating load conditions. *Condition Monitoring and Diagnostic Engineering Management. Comadem 2001. Proceedings of the 14th International Congress.* Manchester, 4-6 September 2001, pp.457-464.

STANDER, C.J. & HEYNS, P.S. 2005. Instantaneous angular speed monitoring of gearboxes under non-cyclic stationary load conditions. *Mechanical Systems and Signal Processing,* 19(4):817 - 835.

STANDER, C.J. & HEYNS, P.S. 2006. Transmission path phase compensation for gear monitoring under fluctuating load conditions. *Mechanical Systems and Signal Processing,* 20(7):1511 - 1522.

TAYLOR, J.I. 2003. The Vibration Analysis Handbook.

Appendix A

Gearbox dimensions

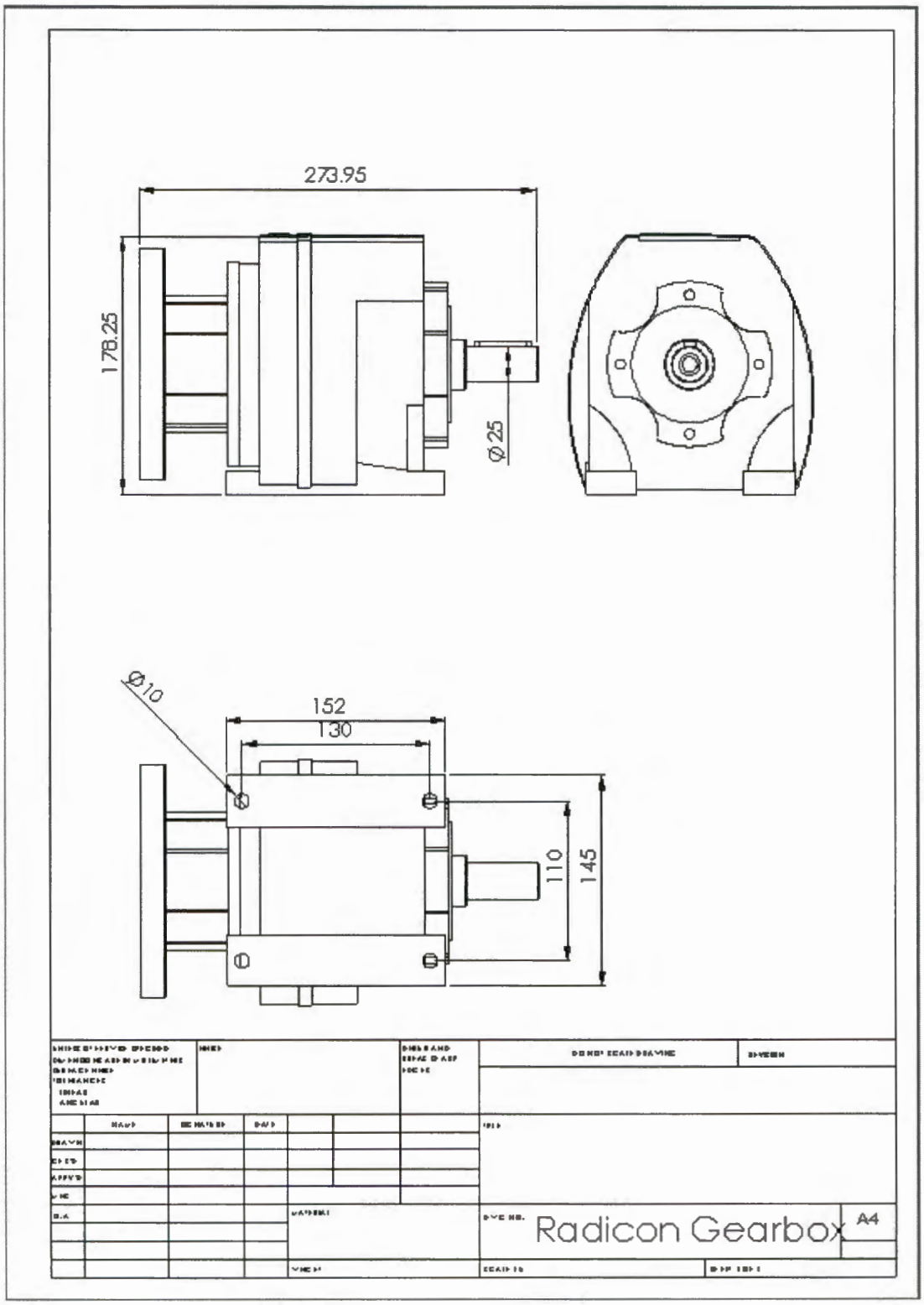

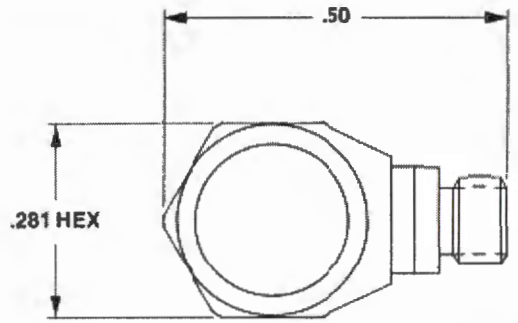

ACTUAL SIZE

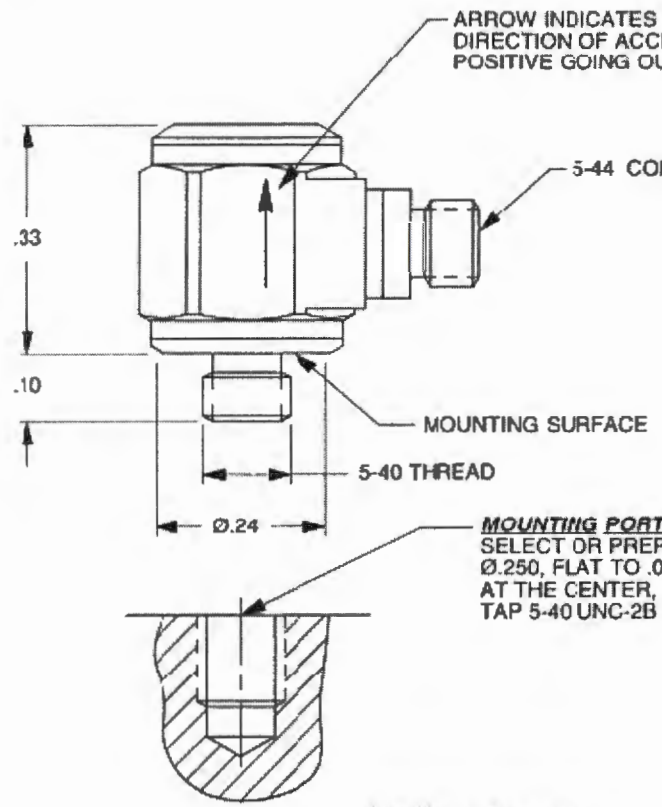

MOUNTING PORT PREPARATION: 3035B
SELECT OR PREPARE A FLAT AREA OF AT LEAST Ø.250, FLAT TO .001 TIR.
AT THE CENTER, DRILL #38 (Ø.101) X .150 DEEP, MIN.
TAP 5-40 UNC-2B X .125 DEEP, MIN.

MODEL 3035B

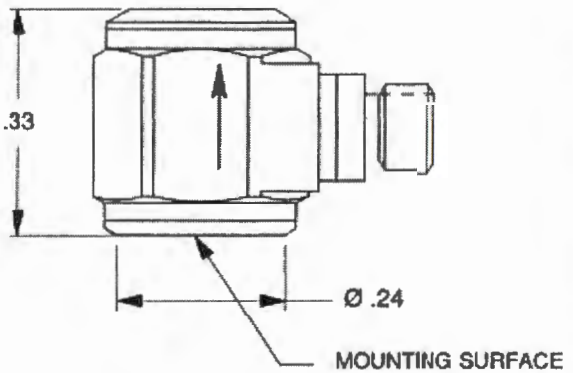

MODEL 3035BG

MOUNTING SURFACE PREPARATION: 3035BG
SELECT OR PREPARE A FLAT AREA OF AT LEAST Ø.250, FLAT TO .001 TIR. CLEAN TO REMOVE CONTAMINANTS. APPLY ADHESIVE TO SURFACE OR TO ACCELEROMETER AND PRESS TOGETHER UNTIL ADHESIVE SETS.

2. MOUNTING TORQUE ON .281 HEX: 3 TO 4 LB.-IN.
1. WEIGHT: 2.5 GRAMS.

DYTRAN INSTRUMENTS, INC.

MASTER
ONLY IF IN RED
CHATSWORTH, CA.

SCALE 4X	REV D	DATE 6/10/04	ECN N/A		
DATE 12/02/02	PART NO. MODELS 3035B, 3035BG				
DRAWN N.C.	CHECKED R.A.	DATE			
APPROVED 6/10/04	NEXT ASSEMBLY		USED ON		

TITLE
OUTLINE/INSTALLATION DRAWING, MODELS 3035B & 3035BG LIVM ACCELEROMETERS

DWG NO. 127-3035B/G

SHEET 1 OF 1

Acceleration meter characteristics

SPECIFICATIONS, MODELS 3035BX & 3035BXG
LIVM ACCELEROMETERS

SPECIFICATIONS BY MODEL

MODEL	RANGE F.S. (g)	MAXIMUM SHOCK (g)	SENSITIVITY (±10%) [1] (mV/g)	ELECTRICAL NOISE (g) (kHz)	NATURAL FREQUENCY (kHz)
3035B & BG	± 50	600/3000	100.0	0.0009	>45
3035B1 & B1G	± 500	600/3000	10.0	0.005	>45
3035B2 & B2G	± 100	600/3000	50.0	0.0015	>45
3035B3 & B3G	± 1000	600/3000	5.0	0.009	>45

COMMON SPECIFICATIONS

SPECIFICATION	VALUE	UNITS
PHYSICAL		
WEIGHT	2.5	grams
SIZE, HEX x HEIGHT	.281 (9/32) x .33	inches
MOUNTING PROVISION, 3035B	5-40 integral stud	
MOUNTING PROVISION, 3035BG	flat surface for adhesive mount	
CONNECTOR, RADIALLY MOUNTED	5-44 coaxial	
MATERIAL, HOUSING AND CONNECTOR	300 Series Stainless Steel	
PERFORMANCE		
FREQUENCY RANGE, ± 10%	0.5 to 10k	Hz
RESONANT FREQUENCY	>45	kHz
EQUIVALENT ELECTRICAL NOISE FLOOR	.007	g rms
LINEARITY [2]	± 1%	% F.S.
TRANSVERSE SENSITIVITY, MAX.	5	%
STRAIN SENSITIVITY	.002	g/με @ 250με
ENVIRONMENTAL		
MAXIMUM VIBRATION/SHOCK	600/3000	± g pk
TEMPERATURE RANGE, 3035B/BG, 3035B2/B2G	-60 to +225	°F
3035B1/B1G, 3035B3/B3G	-60 to +250	°F
SEAL, HERMETIC	Glass-to-metal and TIG welded	
COEFFIEICNT OF THERMAL SENSITIVITY	.04	%/°F
ELECTRICAL		
SUPPLY CURRENT [3]	2 to 20	mA
SUPPLY COMPLIANCE VOLTAGE RANGE	+18 to +30	Volts
OUTPUT IMPEDANCE, TYP.	100	Ω
BIAS VOLTAGE	+11 to +13	Vdc
DISCHARGE TIME CONSTANT	1.0 to 2.0	seconds
OUTPUT SIGNAL POLARITY FOR ACCELERATION TOWARD TOP	Positive	
CASE GROUNDING	Case is grounded to electrical power ground	

Current transformer information

佛山市华新微晶金属有限公司
FOSHAN HUAXIN MICROLITE METAL CO., LTD
地址：广东省佛山市狮山工业园B区工业大道6号 TEL:+86-757-86698378 FAX:+86-757-86698370
Add: 6th,Industrial Road B Sector Shishan Industrial Zone E-mail: huaxin@fshuaxin.com
Foshan City Guangdong Province Http: //www.fshuaxin.com

SPECIFICATION FOR APPROVAL

Customer Name	南非	Rev	C
Description	Split-core Current Transformer	Date	05-16-2010
H.X.Part No	CT234-30M-LC	Customer Part No	

Features:
Small Volume;Low Price; High Linearity; The Split-core current transformer is designed;The installation can be finished at without interrupting the current-carrying wire.

Applications:
Portable Instruments;Electricity Disponser;Power Calibrator;Power Ttansducer;Precision Power Meters;Digital Meters for power System;Serve Motor.

Mechanical Dimensions(unit:mm)

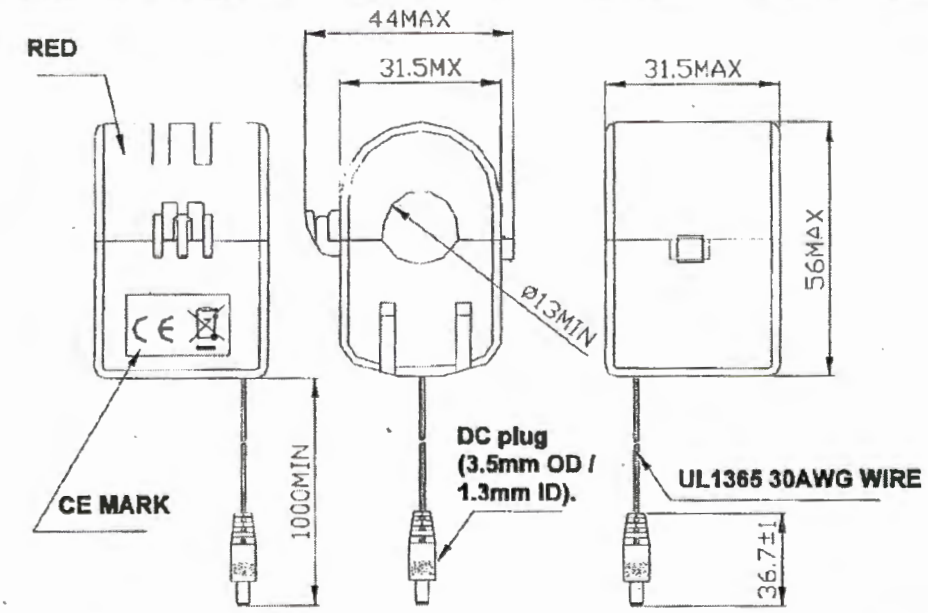

Current transformer circuit diagram

Test circuit: **Bold lines indicate linear regionaccording to formula:**

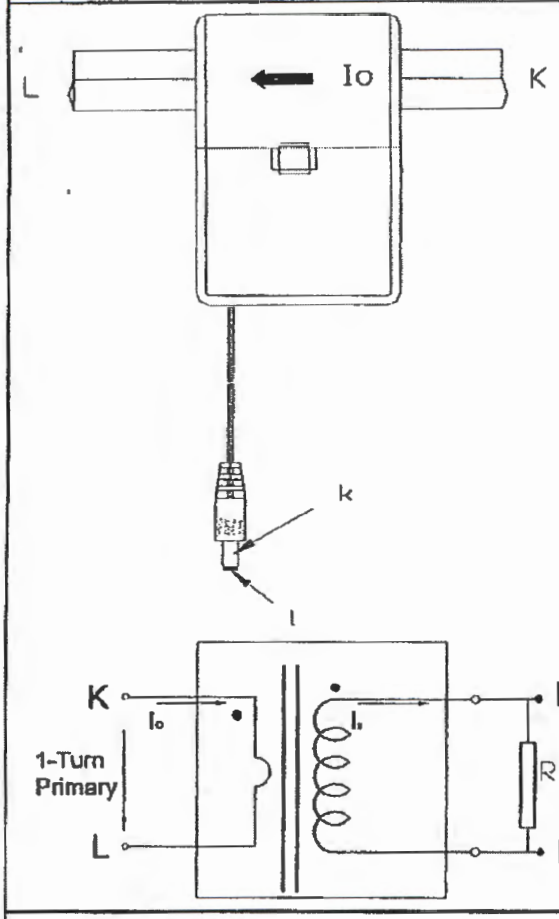

$$Vout = \frac{I_O \times R_L}{N}$$

Vout:Secondary Output Voltage

Io:Primary Current

R_L:Secondary Load

N:Secondary Turns

Remark: Unless requested, the 1-turn primary winding and the terminating resistor RL are not supplied.

Current transformer characteristics

Electrical Characteristics		
No	**Item**	**Specification**
1	Primary Current (Arms 50/60Hz)	30A nom 75A max
2	Secondary Current at primary nominal (rms)	10mA
3	Primary/secondary currents ratio In the nominal range of primary current	3000Ts
4	D.C.Resistance .at25 °C (Ω)	460ΩMAX
5	Maximal burden, resistive load of secondary winding	50Ω
6	Amplitude Error f(%)	±2%
7	Insulation between primary non-insulated wire, touching inside surface of the window, and secondary output must withstand AC rms voltage	1500V/1mA/1min
8	Impulse withstand voltage 1.2/50us	3500V
9	Temperature error of currents ratio	<50ppm/K
10	Ambient operating temperature range	-20°C~60°C
Mechanical Specifications		
No	**Item**	**Describe**
1	Housing	ABS
2	Bobbin	PBT
3	core	Ferrite
4	Tap	Polyethylene Terephthalate (PET)
5	Magnet Wire	2UEW
6	Leader wire	UL1365 30#AWG BLACK + DC PLUG
7	Flame retardant	UL94-V0
8	Marking Logo	
9	Approximate Weight	65g
10	Tolerance	
11	All material to the requirement of ROHS	

Appendix B

Acceleration meter quotation

ESTEQ Test & Measurement (Pty) Ltd | Company Registration No.: 2009/018819/07
Directors: JJ Oosthuizen, E Murison

ESTEQ TEST & MEASUREMENT

Tigervallei Office Park, Block 6
Silverlakers Road, Silverelakes
Pretoria, Gauteng, 0081

Phone: (012) 809 9500
Fax: (012) 809 3396

To:	Stephan Grobler	**Date:**	22-Nov-2013
Company:	**NWU Potchefstroom Kampus**	**Quote No.:**	ETQ14-154-11
Email:	20688245@nwu.ac.za	**[ZAR:USD] ROE:**	10.64
Tel No.:	073 1575 650	**Valid Until:**	6-Dec-2013

QUOTATION

PRODUCT CODE	DESCRIPTION	Qty	PRICE [ZAR]
3035B	50g range, 100mV/g, 5-44 side connector, 5-40 mounting stud	4	R 14,551.39
6207	Adhesive Mounting Base, 3/8 Hex, 5-40 tapped hole	4	R 340.39
6056A/26	Mini-coax, Teflon jacket, low noise, 5-44 to BNC plug, red, 26 ft.	4	R 3,169.86
	University Discount	1	-R 1,354.62
		SubTotal	**R 16,707.02**
		Shipping, Handling & Insurance	R 1,000.00
		TOTAL [Excl. VAT]	**R 17,707.02**

Notes:

1. This Quotation is subjects to the standard conditions of agreement and indebtedness of ESTEQ Test & Measurement (Pty) Ltd, available on request.
2. Prices: All prices quoted in South African Rand (ZAR) with a ROE stated above and exclude VAT and any other applicable taxes.
3. Variation in exchange rate at time of delivery will be for buyers account
4. Where applicable, all Maintenance fees are payable annually in advance.
5. Validity: This quotation is valid for 14 days from date of issue, but pricing remains linked to ROE.
6. Delivery: Six to Eight weeks or earlier, ARO.
7. Payment: 30 Days Net for account holders, all others COD

If you have any questions about this price quote, please contact
Jana Murison, Phone # 012 809 9500 | 083 7737359 | j.murison@esteq.com

Thank You For Your Business!

Postal Adress: PO Box 1771 Faerie Glen 0043 | Standard Bank Acc No 013355856 Lynnwood Ridge Branch Code 0 2 1 45

My Shopping Cart (ZAR Dollar)

Part Number	Description	Est Ship	Unit Price	Qty	Line Total
781424-01	cDAQ-9188, CompactDAQ chassis (8 Slot ENET)	5 - 7	R 18,890.00	1	R 18,890.00
779001-01	NI 9211 4-Ch ±80 mV, 14 S/s, 24-Bit TC and Diff AI	5 - 6	R 4,470.00	1	R 4,470.00
745690-J002	J-Type Thermocouples Wire, Fiberglass (32 deg F to 900 deg F) 2 m	14 - 19	R 380.00	4	R 1,520.00
779680-01	NI 9234 - NI 9234 [qty: 2]	5 - 6	R 22,520.00	2	R 45,040.00
					Total Items: 8
					Subtotal: R 69,920.00
					Shipping in South Africa: Standard: R 0.00
					Order Total: R 69,920.00

Price Excludes VAT

National Instruments - South Africa

G3 - Ground Floor East Midview Building

Thandanani Office Park Invicta Road

Halfway Gardens Ext.25 Midrand

South Africa

Phone 27 82 877 8530

Fax: 27 11 805 8194

Matlab license quotation

Quotation from OPTI-NUM solutions

t +27 11 325 6238 info@optinum.co.za PO Box 412175
f +27 11 325 6239 www.optinum.co.za Craighall 2024 South Africa

Attn: Stephan Grobler - Master's Student
North West University - Mechanical Engineering
Private Bag X 6001
Potchefstroom, North West Province,
South Africa

Fax: Tel: +27 73 157 5650
email: 20688245@nwu.ac.za

We have pleasure in providing you with the following quotation for products and services.

Quote Ref	Quote Date	Expiry Date	Contact	Terms	Our VAT Reg No
Q201410087	2014-10-13	2014-11-12	Vicky Makhathini	30 days nett	4590135457

Line	Code	Qty	Description	Unit Price	Total
1	CMLIN	1	MATLAB (Individual) New	R 35046.30	R 35046.30
2	CDAIN	1	Data Acquisition Toolbox (Individual) New	R 16531.30	R 16531.30
3	CSGIN	1	Signal Processing Toolbox (Individual) New	R 16531.30	R 16531.30
4	COPIN	1	Optimization Toolbox (Individual) New	R 19176.30	R 19176.30
				Excl Total	R 87285.20
				VAT (14%)	R 12219.93
				Quote Total	R 99505.13

Comment: Quote for a Commercial Individual License. Please note this is perpetual license and includes 12 months of Software Maintenance Service (SMS), which covers 12 months of technical support, product updates (released around March and September every year) and only when in maintenance can license changes be made. The annual cost for SMS is 20% of the new product cost.

Notes:

1. Orders must explicitly state the quotation reference given above, as well as terms stated.
2. Orders must include your company VAT registration number, if applicable.
3. OPTI-NUM solutions charges interest of 1.75% per month on overdue invoices.
4. The prices listed in this quotation are firm until the Expiry Date shown above. OPTI-NUM solutions may, at its own discretion, extend the expiry date of this quotation on written notice only. OPTI-NUM solutions reserves the right to refuse orders placed after a quotation has expired.
5. (Software purchases only) All prices include South African duties and surcharges as well as courier delivery charges. Customers in other countries may be liable for local taxes.
6. (Software purchases only) Delivery: By courier, within 14 days of order placement.
7. (Software purchases only) This quotation is subject to OPTI-NUM solutions Commercial Licensing and Ordering Information, available on request.
8. (Software purchases only) Prices are subject to the Rand Dollar exchange rate not exceeding R11.78 = US$1.00 at the time of purchase.

HP Probook 470 laptop quotation

BlueTek Computers CC (1988/19967/23) t/a

Belasting no.: 4060187566

Kwotasie

Tel: (018) 297 0164
Fax: (018) 294 3036

45 Chief Albert Luthuli Drive
PO Box 2495
Potchefstroom 2520

www.bluetek.co.za

Naam: Mnr Carl Nel
Besigheid: Noordwes Universiteit
Tel: 0182991315

Datum: 2014/03/11

Kwotasienr.: Q228934f

Kode	Item	Wty	Hoev	Eenh. prys	Totaal (0% BTW)	Totaal (met BTW)
NTB1287	HP Probook 470 I7-4702MQ ,2.2 GHz, 6 MB cache, 4 cores, (17.3") diagonal LED-backlit HD+ anti-glare (1600 x 900), 8GB RAM, 1TB HDD, Windows 8 Pro Licence DG to Windows 7 Pro 64, AMD Radeon HD 8750M 2GB E9Y70EA	1	1	R 12 599.00	R 12 599.00	R 14 362.86
BAG0033	Targus CNXL1 Extra large notebook case 17"		2	R 503.00	R 1 006.00	R 1 146.84
WAR0470	HP Care Pack -3 year Next business day onsite Notebook Only Service UK703E	3	1	R 765.00	R 765.00	R 872.10
MSE0735	M185 Micro receiver, 3 Button, Wheel, Optical -Swift Grey 910-002235 MO-LM185BS		1	R 155.00	R 155.00	R 176.70
PSU0031	HP ED495AA 90W Powersupply for notebooks		1	R 353.00	R 353.00	R 402.42
HDD2029	Transcend StoreJet 25D3 Series - 1TB 2.5" External HDD - SuperSpeed USB 3.0, Plug & Play, USB Powered - Durable Piano Black Finish TS1TSJ25D3	1	1	R 794.00	R 794.00	R 905.16

Subtotaal (BTW uitgesluit)	R 15 672.00
BTW @ 14%	R 2 194.08
TOTAAL	R 17 866.08

Ons wil u bedank vir die geleentheid om te kwoteer. Indra-waarborge (wty) word gespesifiseer i.t.v. jare. Die kwotasie is geldig vir 'n maksimum periode van 7 dae. Pryse is onderhewig aan die rand/dollar verhouding. Pryse word gekwoteer vir kontant en internetbetalings. Doen asb. navraag oor pryse vir ander metodes van betaling. Geen tjeks word aanvaar tensy vooraf goedkeuring verkry is vanaf bestuur. Internetbetalings moet eers op BlueTek se rekening (ABSA) reflekteer voordat goedere afgelewer of opgetel kan word.

F. & W. U. *Ons hoop u vind alles in orde en verwelkom enige navrae.*

Werner de Villiers
werner@bluetek.co.za

Personal Computing Gold Specialist 2013

GOLD PARTNER

Microsoft Partner
Midmarket Solution Provider

Appendix C

Program A Matlab program code: Gearbox defect frequencies

```
%Shaft speeds:
% Gear mesh frequencies:
% t = number of teeth
% r = reduction at gear pair
t_1 = 39
t_2 = 44
t_3 = 13
t_4 = 58
rpm_1 = 1496.3  %Input Shaft speed


%Gear mesh 1 and harmonics

gmf_1 =(rpm_1*t_1)/60
gmf_11=2*gmf_1
gmf_12=3*gmf_1
gmf_13=4*gmf_1
gmf_14=5*gmf_1
gmf_15=6*gmf_1


%reduction_1
r_1 = t_1/t_2

%Gear mesh 2 and harmonics
rpm_2 = rpm_1*r_1
gmf_2 = (rpm_2*t_3)/60
gmf_21=2*gmf_2
gmf_22=3*gmf_2
gmf_23=4*gmf_2
gmf_24=5*gmf_2
gmf_25=6*gmf_2

%reduction_2
r_2 = (t_3/t_4)
rpm_3 = rpm_2*r_2
gear_ratio=1/r_1+1/r_2



% Bearing defect frequencies
% n = number of balls
% b = Ball diameter
% p = Pitch diameter
% rpm = inner race revolutions per minute
% ftf = fundamental train frequency
% bpfi = ball pass frequency inner
% bpfo = ball pass frequency outer
% bsf = ball spin frequency
% cuf = cage unbalance frequency

%6008/2RS1-C3 = a
n_a=12
```

```
b_a=7.94
p_a=54
rpm_a=rpm_1
beta_a=0
ftf_a=rpm_a/(2*60)*(1-b_a/p_a*cos(beta_a))
bpfi_a = n_a*rpm_a/(2*60)*(1+b_a/p_a*cos(beta_a))
bpfo_a = n_a*rpm_a/(2*60)*(1-b_a/p_a*cos(beta_a))
bsf_a = p_a*rpm_a/(2*60*b_a)*(1-(b_a/p_a)^2*(cos(beta_a))^2)
cuf_a = rpm_a/2*(1-b_a/p_a*cos(beta_a))

%6205-2RS1-C3 = b
n_b=9
b_b=7.94
p_b=39.04
rpm_b=rpm_1
beta_b=0
ftf_b=rpm_b/(2*60)*(1-b_b/p_b*cos(beta_b))
bpfi_b = n_b*rpm_b/(2*60)*(1+b_b/p_b*cos(beta_b))
bpfo_b = n_b*rpm_b/(2*60)*(1-b_b/p_b*cos(beta_b))
bsf_b = p_b*rpm_b/(2*60*b_b)*(1-(b_b/p_b)^2*(cos(beta_b))^2)
cuf_b = rpm_b/2*(1-b_b/p_b*cos(beta_b))

%6202/C3 = c
n_c=8
b_c=6
p_c=25.26
rpm_c=rpm_2
beta_c=0
ftf_c=rpm_c/(2*60)*(1-b_c/p_c*cos(beta_c))
bpfi_c = n_c*rpm_c/(2*60)*(1+b_c/p_c*cos(beta_c))
bpfo_c = n_c*rpm_c/(2*60)*(1-b_c/p_c*cos(beta_c))
bsf_c = p_c*rpm_c/(2*60*b_c)*(1-(b_c/p_c)^2*(cos(beta_c))^2)
cuf_c = rpm_c/2*(1-b_c/p_c*cos(beta_c))

%6005/C3 = e
n_e=10
b_e=6.75
p_e=36
rpm_e=rpm_3
beta_e=0
ftf_e=rpm_e/(2*60)*(1-b_e/p_e*cos(beta_e))
bpfi_e = n_e*rpm_e/(2*60)*(1+b_e/p_e*cos(beta_e))
bpfo_e = n_e*rpm_e/(2*60)*(1-b_e/p_e*cos(beta_e))
bsf_e = p_e*rpm_e/(2*60*b_e)*(1-(b_e/p_e)^2*(cos(beta_e))^2)
cuf_e = rpm_e/2*(1-b_e/p_e*cos(beta_e))

%6206-2Z/C3 = f
n_f=9
b_f=9.52
p_f=46
rpm_f=rpm_3
beta_f=0
ftf_f=rpm_f/(2*60)*(1-b_f/p_f*cos(beta_f))
bpfi_f = n_f*rpm_f/(2*60)*(1+b_f/p_f*cos(beta_f))
bpfo_f = n_f*rpm_f/(2*60)*(1-b_f/p_f*cos(beta_f))
bsf_f = p_f*rpm_f/(2*60*b_f)*(1-(b_f/p_f)^2*(cos(beta_f))^2)
cuf_f = rpm_f/2*(1-b_f/p_f*cos(beta_f))
```

Appendix D

Program B Matlab program code: Vibration signal construction, power and torque

```
%
%=========================================================================
% Stephan Grobler
% Measure and display data measured from NI hardware
% 4 Temperature Channels
% 2 Current readings for Power calculation
% 4 Vibration Channels
%
% !!!!!ALARMS!!!!!  (These values must be changed in the program as needed)
% Load above 3000 W
% Temps above 50degC 4 sensors
% RMS Xdotdot above 150% of startup 4 sensors
%=========================================================================
%
clc;
clear;
clf reset
daq.reset
daq.getDevices
%
%=========================================================================
% Create matrix and for loop to measure for a certain number of times.
%=========================================================================
%

q=1;              %number of measurements taken for trends
z=5;             %time between measurements in seconds
srate=20000;     %Specify the sample rate for vibration signals
stime=30       %Specify the sample time for a vibration signal
I=zeros(q,18)

for (i = 1:q)
%
%=========================================================================
% Create session
%=========================================================================
%

s = daq.createSession('ni')

%
%=========================================================================
% Create 4  Thermocouple channels
%=========================================================================
%

[ch, idx]= s.addAnalogInputChannel( 'cDAQ9188-
16D666AMod2',0:3,'Thermocouple');
s.Channels(1).ThermocoupleType = 'J'
s.Channels(2).ThermocoupleType = 'J'
s.Channels(3).ThermocoupleType = 'J'
s.Channels(4).ThermocoupleType = 'J'

%
```

```
%=========================================================================
% Collect data on 4 Thermocouple channels
%=========================================================================
%

s.DurationInSeconds = 0.2
[temp,clock]=inputSingleScan(s)
I(i,1)=temp(1,1)
I(i,2)=temp(1,2)
I(i,3)=temp(1,3)
I(i,4)=temp(1,4)

%
%=========================================================================
% Create session and 2 power channel
%=========================================================================
%

s=0;
s = daq.createSession('ni')
ch1=s.addAnalogInputChannel( 'cDAQ9188-16D666AMod3',0:1,'Voltage');
%
%=========================================================================
% Collect current (A) data
%=========================================================================
%
s.DurationInSeconds = 0.2
[power,powtime] = s.startForeground;

%
%=========================================================================
% Create session and 4 vibration channels
%=========================================================================
%
%
s=0;
s = daq.createSession('ni')
s.addAnalogInputChannel( 'cDAQ9188-16D666AMod1',0:3,'Accelerometer');
%
%=========================================================================
% Collect data from 4 vibration channels, change the Rate and duration
%=========================================================================
%

s.Rate=srate;
s.DurationInSeconds = stime;
s.Channels(1).Sensitivity = 0.01039;
s.Channels(2).Sensitivity = 0.01028;
s.Channels(3).Sensitivity = 0.01040;
s.Channels(4).Sensitivity = 0.01024;

[vibdata,vibtime] = s.startForeground;
Fs=s.Rate
d= detrend(vibdata,'constant');

%
%=========================================================================
% Store vibration data in matrix V
%=========================================================================
%
```

```
vn=length(vibdata)
V=zeros(vn,5);
V(:,1)=d(:,1);
V(:,2)=d(:,2);
V(:,3)=d(:,3);
V(:,4)=d(:,4);
V(:,5)=vibtime;
%
%=========================================================================
% Power calculations
%=========================================================================
%

sensitivity_1=0.531885952 %V/A from CT1 calibration
sensitivity_2=0.568649141 %V/A from CT2 calibration
I(i,5)=(rms(power(:,1)))/sensitivity_1 % Ampere reading
(amps=power*sensitivity)
I(i,18)=(rms(power(:,2)))/sensitivity_2 % Ampere reading
(amps=power*sensitivity

v=407  %constant
RPM=1500  %input
rend=0.8184 %Rendement (calculated from motor)

%Power calc
I(i,6)=((I(i,5)*v*(3^0.5)*0.84)+(I(i,18)*v*(3^0.5)*0.84))/2 *rend % Power
in Watts

% Torque calculation
I(i,7)=I(i,6)*60/(2*pi*RPM) % Torque in N.m

% Load percentage
I(i,8)=I(i,6)/3000*100 % Percentage of max
I(i,9)=now % Time the measurements are taken

%
%=========================================================================
% Plots and alarms
% Figure 1: 5 Graphs on one window Temps + Power
% Figure 2: Vibration on 4 channels
%=========================================================================
%

%
%=========================================================================
% Power plots
%=========================================================================
%
%Amps
figure(1);
subplot(4,4,1),plot(I(1:i,9),I(1:i,5),'--ro',I(1:i,9),I(1:i,18),'--
rx');set(gca,'FontSize',6)
datetick('x', 'dd/mm/yy-HHPM'); % print time in date format of '0'
title('Plot of Amps over Time') % title
ylabel('Current [A]') % label for y axis
xlabel('Time (h)') % label for x axis
legend('A1','A2')
legend('Location','NorthWest') % move legend to upper left
grid on
```

```
%Power
subplot(4,4,2),plot(I(1:i,9),I(1:i,6),'--ro');set(gca,'FontSize',6)
datetick('x', 'dd/mm/yy-HHPM'); % print time in date format of '0'
title('Plot of Load over Time') % title
ylabel('Power [W]') % label for y axis
xlabel('Time (h)') % label for x axis
legend('P')
legend('Location','NorthWest') % move legend to upper left
grid on

% Alarm on load !!!!
if I(i,(6))> 3000
    warningstring=' Load on gearbox is too high'
dlgname= 'Load warning'
h = warndlg(warningstring,dlgname)

for ss=1:10

    pause(0.5)
    WarnWave = [sin(1:.6:400), sin(1:.7:400), sin(1:.4:400)];
Audio = audioplayer(WarnWave, 22050);
play(Audio);
end

end

%Torque
subplot(4,4,3),plot(I(1:i,9),I(1:i,7),'--ro');set(gca,'FontSize',6)
datetick('x', 'dd/mm/yy-HHPM'); % print time in date format of '0'
title('Plot of Torque over Time') % title
ylabel('Torque [N-m]') % label for y axis
xlabel('Time (h)') % label for x axis
legend('T')
legend('Location','NorthWest') % move legend to upper left
grid on

% % Power
subplot(4,4,4),plot(I(1:i,9),I(1:i,8),'--ro');set(gca,'FontSize',6)
datetick('x', 'dd/mm/yy-HHPM'); % print time in date format of '0'
title('Plot of Load % over Time') % title
ylabel('% of full load') % label for y axis
xlabel('Time (h)') % label for x axis
legend('%')
legend('Location','NorthWest') % move legend to upper left
grid on

%
%=========================================================================
% Temperature plots
%=========================================================================
%

%subplot(4,4,13),plot((I(1:i,9)),(I(1:i,1)),'--ro',(I(1:i,9)),(I(1:i,2)),'-
--g*',(I(1:i,9)),(I(1:i,3)),'--bx',(I(1:i,9)),(I(1:i,4)),'--
kv');set(gca,'FontSize',6)
%datetick('x', 0); % print time in date format of '0'
%title('Plot of Temperature over Time') % title
%ylabel('Temp (oC)') % label for y axis
%xlabel('Time (h)') % label for x axis
%temp_legend=legend('Input shaft', 'Interm. shaft', 'Output shaft', 'Oil')
```

```
%temp_legend=legend('Location','NorthWest') % move legend to upper left
%set(temp_legend,'FontSize',6);
%grid on
%ylim([15 80])
%
%=========================================================================
% Channel 1 Input shaft Temp
%=========================================================================
%
% Alarm on Input shaft Temperature !!!!
if I(i,1)> 57
    warningstring='Temperature on input shaft is too high'
dlgname= 'Temp warning'
h = warndlg(warningstring,dlgname)

for ss=1:10

    pause(0.5)
    WarnWave = [sin(1:.6:400), sin(1:.7:400), sin(1:.4:400)];
Audio = audioplayer(WarnWave, 22050);
play(Audio);
end

end

%plot
subplot(4,4,13),plot((I(1:i,9)),(I(1:i,1)),'--ro');set(gca,'FontSize',6)
datetick('x', 'dd/mm/yy-HHPM'); % print time in date format of '0'
title('Input shaft Temp trend') % title
ylabel('I S Temp [oC]') % label for y axis
xlabel('Time [h]') % label for x axis
temp_legend=legend('Input shaft')
temp_legend=legend('Location','NorthWest') % move legend to upper left
set(temp_legend,'FontSize',6);
grid on
%ylim([15 80])
%
%=========================================================================
% Channel 2 Intermediate shaft Temp
%=========================================================================
%
% Alarm on Intermediate shaft Temperature !!!!
if I(i,2)> 50
    warningstring='Temperature on intermediate shaft is too high';
dlgname= 'Temp warning'
h = warndlg(warningstring,dlgname)

for ss=1:10

    pause(0.5)
    WarnWave = [sin(1:.6:400), sin(1:.7:400), sin(1:.4:400)];
Audio = audioplayer(WarnWave, 22050);
play(Audio);
end

end

%plot
subplot(4,4,14),plot((I(1:i,9)),(I(1:i,2)),'--g*');set(gca,'FontSize',6)
datetick('x', 'dd/mm/yy-HHPM'); % print time in date format of '0'
```

```
title('Intermediate shaft Temp trend') % title
ylabel('It S Temp [oC]') % label for y axis
xlabel('Time [h]') % label for x axis
temp_legend=legend('Interm shaft')
temp_legend=legend('Location','NorthWest') % move legend to upper left
set(temp_legend,'FontSize',6);
grid on
%

%=========================================================================
% Channel 3 Output shaft Temp
%=========================================================================
%
% Alarm on output shaft Temperature !!!!
if I(i,3)> 60
    warningstring='Temperature on output shaft is too high';
dlgname= 'Temp warning'
h = warndlg(warningstring,dlgname)

for ss=1:10

    pause(0.5)
    WarnWave = [sin(1:.6:400), sin(1:.7:400), sin(1:.4:400)];
Audio = audioplayer(WarnWave, 22050);
play(Audio);
end

end

%plot
subplot(4,4,15),plot((I(1:i,9)),(I(1:i,3)),'--bx');set(gca,'FontSize',6)
datetick('x', 'dd/mm/yy-HHPM'); % print time in date format of '0'
title('Output shaft Temp trend') % title
ylabel('O S Temp [oC]') % label for y axis
xlabel('Time [h]') % label for x axis
temp_legend=legend('Output shaft')
temp_legend=legend('Location','NorthWest') % move legend to upper left
set(temp_legend,'FontSize',6);
grid on
%ylim([15 80])
%
%=========================================================================
% Channel 4 Oil Temp
%=========================================================================
%
% Alarm on oil Temperature !!!!
if I(i,4)> 65
    warningstring='Temperature on oilt is too high';
dlgname= 'Temp warning'
h = warndlg(warningstring,dlgname)

for ss=1:10

    pause(0.5)
    WarnWave = [sin(1:.6:400), sin(1:.7:400), sin(1:.4:400)];
Audio = audioplayer(WarnWave, 22050);
play(Audio);
end

end
```

```
%plot
subplot(4,4,16),plot((I(1:i,9)),(I(1:i,4)),'--kv');set(gca,'FontSize',6)
datetick('x', 'dd/mm/yy-HHPM'); % print time in date format of '0'
title('Oil Temp trend') % title
ylabel('Oil Temp [oC]') % label for y axis
xlabel('Time [h]') % label for x axis
temp_legend=legend('Oil')
temp_legend=legend('Location','NorthWest') % move legend to upper left
set(temp_legend,'FontSize',6);
grid on
%ylim([15 80])

%
%=========================================================================
% Vibration data analysis and plots
%=========================================================================
%
%
%=========================================================================
% Plot channel 1 data over time [ms^2]
%=========================================================================
%

figure(2)
subplot(3,4,1);plot(V(:,5),V(:,1));set(gca,'FontSize',6)
title('Input shaft Vertical ') % title
ylabel('I V Acce (Xdotdot) [m/s^2]') % label for y axis
xlabel('Time (s)') % label for x axis
grid on
%pause;

%
%=========================================================================
% Determine FFT on time domain signal
%=========================================================================
% old: fs=2500;
t=vibtime;
fs=1/t(2);
Xdotdot=d(:,1);

%%%%%%%%%%%%%%%%%%%%%%%%%%%%%%%
np=length(t);
f=fs*(0:np-1)/np;

FXdotdot=fft(Xdotdot);
PXdotdot=abs(FXdotdot)*2/np;
aXdotdot=angle(FXdotdot);

% Remove unwanted inaccurate energy between approx 0 to 2 Hz
% because of piezo cristal

aantalf=(2/f(2))+1
for a=1:aantalf
   PXdotdot(a) =  0.000000;
end

%=========================================================================
% Plot spectra - Acceleration Peak Amplitude and Phase
```

```
%=========================================================================
%npl=1:(86);
% (lenghth of t) / 2
npl=1:(np/2);

%figure(3);
subplot(3,4,5);plot(f(npl),PXdotdot(npl),'b');set(gca,'FontSize',6)
%title('Channel 1')
ylabel('I V Peak Acce (Xdotdot) [m/s^2]')
xlabel('Frequency [Hz]')

%subplot(2,1,2);plot(f(npl),aXdotdot(npl),'b')
%ylabel('Acce Phase (aXdotdot) [rad]')
%xlabel('Frequency [Hz]'),pause
%

%=========================================================================
% Convert Acceleration to Velocity - Amplitude and Phase
%=========================================================================
% NB: Length of f (old: f = 6827)
lf = length(f);

% Velocity signal - Peak Amplitude, Note: mm/s
j=0;
for j = 1:(lf-1);
j=j+1;
PXdot(j) =( 1000*PXdotdot(j)/(f(j)*2*pi));
end;

% TEST:
%%PXdot= PXdotdot(10)/f(10)*2*pi

%test1 = 11111
%pause

% Remove unwanted inaccurate energy between approx 0 to 2 Hz
% because of piezo cristal

%test2 = 22222
%pause

% Velocity phase angle - Peak Amplitude, Note: mm/s
% Angular relationship between acceleration and velocity vectors
% (pi/2 rad = 90 degrees)
j=0;
for j = 1:(lf-1);
j=j+1;
aXdot(j) =  (aXdotdot(j)- pi/2);

if aXdot(j)  <= -pi
        aXdot(j) = (aXdot(j) + 2*pi);
       else
          aXdot(j) = aXdot(j);
       end;

end;

%test3 = 33333
%pause
```

```
%=========================================================================
% Plot spectra - Velocity Peak Amplitude and Phase
%=========================================================================
%figure(4)

subplot(3,4,9);plot(f(npl),PXdot(npl),'b');set(gca,'FontSize',6)
%title('Channel 1')
ylabel('I V Peak Veloc (Xdot) [mm/s]')
xlabel('Frequency [Hz]')
%print

%subplot(2,1,2);plot(f(npl),aXdot(npl),'b')
%ylabel('Veloc Phase (aXdot) [rad]')
%xlabel('Frequency [Hz]'),pause
%

%=========================================================================
% Fourier coefficients for Acceleration
%=========================================================================

datXdotdot=[2*pi*f(npl); PXdotdot(npl)'; aXdotdot(npl)'];

%=========================================================================
% Reconstruct time domain Acceleration signal with Fourier coefficients,
note s
%=========================================================================
%Please note: E = length of t
E=length(t);

for j=1:E;
Xdotdots(j)=sum(datXdotdot(2,:).*cos(datXdotdot(1,:)*t(j)+datXdotdot(3,:)))
;
end;

% Mean acceleration - overall magnitude
MEAN_Xdotdots = mean( abs (Xdotdots))

% RMS acceleration - overall magnitude
%%coverts average to RMS (SA cc course notes: SKF guide: p 2)
RMS_Xdotdots = 1.11*mean( abs (Xdotdots))
I(i,10)=RMS_Xdotdots;

%=========================================================================
% Fourier coefficients for Velocity
%=========================================================================

datXdot = [2*pi*f(npl); PXdot(npl); aXdot(npl)];

%=========================================================================
% Construct time domain Velocity signal with Fourier coefficients, note s
%=========================================================================
E=length(t);

for j=1:E;
Xdots(j)=sum(datXdot(2,:).*cos(datXdot(1,:)*t(j)+datXdot(3,:)));
end;
```

```
% Mean acceleration - overall magnitude
MEAN_Xdots = mean( abs (Xdots))

% RMS velocity - overall magnitude
%%coverts average to RMS (SA cc course notes: SKF guide: p 2)
RMS_Xdots = 1.11*mean( abs (Xdots))
I(i,11)=RMS_Xdots;

%
%=========================================================================
% Plot channel 1 RMS trend on figure(1)
%=========================================================================
%

% Alarm on Input shaft vertical RMS !!!!
if I(i,10)> 7.5
    warningstring='RMS Xdotdot limit overreached:Input shaft vertical'
dlgname= 'Vibration warning'
h = warndlg(warningstring,dlgname)

for ss=1:10

    pause(0.5)
    WarnWave = [sin(1:.6:400), sin(1:.7:400), sin(1:.4:400)];
Audio = audioplayer(WarnWave, 22050);
play(Audio);
end

end
%plot
figure(1)
subplot(4,4,5),plot(I(1:i,9),I(1:i,10),'--ro');set(gca,'FontSize',6)
datetick('x', 'dd/mm/yy-HHPM'); % print time in date format of '0'
title('Input vert RMSXdotdots') % title
ylabel('I V RMSXdotdot') % label for y axis
xlabel('Time (h)') % label for x axis
legend('RMS')
legend('Location','NorthWest') % move legend to upper left
grid on
%
subplot(4,4,9),plot(I(1:i,9),I(1:i,11),'--ro');set(gca,'FontSize',6)
datetick('x', 'dd/mm/yy-HHPM'); % print time in date format of '0'
title('Input vert RMSXdots') % title
ylabel('I V RMSXdot') % label for y axis
xlabel('Time (h)') % label for x axis
legend('RMS')
legend('Location','NorthWest') % move legend to upper left
grid on


%=========================================================================
% Plot channel 2 data over time [ms^2]
%=========================================================================
%

figure(2)
subplot(3,4,2);plot(V(:,5),V(:,2));set(gca,'FontSize',6)
title('Input shaft Horizontal') % title
ylabel('I H Acce (Xdotdot) [m/s^2]') % label for y axis
```

```
xlabel('Time (s)') % label for x axis
grid on
%pause;

%
%=========================================================================
% Determine FFT on time domain signal
%=========================================================================
% old: fs=2500;
t=vibtime;
fs=1/t(2);
Xdotdot=d(:,2);

%%%%%%%%%%%%%%%%%%%%%%%%%%%%%%
np=length(t);
f=fs*(0:np-1)/np;

FXdotdot=fft(Xdotdot);
PXdotdot=abs(FXdotdot)*2/np;
aXdotdot=angle(FXdotdot);
% Remove unwanted inaccurate energy between approx 0 to 2 Hz
% because of piezo cristal

aantalf=2/f(2)+1
for a=1:aantalf
   PXdotdot(a) =  0.000000;
end

%=========================================================================
% Plot spectra - Acceleration Peak Amplitude and Phase
%=========================================================================
%npl=1:(86);
% (lenghth of t) / 2
npl=1:(np/2);

%figure(6);
subplot(3,4,6);plot(f(npl),PXdotdot(npl),'b');set(gca,'FontSize',6)
%title('Channel 2')
ylabel('I H Peak Acce (Xdotdot) [m/s^2]')
xlabel('Frequency [Hz]')

%subplot(2,1,2);plot(f(npl),aXdotdot(npl),'b')
%ylabel('Acce Phase (aXdotdot) [rad]')
%xlabel('Frequency [Hz]'),pause
%

%=========================================================================
% Convert Acceleration to Velocity - Amplitude and Phase
%=========================================================================
% NB: Length of f (old: f = 6827)
lf = length(f);

% Velocity signal - Peak Amplitude, Note: mm/s
j=0;
for j = 1:(lf-1);
j=j+1;
PXdot(j) =( 1000*PXdotdot(j)/(f(j)*2*pi));
end;
```

```
% TEST:
%%PXdot= PXdotdot(10)/f(10)*2*pi

%test1 = 11111
%pause

%test2 = 22222
%pause

% Velocity phase angle - Peak Amplitude, Note: mm/s
% Angular relationship between acceleration and velocity vectors
% (pi/2 rad = 90 degrees)
j=0;
for j = 1:(lf-1);
j=j+1;
aXdot(j) =  (aXdotdot(j)- pi/2);

if aXdot(j)  <= -pi
        aXdot(j) = (aXdot(j) + 2*pi);
       else
          aXdot(j) = aXdot(j);
       end;

end;

%test3 = 33333
%pause

%=========================================================================
% Plot spectra - Velocity Peak Amplitude and Phase
%=========================================================================
%figure(7)
subplot(3,4,10);plot(f(npl),PXdot(npl),'b');set(gca,'FontSize',6)
%title('Channel 2')
ylabel('I H Peak Veloc (Xdot) [mm/s]')
xlabel('Frequency [Hz]')
%print

%subplot(2,1,2);plot(f(npl),aXdot(npl),'b')
%ylabel('Veloc Phase (aXdot) [rad]')
%xlabel('Frequency [Hz]'),pause
%
%=========================================================================
% Fourier coefficients for Acceleration
%=========================================================================

datXdotdot=[2*pi*f(npl); PXdotdot(npl)'; aXdotdot(npl)'];

%=========================================================================
% Reconstruct time domain Acceleration signal with Fourier coefficients,
note s
%=========================================================================
%Please note: E = length of t
E=length(t);

for j=1:E;
Xdotdots(j)=sum(datXdotdot(2,:).*cos(datXdotdot(1,:)*t(j)+datXdotdot(3,:)))
;
end;
```

```
% Mean acceleration - overall magnitude
MEAN_Xdotdots = mean( abs (Xdotdots))

% RMS acceleration - overall magnitude
%%coverts average to RMS (SA cc course notes: SKF guide: p 2)
RMS_Xdotdots = 1.11*mean( abs (Xdotdots))
I(i,12)=RMS_Xdotdots;

%=========================================================================
% Fourier coefficients for Velocity
%=========================================================================

datXdot = [2*pi*f(npl); PXdot(npl); aXdot(npl)];

%=========================================================================
% Construct time domain Velocity signal with Fourier coefficients, note s
%=========================================================================
E=length(t);

for j=1:E;
Xdots(j)=sum(datXdot(2,:).*cos(datXdot(1,:)*t(j)+datXdot(3,:)));
end;

% Mean acceleration - overall magnitude
MEAN_Xdots = mean( abs (Xdots))

% RMS velocity - overall magnitude
%%coverts average to RMS (SA cc course notes: SKF guide: p 2)
RMS_Xdots = 1.11*mean( abs (Xdots))
I(i,13)=RMS_Xdots;

%
%=========================================================================
% Plot channel 2 RMS trend on figure(1)
%=========================================================================
%
figure(1)
subplot(4,4,6),plot(I(1:i,9),I(1:i,12),'--ro');set(gca,'FontSize',6)
datetick('x', 'dd/mm/yy-HHPM'); % print time in date format of '0'
title('Input Horz RMSXdotdots') % title
ylabel('I H RMSXdotdot') % label for y axis
xlabel('Time (h)') % label for x axis
legend('RMS')
legend('Location','NorthWest') % move legend to upper left
grid on
%

% Alarm on Input shaft Horizontal RMS !!!!
if I(i,12)> 7.5
    warningstring='RMS Xdotdot limit overreached:Input shaft horizontal'
dlgname= 'Vibration warning'
h = warndlg(warningstring,dlgname)

for ss=1:10

    pause(0.5)
    WarnWave = [sin(1:.6:400), sin(1:.7:400), sin(1:.4:400)];
Audio = audioplayer(WarnWave, 22050);
```

```
play(Audio);
end

end
%plot

subplot(4,4,10),plot(I(1:i,9),I(1:i,13),'--ro');set(gca,'FontSize',6)
datetick('x', 'dd/mm/yy-HHPM'); % print time in date format of '0'
title('Input Horz RMSXdots') % title
ylabel('I H RMSXdot') % label for y axis
xlabel('Time (h)') % label for x axis
legend('RMS')
legend('Location','NorthWest') % move legend to upper left
grid on
%
%
%=========================================================================
% Plot channel 3 data over time [ms^2]
%=========================================================================
%

figure(2)
subplot(3,4,3);plot(V(:,5),V(:,3));set(gca,'FontSize',6)
title('Output shaft Vertical') % title
ylabel('O V Acce (Xdotdot) [m/s^2]') % label for y axis
xlabel('Time (s)') % label for x axis
grid on
%pause;

%
%=========================================================================
% Determine FFT on time domain signal
%=========================================================================
% old: fs=2500;
t=vibtime;
fs=1/t(2);
Xdotdot=d(:,3);

%%%%%%%%%%%%%%%%%%%%%%%%%%%%%
np=length(t);
f=fs*(0:np-1)/np;

FXdotdot=fft(Xdotdot);
PXdotdot=abs(FXdotdot)*2/np;
aXdotdot=angle(FXdotdot);
% Remove unwanted inaccurate energy between approx 0 to 2 Hz
% because of piezo cristal

aantalf=2/f(2)+1
for a=1:aantalf
   PXdotdot(a) =  0.000000;
end

%=========================================================================
% Plot spectra - Acceleration Peak Amplitude and Phase
%=========================================================================
%npl=1:(86);
% (lenghth of t) / 2
npl=1:(np/2);
```

```
%figure(9);
subplot(3,4,7);plot(f(npl),PXdotdot(npl),'b');set(gca,'FontSize',6)
%title('Channel 3')
ylabel(' O V Peak Acce (Xdotdot) [m/s^2]')
xlabel('Frequency [Hz]')

%subplot(2,1,2);plot(f(npl),aXdotdot(npl),'b')
%ylabel('Acce Phase (aXdotdot) [rad]')
%xlabel('Frequency [Hz]'),pause
%

%=========================================================================
% Convert Acceleration to Velocity - Amplitude and Phase
%=========================================================================
% NB: Length of f (old: f = 6827)
lf = length(f);

% Velocity signal - Peak Amplitude, Note: mm/s
j=0;
for j = 1:(lf-1);
j=j+1;
PXdot(j) =( 1000*PXdotdot(j)/(f(j)*2*pi));
end;

% TEST:
%%PXdot= PXdotdot(10)/f(10)*2*pi

%test1 = 11111
%pause


%test2 = 22222
%pause

% Velocity phase angle - Peak Amplitude, Note: mm/s
% Angular relationship between acceleration and velocity vectors
% (pi/2 rad = 90 degrees)
j=0;
for j = 1:(lf-1);
j=j+1;
aXdot(j) =  (aXdotdot(j)- pi/2);

if aXdot(j)  <= -pi
        aXdot(j) = (aXdot(j) + 2*pi);
       else
          aXdot(j) = aXdot(j);
       end;

end;

%test3 = 33333
%pause

%=========================================================================
% Plot spectra - Velocity Peak Amplitude and Phase
%=========================================================================
%figure(10)
subplot(3,4,11);plot(f(npl),PXdot(npl),'b');set(gca,'FontSize',6)
```

```
%title('Channel 3')
ylabel('O V Peak Veloc (Xdot) [mm/s]')
xlabel('Frequency [Hz]')
%print

%subplot(2,1,2);plot(f(npl),aXdot(npl),'b')
%ylabel('Veloc Phase (aXdot) [rad]')
%xlabel('Frequency [Hz]'),pause
%
%=========================================================================
% Fourier coefficients for Acceleration
%=========================================================================

datXdotdot=[2*pi*f(npl); PXdotdot(npl)'; aXdotdot(npl)'];

%=========================================================================
% Reconstruct time domain Acceleration signal with Fourier coefficients,
note s
%=========================================================================
%Please note: E = length of t
E=length(t);

for j=1:E;
Xdotdots(j)=sum(datXdotdot(2,:).*cos(datXdotdot(1,:)*t(j)+datXdotdot(3,:)))
;
end;

% Mean acceleration - overall magnitude
MEAN_Xdotdots = mean( abs (Xdotdots))

% RMS acceleration - overall magnitude
%%coverts average to RMS (SA cc course notes: SKF guide: p 2)
RMS_Xdotdots = 1.11*mean( abs (Xdotdots))
I(i,14)=RMS_Xdotdots;

%=========================================================================
% Fourier coefficients for Velocity
%=========================================================================

datXdot = [2*pi*f(npl); PXdot(npl); aXdot(npl)];

%=========================================================================
% Construct time domain Velocity signal with Fourier coefficients, note s
%=========================================================================
E=length(t);

for j=1:E;
Xdots(j)=sum(datXdot(2,:).*cos(datXdot(1,:)*t(j)+datXdot(3,:)));
end;

% Mean acceleration - overall magnitude
MEAN_Xdots = mean( abs (Xdots))

% RMS velocity - overall magnitude
%%coverts average to RMS (SA cc course notes: SKF guide: p 2)
RMS_Xdots = 1.11*mean( abs (Xdots))
I(i,15)=RMS_Xdots;

%
```

```
%=========================================================================
% Plot channel 3 RMS trend on figure(1)
%=========================================================================
%
figure(1)
subplot(4,4,7),plot(I(1:i,9),I(1:i,14),'--ro');set(gca,'FontSize',6)
datetick('x', 'dd/mm/yy-HHPM'); % print time in date format of '0'
title('Output vert RMSXdotdots') % title
ylabel('O V RMSXdotdot') % label for y axis
xlabel('Time (h)') % label for x axis
legend('RMS')
legend('Location','NorthWest') % move legend to upper left
grid on
%

% Alarm on Output shaft Vertical RMS !!!!
if I(i,14)> 7.5
    warningstring='RMS Xdotdot limit overreached:Output shaft vertical'
dlgname= 'Vibration warning'
h = warndlg(warningstring,dlgname)

for ss=1:10

    pause(0.5)
    WarnWave = [sin(1:.6:400), sin(1:.7:400), sin(1:.4:400)];
Audio = audioplayer(WarnWave, 22050);
play(Audio);
end

end
%plot
subplot(4,4,11),plot(I(1:i,9),I(1:i,15),'--ro');set(gca,'FontSize',6)
datetick('x', 'dd/mm/yy-HHPM'); % print time in date format of '0'
title('Output vert RMSXdots') % title
ylabel('O V RMSXdot') % label for y axis
xlabel('Time (h)') % label for x axis
legend('RMS')
legend('Location','NorthWest') % move legend to upper left
grid on
%
%
%
%=========================================================================
% Plot channel 4 data over time [ms^2]
%=========================================================================
%

figure(2)
subplot(3,4,4); plot(V(:,5),V(:,1));set(gca,'FontSize',6)
title('Output shaft Horizontal') % title
ylabel('O H Acce (Xdotdot) [m/s^2]') % label for y axis
xlabel('Time (s)') % label for x axis
grid on
%pause;

%
%=========================================================================
% Determine FFT on time domain signal
%=========================================================================
% old: fs=2500;
```

```
t=vibtime;
fs=1/t(2);
Xdotdot=d(:,4);

%%%%%%%%%%%%%%%%%%%%%%%%%%%%%%%%
np=length(t);
f=fs*(0:np-1)/np;

FXdotdot=fft(Xdotdot);
PXdotdot=abs(FXdotdot)*2/np;
aXdotdot=angle(FXdotdot);
% Remove unwanted inaccurate energy between approx 0 to 2 Hz
% because of piezo cristal

aantalf=2/f(2)+1
for a=1:aantalf
   PXdotdot(a) =  0.000000;
end

%=========================================================================
% Plot spectra - Acceleration Peak Amplitude and Phase
%=========================================================================
%npl=1:(86);
% (lenghth of t) / 2
npl=1:(np/2);

%figure(12);
subplot(3,4,8);plot(f(npl),PXdotdot(npl),'b');set(gca,'FontSize',6)
%title('Channel 4')
ylabel('O H Peak Acce (Xdotdot) [m/s^2]')
xlabel('Frequency [Hz]')

%subplot(2,1,2);plot(f(npl),aXdotdot(npl),'b')
%ylabel('Acce Phase (aXdotdot) [rad]')
%xlabel('Frequency [Hz]'),pause
%

%=========================================================================
% Convert Acceleration to Velocity - Amplitude and Phase
%=========================================================================
% NB: Length of f (old: f = 6827)
lf = length(f);

% Velocity signal - Peak Amplitude, Note: mm/s
j=0;
for j = 1:(lf-1);
j=j+1;
PXdot(j) =( 1000*PXdotdot(j)/(f(j)*2*pi));
end;

% TEST:
%%PXdot= PXdotdot(10)/f(10)*2*pi

%test1 = 11111
%pause

%test2 = 22222
%pause
```

```
% Velocity phase angle - Peak Amplitude, Note: mm/s
% Angular relationship between acceleration and velocity vectors
% (pi/2 rad = 90 degrees)
j=0;
for j = 1:(lf-1);
j=j+1;
aXdot(j) =  (aXdotdot(j)- pi/2);

if aXdot(j)  <= -pi
        aXdot(j) = (aXdot(j) + 2*pi);
       else
          aXdot(j) = aXdot(j);
       end;

end;

%test3 = 33333
%pause

%=========================================================================
% Plot spectra - Velocity Peak Amplitude and Phase
%=========================================================================
%figure(13)
subplot(3,4,12);plot(f(npl),PXdot(npl),'b');set(gca,'FontSize',6)
%title('Channel 4')
ylabel('O H Peak Veloc (Xdot) [mm/s]')
xlabel('Frequency [Hz]')
%print

%subplot(2,1,2);plot(f(npl),aXdot(npl),'b')
%ylabel('Veloc Phase (aXdot) [rad]')
%xlabel('Frequency [Hz]'),pause
%
%=========================================================================
==
% Fourier coefficients for Acceleration
%=========================================================================
==

datXdotdot=[2*pi*f(npl); PXdotdot(npl)'; aXdotdot(npl)'];

%=========================================================================
% Reconstruct time domain Acceleration signal with Fourier coefficients,
note s
%=========================================================================
%Please note: E = length of t
E=length(t);

for j=1:E;
Xdotdots(j)=sum(datXdotdot(2,:).*cos(datXdotdot(1,:)*t(j)+datXdotdot(3,:)))
;
end;

% Mean acceleration - overall magnitude
MEAN_Xdotdots = mean( abs (Xdotdots))

% RMS acceleration - overall magnitude
%%coverts average to RMS (SA cc course notes: SKF guide: p 2)
RMS_Xdotdots = 1.11*mean( abs (Xdotdots))
```

```
I(i,16)=RMS_Xdotdots;

%=========================================================================
==
% Fourier coefficients for Velocity
%=========================================================================

datXdot = [2*pi*f(npl); PXdot(npl); aXdot(npl)];

%=========================================================================
% Construct time domain Velocity signal with Fourier coefficients, note s
%=========================================================================
E=length(t);

for j=1:E;
Xdots(j)=sum(datXdot(2,:).*cos(datXdot(1,:)*t(j)+datXdot(3,:)));
end;

% Mean acceleration - overall magnitude
MEAN_Xdots = mean( abs (Xdots))

% RMS velocity - overall magnitude
%%coverts average to RMS (SA cc course notes: SKF guide: p 2)
RMS_Xdots = 1.11*mean( abs (Xdots))
I(i,17)=RMS_Xdots;
%
%
%=========================================================================
% Plot channel 4 RMS trend on figure(1)
%=========================================================================
%
figure(1)
subplot(4,4,8),plot(I(1:i,9),I(1:i,16),'--ro');set(gca,'FontSize',6)
datetick('x', 'dd/mm/yy-HHPM'); % print time in date format of '0'
title('Output Horz RMSXdotdots') % title
ylabel('O H RMSXdotdot') % label for y axis
xlabel('Time (h)') % label for x axis
legend('RMS')
legend('Location','NorthWest') % move legend to upper left
grid on
%
% Alarm on Output shaft Horizontal RMS !!!!
if I(i,16)> 7.5
    warningstring='RMS Xdotdot limit overreached:Output shaft horizontal'
dlgname= 'Vibration warning'
h = warndlg(warningstring,dlgname)

for ss=1:10

    pause(0.5)
    WarnWave = [sin(1:.6:400), sin(1:.7:400), sin(1:.4:400)];
Audio = audioplayer(WarnWave, 22050);
play(Audio);
end

end
%plot
subplot(4,4,12),plot(I(1:i,9),I(1:i,17),'--ro');set(gca,'FontSize',6)
datetick('x', 'dd/mm/yy-HHPM'); % print time in date format of '0'
```

```
title('Output Horz RMSXdots') % title
ylabel('O H RMSXdot') % label for y axis
xlabel('Time (h)') % label for x axis
legend('RMS')
legend('Location','NorthWest') % move legend to upper left
grid on
%
data=0
clock=0

%
%
%=========================================================================
% Save all variables as Current date and time
%=========================================================================
%

datetime=datestr(now);
datetime=strrep(datetime,':','_'); %Replace colon with underscore
datetime=strrep(datetime,'-','_');%Replace minus sign with underscore
datetime=strrep(datetime,' ','_');%Replace space with underscore
save(datetime)    %save all variables as date and time


for j = z:-1:1 %Time increments in seconds between measurements
pause(1)
disp(j)

end
end

%Vibrasie
datetime=datestr(now);
datetime=strrep(datetime,':','_'); %Replace colon with underscore
datetime=strrep(datetime,'-','_');%Replace minus sign with underscore
datetime=strrep(datetime,' ','_');%Replace space with underscore
%save(datetime)    %save all variables as date and time
```